DISSERTATION

HUMAN T LYMPHOTROPIC VIRUS TYPE 1 PROTEIN TAX REDUCES HISTONE LEVELS

Submitted by

James M. Bogenberger

Graduate Degree Program in Cell and Molecular Biology

In partial fulfillment of the requirements

For the Degree of Doctor of Philosophy

Colorado State University

Fort Collins, Colorado

Spring 2008

COLORADO STATE UNIVERSITY

April 7, 2008

WE HEREBY RECOMMEND THAT THE DISSERTATION PREPARED UNDER OUR SUPERVISION BY JAMES M. BOGENBERGER ENTITLED "HUMAN T LYMPHOTROPIC VIRUS TYPE 1 PROTEIN TAX REDUCES HISTONE LEVELS" BE ACCEPTED AS FULFILLING IN PART REQUIREMENTS FOR THE DEGREE OF DOCTOR OF PHILOSOPHY.

Committee on Graduate Work

Dr. Jennifer Nyborg

Dr. Susan Bailey

Dr. Howard Liber

Dr. Paul Laybourn, Advisor

Dr. Norm Curthoys, Director

ABSTRACT OF DISSERTATION

HUMAN T LYMPHOTROPIC VIRUS TYPE 1 PROTEIN TAX REDUCES HISTONE LEVELS

Human T Lymphotropic Virus Type 1 (HTLV-1) is an oncogenic retrovirus that causes adult T-cell leukemia/lymphoma (ATLL). The virally encoded Tax protein is thought to be necessary and sufficient for T-cell leukemogenesis. Tax promotes cell proliferation, represses multiple DNA repair mechanisms, deregulates cell cycle checkpoints, inhibits apoptosis and induces genomic instability. All of these effects of Tax are thought to cooperate in the development of ATLL. In this study, we demonstrate that histone protein levels are reduced in HTLV-1 infected T-cell lines as compared to uninfected T-cell lines, while the relative amount of DNA per haploid complement is unaffected. In addition, we show that replication-dependent histone transcript levels are reduced in HTLV-1 infected T-cell lines, relative to uninfected T-cell lines. Furthermore, we show that Tax expression is sufficient for reduction of replication-dependent histone transcript levels. These results demonstrate that Tax disrupts the proper regulation of replication-dependent histone gene expression. Further, our findings suggest that HTLV-1 infection uncouples replication-dependent histone gene expression and DNA replication, allowing the depletion of histone proteins with cell division. Histone proteins are involved in the regulation of all metabolic processes involving DNA including transcription,

replication, repair and recombination. This study provides a previously unidentified mechanism by which Tax may directly induce chromosomal instability and deregulate gene expression through reduced histone levels.

James M. Bogenberger
Graduate Degree Program in Cell and Molecular Biology
Colorado State University
Fort Collins, CO 80523
Spring 2008

ACKNOWLEDGEMENTS

First and foremost I thank my advisor, Dr. Paul Laybourn, for all he has done to help me grow as a scientist. I greatly appreciate all of the stimulating and thought-provoking discussions that we shared. I thank my committee members Drs. Jennifer Nyborg, Susan Bailey and Howard Liber for all of their support and for all of their helpful suggestions. I thank all of the members of the Nyborg laboratory for all of their help. I thank Drs. Nicholas Polakowski and Isabelle Lemasson for all of their technical assistance at the bench and for many insightful discussions of my project. I thank Leslie Armstrong for her help in collecting flow cytometry data over the course of my project. I thank Dr. Mike Fox for taking time to discuss my flow cytometry data on several occasions. I thank all of the members of the Cell and Molecular Biology Program and the Department of Biochemistry and Molecular Biology at Colorado State University for many useful discussions of my project.

Table of Contents

Chapter 3 Figures

Chapter 1

Introduction

1.1 HTLV-1: PATHOGENESIS AND ASSOCIATED DISEASES

Human T Lymphotropic Virus Type 1 (HTLV-1) is a complex retrovirus originally isolated in 1980 from a patient with cutaneous T-cell lymphoma (1). After the identification of HTLV-1 as the first human retrovirus, it was demonstrated to be associated with a malignancy of T-lymphocytes known as adult T-cell leukemia/lymphoma (ATLL) (2-6). ATLL is now known to be a direct result of HTLV-1 infection (7). HTLV-1 is also associated with the non-malignant, neurodegenerative disease tropical spastic paraparesis/HTLV-1 associated myelopathy (TSP/HAM) (8). HTLV-1 is suspected to be associated with several other inflammatory diseases such as uveitis, arthritis and polymiositis (8-10).

Although the exact mechanistic details of T-cell transformation by HTLV-1 remain unknown, it is clear that HTLV-1 induced transformation is different from that of other known retroviruses. Unlike the acutely transforming retroviruses, which encode a viral homolog of a cellular proto-oncogene, HTLV-1 does not encode an oncogene transduced from a host genome (11). Additionally, development of ATLL does not correlate with a specific HTLV-1 proviral integration site (12). While malignant cells within a single individual exhibit a common site of proviral integration, the site of proviral integration varies amongst malignant cells of different individuals (13-15). Thus, HTLV-1 induces ATLL independently of the cis-acting effects of proviral integration, distinguishing it from the slowly transforming, cis-acting retroviruses.

Like all retroviruses, the HTLV-1 genome consists of two long-terminal repeats (LTRs) flanking the structural retroviral genes *gag, pro, pol* and *env* (11).

HTLV-1 contains an additional genomic segment between the *env* gene and the 3′ LTR, called the pX region (16). The pX region contains four partially overlapping open reading frames (ORFs), encoding several nonstructural and accessory viral gene products required for viral replication and infectivity (**Figure 1.1**) (17-22). ORF IV encodes the viral transcription factor Tax (16). Tax is essential for replication of the HTLV-1 genome and is required for HTLV-1 pathogenesis. Although there is no known cellular homolog of Tax, it is considered to be an oncoprotein. Tax has been shown to be necessary and sufficient in the transformation of primary T-cells and in the formation of tumors in transgenic mice (2, 23-27).

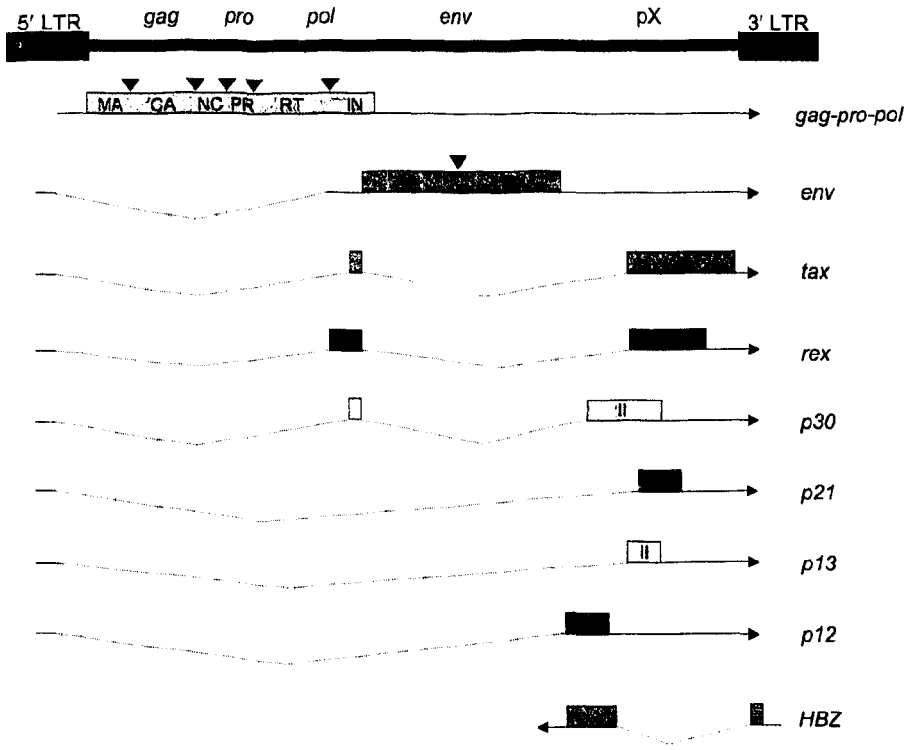

Figure 1.1. HTLV-1 genome and transcripts. HTLV-1 mRNAs are shown below the proviral genome. Boxes correspond to the open reading frames utilized for translation of the indicated mRNA. The triangles above the gag-pro-pol and env mRNAs show the protease cleavage sites in the corresponding protein products. MA = Matrix, CA = Capsid, NC = Nucleocapsid, PR = Protease, RT = Reverse Transcriptase, IN = Integrase, SU = Surface Protein, TM = Transmembrane Protein. The roman numerals indicate the open reading frames of the pX region utilized in the translation of the indicated mRNA.

Cell-free HTLV-1 virions are essentially non-infectious (28, 29). It has been demonstrated that a small percentage of HTLV-1 infected T-cells do complete a replication cycle and are able to infect additional T-cells through a virological synapse mediated by cell-to-cell contacts (30). HTLV-1 mRNAs and proteins are usually undetectable in the circulating peripheral blood mononuclear cells of HTLV-1 individuals with a high proportion of T-cells containing integrated HTLV-1 provirus (31, 32). HTLV-1 virions are not detected in the plasma of HTLV-1 infected individuals (33). Studies have shown that inhibitors of reverse transcriptase do not reduce the number of T-cells containing provirus in HTLV-1 infected individuals (34). Furthermore, reverse transcriptase is a highly error-prone polymerase, yet variations in HTLV-1 coding-sequences are limited when compared to other retroviruses, such as Human Immunodeficiency Virus Type 1 (HIV-1), that rely on viral transmission to uninfected cells to increase the number of infected cells (35). The aforementioned observations have led to the conclusion that persistent HTLV-1 infection is maintained by proliferation of HTLV-1 infected cells, rather than completion of the viral replication cycle. This requirement for cellular proliferation to replicate the proviral genome has likely provided the selective pressure for HTLV-1 to evolve strategies to induce inappropriate cellular proliferation. HTLV-1 Tax protein is known to induce cellular proliferation of HTLV-1 infected T-cells (36). While the induction of inappropriate cell division effectively replicates the proviral genome, it also has important consequences with respect to cellular transformation and the development of ATLL.

Evidence from clinical studies suggests that fewer than seven percent of HTLV-1 infected individuals develop ATLL (37). In addition, manifestation of ATLL occurs after a long latent period ranging from twenty to sixty years (38). Both of these observations suggest that subsequent events are required in the progression from HTLV-1 infection to T-cell transformation and the development of ATLL. The function of the HTLV-1 oncogenic protein Tax is fundamentally different from that of other viral oncoproteins. While other cancer-causing viruses require continuous expression of viral oncoprotein to perpetuate the transformed phenotype (39), Tax expression is not required to maintain the ATLL phenotype (40, 41). Thus, it is thought that the HTLV-1 encoded protein Tax creates a cellular environment more conducive to multi-step oncogenesis. As multi-step oncogenesis is accelerated by reduced DNA repair capacity and/or genomic instability (42), Tax expression may establish either or both of these conditions. Reduced DNA repair capacity and/or genomic instability may induce permanent changes in cellular homeostasis that mediate and/or perpetuate neoplastic transformation if and when Tax expression is silenced.

Tax is also linked to the non-malignant, inflammatory diseases associated with HTLV-1 infection, such as tropical spastic paraparesis/HTLV-1 associated myelopathy (TSP/HAM). Evidence suggests that two independent factors; the host immune response and the probability that an HTLV-1 infected T-cell expresses Tax, play a pivotal role in the development of these diseases (43, 44). Host immunosurveillance of HTLV-1-specific antigen presentation and lysis of HTLV-1 infected T-cells by cytotoxic T lymphocytes (CTLs) eliminates T-cells

expressing HTLV-1 proteins (44-46). While many HTLV-1 proteins are recognized, the dominant antigenic target of HTLV-1-specific CTLs is the Tax protein (47, 48). Mutations resulting in CTL escape are not observed with HTLV-1 infection, as with infection by Human Immunodeficiency Virus Type 1 (HIV-1) (49). Despite a CTL response to HTLV-1 gene expression, steady-state populations of HTLV-1 infected T-cells exhibiting clonal proviral integration are maintained in infected hosts (50). While the number of HTLV-1 infected T-cells in a given host remain constant prior to leukemogenesis, the number of HTLV-1 infected T-cells between different hosts has been observed to differ by more than 10^3-fold (51). TSP/HAM patients have been observed to have a greater number of HTLV-1 infected cells than asymptomatic carriers (52). Differences in the rate of CTL lysis have been reported between different HTLV-1 positive individuals, with reduced CTL antiviral efficacy correlating with the occurrence of a greater number of HTLV-1 infected cells (53). The number of HTLV-1 infected T-cells expressing Tax has been estimated to range from 0.3% to 3.0% daily between different hosts, with higher levels of Tax expression correlating with TSP/HAM patients and lower levels of Tax expression correlating with asymptomatic carriers (44). These observations suggest that the proliferative advantage gained through Tax expression surpasses the deleterious effects of immunosurveillance. While the mechanism by which HTLV-1 infected T-cells cause inflammatory disease is not known, efficacy of the host immune response and levels of Tax expression are determinants in the development of TSP/HAM.

Maintenance of a persistent viral infection is essential to all pathologies associated with HTLV-1. While many of the HTLV-1 accessory gene products encoded by the pX region are required for maintaining HTLV-1 infection in vivo, Tax protein is unique in that it is the only HTLV-1 accessory gene product that is sufficient to induce T-cell transformation.

1.2 FUNCTIONS OF HTLV-1 TAX PROTEIN

Tax exhibits many properties with respect to regulating the HTLV-1 replication cycle. Tax functions as a transcriptional activator regulating expression of the HTLV-1 genome (54). In addition, Tax exhibits many cellular properties not directly involved in regulating transcription of the HTLV-1 genome. However, these other cellular properties of Tax do function to replicate the proviral genome through induced proliferation and promotion of survival of HTLV-1 infected cells.

1.2a Tax as a Transcription Factor

Tax activates transcription of the HTLV-1 genome (54). The LTRs of HTLV-1 contain three degenerate copies of a recognition element known as a viral cAMP response element (vCRE). The vCREs have a central portion similar to cellular cAMP response elements and thus bind the cAMP-response element binding protein (CREB). Tax interacts with GC-rich sequences adjacent to the vCREs in a CREB-dependent manner (55-58). A historical model for

CREB-dependent transcription suggests that signal-mediated phosphorylation of CREB is responsible for recruitment of the coactivators CBP/p300 and for transcriptional activation. However, more recent evidence suggests that promoter-bound phosphorylated CREB is not sufficient for CBP/p300 recruitment (59, 60). While Tax has been shown to induce CREB phosphorylation in vivo (61), evidence suggests that Tax exhibits activator function beyond that of simply inducing CREB phosphorylation (60, 62). Tax interactions with CREB/ATF proteins have been reported to contribute to deregulated transcriptional control of some cellular genes (63). However, studies have shown that a Tax mutant defective for CREB/ATF activation is still capable of inducing T-cell immortalization (64).

1.2b HTLV-1 Tax in T-Cell Transformation

Cells employ several barriers that protect against neoplastic transformation. These include the multiple levels of regulation impinging on cell proliferation, cellular checkpoints that terminate with repair or apoptosis upon detection of different types of DNA damage or gross chromosomal abnormalities, and regulation of senescence and apoptosis. HTLV-1 infected T-cells must breach these protective barriers before ATLL can emerge. Tax deregulates several aspects of cellular homeostasis governing these protective barriers. The expression of Tax results in replication of the proviral genome through cell proliferation and increased survival of cells containing provirus.

Cellular proliferation is required for replication of the proviral genome, and the viral protein Tax exhibits several activities that result in the induction of cell proliferation. Tax activates expression of D type cyclins, which participate in regulating the G1 restriction point (65). Tax activation of D type cyclin expression is thought to occur primarily through increased IL-2 receptor signaling (66-68). In addition, Tax binds to cyclin-dependent kinases (CDKs), leading to signal-independent hyperphosphorylation of the retinoblastoma (Rb) protein and thus activation of the E2F transcription program regulating genes necessary for DNA replication (69, 70). Tax has also been reported to induce proteosomal degradation of the Rb protein (71). Tax is known to interfere with the activity of several CDK inhibitors. This occurs through direct Tax binding of the CDK inhibitors (INK4A and INK4B) (72, 73) and through direct transcriptional repression of the INK4C, INK4d and KIP1 genes by Tax binding of E-box binding factors required for transcriptional activation of these CDK inhibitors (74, 75). The net effect of Tax on D cyclin expression, cyclin-dependent kinases and cyclin-dependent kinase inhibitors, is the induction of signal-independent cell proliferation.

Tax is known to inhibit multiple DNA repair mechanisms. Tax represses transcription of polymerase β, which is involved in base excision repair, nucleotide excision repair and mismatch repair (76). The ability of cell cycle checkpoints to impede cell division until damage can be repaired or signal the induction of apoptosis if damage cannot be repaired greatly reduces the accumulation of mutations resulting from impaired repair processes. Checkpoint

Kinase 1 (Chk1) functions in the activation of S and G2 checkpoints in response to DNA damage. Tax has been reported to directly interact with Chk1 resulting in an inhibition of G2 arrest in response to γ-irradiation (77). Moreover, Tax is also known to inactivate p53 function, through several putative mechanisms (78-80). Although the mechanistic details are currently controversial, it is clear that p53 function is abrogated in Tax expressing cells (81). Tax has also been reported to deregulate the spindle assembly checkpoint (SAC) by binding to MAD1 (82). Tax deregulation of cell cycle checkpoints results in an increased rate of cellular proliferation and favors replication of the HTLV-1 proviral genome.

In addition to inducing inappropriate proliferation and deregulating multiple cell cycle checkpoints, Tax has been reported to promote cell survival. Tax binds directly to phosphatidylinositol 3-kinase (PI3K) and promotes phosphorylation of Akt, which initiates a survival signal though downstream effectors (83). Tax has been shown to promote NF-κB nuclear localization thereby inducing expression of NF-κB responsive genes, including those involved in promoting cell survival (84, 85). Tax promoted cell survival increases the number of HTLV-1 infected cells.

While Tax has been shown to be necessary and sufficient for T-cell transformation, Tax expression is only detected in about forty percent of ATLL cells (40, 86-88). These observations have led to the conclusion that Tax is required to initiate transformation but is not required to perpetuate the transformed phenotype in ATLL cells. As Tax protein is the major target of CTLs, cells not expressing Tax have a clear advantage in evading the host immune

response. While Tax protein is known to bypass many of the barriers to neoplastic transformation, it is not known exactly what cellular changes induced by Tax allow for the continued progression and/or maintenance of the ATLL phenotype after Tax expression has been silenced.

1.3 HTLV-1 ACCESSORY PROTEIN FUNCTION IN INFECTION AND T-CELL TRANSFORMATION

In addition to the pleiotropic Tax protein, the HTLV-1 genome encodes six other accessory proteins, p12, p21, p30, p13, HBZ and Rex. While these accessory proteins are not essential for viral replication in vitro (89), experiments in animal models have demonstrated that these proteins are important for productive infection in vivo (90-93). Accessory protein p12 localizes to the endoplasmic reticulum and Golgi and appears to promote cell survival through increased cytoplasmic calcium levels (94). This protein may also participate in the evasion of HTLV-1 specific CTLs through a reduction of major histocompatibility complex type I expression (95). p30 may function to promote cell proliferation through effects on the cellular coactivators CBP/p300 (96-98). Additionally, p30 may promote viral latency by preventing the nuclear export of Tax and Rex mRNA (99). Accessory protein p13 localizes to the mitochondrial inner membrane and affects potassium and calcium uptake, suggesting a function through calcium signaling along with p12 (100). Rex recognizes a sequence in HTLV-1 RNA and represses splicing, which governs the transition to

production of full-length genomic RNA (101, 102). Rex has also been shown to promote nuclear export of viral RNA (103). The function of p21 is currently unknown.

Unlike the previously mentioned HTLV-1 accessory proteins, the HBZ open reading frame is transcribed from the minus stand of the provirus (104, 105). The HBZ open reading frame is thought to produce a protein product and a functional RNA product. While HBZ protein suppresses transcriptional activation by Tax, HBZ RNA appears to promote T-cell proliferation through up-regulation of E2F1 transcription, as well as E2F1 target genes (106-108). While the non-Tax accessory gene products of HTLV-1 are not sufficient for T-cell transformation, they are required for maintaining a persistent viral infection in vivo. Thus, these other accessory proteins are critical to the pathologies associated with HTLV-1.

1.4 CHROMOSOMAL ABNORMALITIES IN ATLL, HTLV-1 INFECTED AND TAX EXPRESSING T-CELLS

ATLL cells exhibit a broad spectrum of chromosomal abnormalities, including deletions, duplications, translocations and aneuploidy (109, 110). Tax expression and DNA damage have been correlated in studies demonstrating that Tax expression results in the formation of micronuclei (111, 112). Micronuclei are small nuclei containing whole chromosomes or chromosomal fragments, separate from the main nucleus. Micronuclei can result from damage to

chromosomes (113, 114). Tax expression has been correlated with an increase in double-strand DNA breaks (115). Tax expression has been shown to induce gene amplification (116), an indication of genomic instability. Tax expression has also been observed to cause an uncoupling of DNA synthesis from cell division, resulting in the formation of multinucleated giant cells with decondensed chromatin (117). These giant cells feature less heterochromatin near the nuclear periphery, as suggested by an absence of the dark, condensed material normally observed just under the nuclear membrane. In addition to decondensed chromatin, these giant cells exhibit lobulated nuclei. The lobulated nuclei phenotype of Tax expressing cells is similar to that of the large lymphocytes with convoluted nuclear outlines, known as "flower cells," observed at higher frequencies in HTLV-1 infected individuals and ATLL patients (118). The chromatin of ATLL cells has been described as being clumped and more homogenous than that of normal T-cells (118). Currently there is not a clear mechanism for how these chromosomal abnormalities arise in Tax expressing and HTLV-1 infected T-cells.

1.5 CHROMATIN: OVERVIEW

In a broad sense, chromatin refers to the nucleoprotein fiber that is the foundation of the chromosome. This chromatin fiber is composed of a long, linear polymer of genomic DNA in association with a roughly equal mass of histone proteins, in addition to many other proteins with enzymatic and structural

functions. While much is known about the smallest and most fundamental units of the chromatin fiber, little is known about how the chromatin fiber is arranged into a chromosome.

The histone proteins are critical components of chromatin. The core histones assemble with DNA into nucleosome core particles, the fundamental units of chromatin (119). This is achieved by assembling two of each of the core histones (H2A, H2B, H3 and H4) into a histone octamer, around which 146 base pairs of DNA is wrapped (120). Arrays of nucleosome core particles constitute a chromatin fiber, the primary level of chromatin structure. The chromatin fiber is a highly dynamic and heterogeneous macromolecule in vivo. The chromatin fiber is further compacted through the formation of additional levels of higher order structure. Linker histones are thought to modulate nucleosome dynamics and higher order chromatin structure. Ultimately, the chromatin fiber is compacted by non-histone proteins forming metaphase chromosomes, the most compacted state of genomic DNA (**Figure 1.2**). Histones and chromatin structure play a central role in the regulation of all DNA metabolic processes, including transcription, replication, repair and recombination.

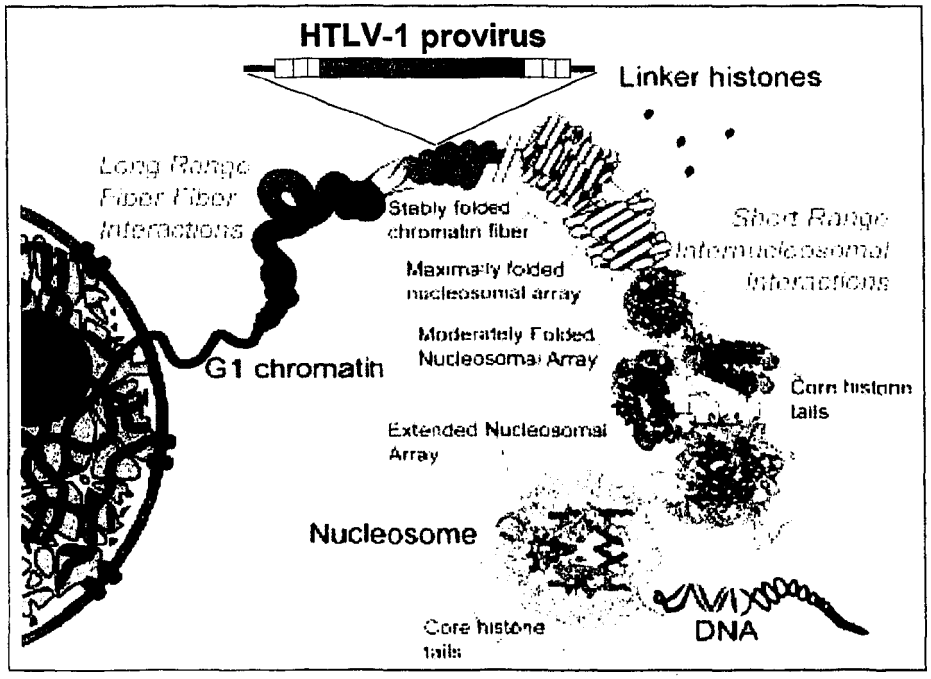

Figure 1.2. Chromatin hierarchical structure. DNA is wrapped around the histone octamer to form a nucleosome. Arrays of nucleosomes are arranged to form a chromatin fiber, the primary level of chromatin structure. The chromatin fiber is compacted into higher-order chromatin structures, with the most compacted state occurring during metaphase of mitosis. The interphase chromatin fiber and the higher order structures of the chromatin fiber are relatively uncharacterized in vivo. (Figure from Jeff Hansen and Karolin Luger)

As nearly every cell in a multi-cellular organism contains the same genomic information, cell differentiation and specialization require that distinct transcriptional programs are established and maintained. Post-translational modifications to the histone tails are thought to impart cellular differentiation through epigenetic control of the genome (121).

Chromatin structure, energy-dependent octamer sliding and the epigenetic information on the histone tails are all known to participate in double-strand DNA break repair (122, 123). Defects in nucleosome assembly have been shown to interfere with the repair of double-strand DNA breaks. Cells lacking the chromatin assembly factors CAF-1 and RCAF are hypersensitive to irradiation and to DNA-damaging agents such as methyl methanesulfonate. Furthermore, assays developed to quantify site-specific double-strand break repair by both non-homologous end joining and recombination pathways demonstrate repair defects in CAF-1 and RCAF mutants (124). Inhibition of chromatin assembly during DNA replication directly induces double-strand DNA breaks (125). Double-strand DNA breaks are potent inducers of genomic instability as they are repaired by the error-prone process of non-homologous end joining when a sister chromatid is not available for the higher fidelity process of recombination-mediated repair (126). Furthermore, partial depletion of histone H4 has been shown to increase homologous recombination-mediated genetic instability (127).

1.6 REPLICATION-DEPENDENT HISTONE GENE EXPRESSION

In normal somatic cells, expression of the majority of histone genes is tightly coupled to the rate of DNA replication during S phase of the cell cycle. Thus, they are called replication-dependent histone genes. Under normal circumstances inhibition of histone synthesis results in inhibition of DNA replication. Conversely, blocking DNA replication results in inhibition of histone expression (128). The coordination of histone gene expression and DNA synthesis is critical in the maintenance of chromosomal integrity (129). Histone chaperones and chromatin assembly factors normally cooperate in the deposition of histones onto nascent DNA as it emerges from the replication fork (130, 131). Since there is no significant pool of non-nucleosomal histones, nucleosome assembly at the replication fork is dependent on de novo histone expression and redistribution of existing histones (132, 133).

Mammalian cell division requires the synthesis of 10^8 histone proteins during a brief S phase. It is thought that cells contain multiple copies of the replication-dependent histone genes in order to meet these histone protein demands. Genomic sequence analysis has revealed fifty-nine replication-dependent core histone genes and six replication-dependent linker histone genes, clustered at four different chromosomal loci in human cells (134). The expression of all the replication-dependent histone genes is coordinately regulated during the DNA synthesis (S) phase of the cell cycle. This coordinate regulation is mediated by transcriptional and post-transcriptional mechanisms. It is not known how the transcriptional and post-transcriptional mechanisms of

histone gene regulation are coupled to the rate of DNA synthesis in proliferating cells.

1.6a Transcriptional Regulation of Replication-Dependent Histone Gene Expression

The rate of transcription of all the replication-dependent histone genes increases three- to five-fold as cells enter S phase (135). Studies have shown that proper cell cycle-dependent transcriptional regulation of each histone subtype involves unique cis-regulatory elements and unique transcription factors for each histone subtype (136, 137). It is not known how these different DNA-binding transcription factors are coordinated to activate transcription of all the replication-dependent histone genes in response to cell cycle signaling. Recently, non DNA-binding proteins have been identified that may be involved in coordinating histone gene transcription. Hir1p and Hir2p are cell cycle regulators thought to be responsible for transcriptional repression of histone gene expression in the budding yeast, *Saccharomyces cerevisiae* (138). HIRA is the mammalian homolog of these yeast proteins and may regulate histone gene expression in mammalian cells. HIRA has been shown to display histone chaperone function independent of DNA synthesis (139). HIRA has been shown to be phosphorylated by cyclin E/cdk2 during S phase of the cell cycle and HIRA activity is thought to be inhibited by this phosphorylation. The ectopic expression of HIRA is known to result in S phase arrest and reduced histone transcript

levels, suggesting a negative function for HIRA in replication-dependent histone gene expression outside of S phase (140).

NPAT is another mammalian protein thought to function in the coordinate expression of replication-dependent histone genes. Like HIRA, NPAT has also been shown to be an in vivo substrate of cyclin E/cdk2. Phosphorylation of NPAT correlates with the colocalization of NPAT to histone processing bodies (141, 142). Inhibition of NPAT gene expression impedes cell cycle progression and decreases histone gene expression in mammalian cells (143). Thus, NPAT is thought to participate in the up-regulation of replication-dependent histone gene expression during S phase.

Cajal bodies are multifunctional nuclear organelles known to accumulate high concentrations of small nuclear ribonucleoproteins (snRNPs) and other factors involved with histone pre-mRNA processing, including U7 snRNP and stem-loop binding protein (SLBP) (144-146). Histone gene clusters are intimately associated with Cajal bodies in a number of different organisms (147). In the fruit fly *Drosophila*, U7 snRNP resides in a distinct nuclear cluster distinguishable from the Cajal body, known as the histone locus body (HLB) (148). The FADD-like IL-1 β-converting enzyme associated huge (FLASH) protein has been identified as a component of the histone gene expression machinery. Reduction of FLASH expression reduces histone gene transcription, results in S-phase arrest and disrupts normal Cajal body architecture, including a loss of NPAT from histone gene clusters. FLASH is reported to interact with

NPAT and chromatin immunoprecipitation reveals that FLASH interacts with histone promoter sequences (149).

1.6b Post-Transcriptional Regulation of Replication-Dependent Histone Gene Expression

Post-transcriptional mechanisms of histone gene expression are responsible for an additional eight- to ten-fold increase in histone mRNA levels as cells enter S phase (135, 150). The replication-dependent histones are unique amongst genes transcribed by RNA polymerase II in that they do not contain introns and are not polyadenylated. Instead, they all contain a very similar 3′ stem-loop structure that is bound by a conserved protein in mammals, stem-loop binding protein (SLBP) (151, 152). SLBP mediates the only RNA processing event required for production of mature histone mRNAs, a 3′ endonucleolytic cleavage (153). In addition, SLBP regulates the nuclear export, half-life and translational efficiency of histone mRNAs (154-156).

1.7 STATEMENT OF PURPOSE

1.7a Historical Perspective

Initially the aim of this project was to examine the phosphorylation status and the global stoichiometry of the somatic histone H1 isoforms in HTLV-1 infected T-cell lines as compared to uninfected T-cell lines. The rationale for this initial investigation was based on two separate hypotheses. The HTLV-1 protein

Tax deregulates cyclin-dependent kinase activities, thus we hypothesized that histone H1 phosphorylation status would be altered during the cell cycle. Additionally, we sought to investigate the hypothesis that the linker histone isoforms are functionally distinct with respect to transcriptional competency. We reasoned that changes in gene expression in HTLV-1 infected cells may correlate with both global and local changes in linker histone isoform stoichiometry. The phosphorylation status of histone H1 isoforms was determined by specifically extracting histone H1 from HTLV-1 infected and uninfected T-cell lines using a perchloric acid extraction method and subsequently analyzing the extracts by mass spectrometry. Mass spectrometry revealed that all of the histone H1 isoforms were less phosphorylated in HTLV-1 infected T-cell lines than in uninfected T-cell lines. To determine the global stoichiometry of the somatic histone isoforms, a rigorous absolute real-time PCR approach was used to analyze transcript levels for each of the somatic histone H1 isoforms. Surprisingly, we discovered that transcripts for all of the somatic H1 isoforms were reduced in HTLV-1 infected T-cell lines as compared to uninfected T-cell lines. In light of this result, it became clear why acid extraction of linker histone, normalized to cell number, consistently yielded less linker histone from HTLV-1 infected T-cell lines, than from uninfected T-cell lines. As linker histone gene expression is regulated by the same mechanisms as the core histones, we began to analyze core histone transcript and protein levels in HTLV-1 infected and uninfected T-cell lines. Both northern blots and western blots revealed a

reduction of core and linker histone transcript and protein levels in HTLV-1 infected T-cell lines as compared to uninfected T-cell lines.

1.7b Significance

There is ample evidence showing the importance of histones and chromatin in the regulation of all aspects of DNA-based metabolism. Thus, the purpose of my research became the demonstration of the unprecedented finding that histone levels are reduced in HTLV-1 infected T-cell lines. This demonstration culminated in the development of a flow cytometry-based assay to measure histone protein and DNA content simultaneously in individual T-cells. Through this approach my research has unequivocally demonstrated a reduction of histone:DNA ratios in HTLV-1 infected T-cell lines as compared to uninfected T-cell lines. To begin to address the mechanism by which HTLV-1 reduces histone levels and to correlate our finding with the oncogenic capacity of HTLV-1, this research has also revealed that Tax expression is sufficient to reduce histone transcript levels in an uninfected T-cell line.

Chapter 2

Materials and Methods

2.1 CELL LINES AND CELL CULTURE

The following HTLV-1 infected T-cell lines, C8166-45 (C81), HuT102, MT-2 and SLB-1 and uninfected T-cell lines, CEM, Jurkat and Molt-4 were cultured in Iscove's Modified Dulbecco's Media (IMDM; Sigma-Aldrich) supplemented with 10% fetal bovine serum (Atlas Biologicals), 50,000 units/liter each streptomycin/penicillin and 2 mM L-glutamine. All T-cell lines were cultured at 37°C in the presence of 5% CO_2.

2.2 ISOLATION OF PRIMARY $CD4^+$ LYMPHOCYTES FROM PERIPHERAL BLOOD SAMPLES

2.2a Density Gradient Centrifugation

Peripheral blood samples where obtained from Bonfils Blood Center. Blood samples were diluted 1:1 with 0.5% BSA-PBS pH 7.4. Diluted samples (10 mL) were layered on 5 mL of Ficoll-Paque PLUS (Amersham Biosciences) in 15 mL conical tubes. Samples were centrifuged at 400 x g for 40 minutes at room temperature. The upper layer was carefully aspirated off after centrifugation. Cells at the interphase were transferred to 50 mL conical tubes (4 per 50 mL conical tube) and each tube was filled to the 50 mL mark with 0.5% BSA-PBS. Tubes were centrifuged at 300 x g for 10 minutes at room temperature. The supernatant was aspirated off and the cell pellet was washed by resuspending in 50 mL of 0.5% BSA-PBS and centrifuged at 200 x g for 15 minutes at room temperature to remove platelets. This wash step was repeated

once. The cell pellet was resuspended in 1 mL of 0.5% BSA-PBS and cell densities were determined.

2.2b Magnetic Labeling and Column Separation of $CD4^+$ Lymphocytes

Gradient purified cells were washed with 2 mL of 0.5% BSA-PBS per 10^7 cells and centrifuged at 300 x g for 10 minutes at room temperature. Cell pellets were resuspended in 80 μL of 0.5% BSA-PBS per 10^7 cells. Microbeads conjugated to $CD4^+$ antibodies (Miltenyi Biotech) were added at a concentration of 20 μL per 10^7 cells. Cell-microbead suspensions were incubated for 15 minutes at 4°C while rotating. After incubation, 2 mL of 0.5% BSA-PBS was added per 10^7 cells and suspensions were centrifuged at 300 x g for 10 minutes at 4°C. The cell-microbead suspension was resuspended in 500 μL of 0.5% BSA-PBS per 10^8 cells.

An LS magnetic separation column (Miltenyi Biotech) was placed into a magnetic field stand (Miltenyi Biotech) and equilibrated with 3 mL of 0.5% BSA-PBS. The cell-microbead suspension was then loaded onto the column. The column was washed 3 times with 3 mL of 0.5% BSA-PBS. After the last wash, the column was removed from the magnetic field stand and placed into a 15 mL conical tube. Cells were flushed out of the column with 5 mL of 0.5% BSA-PBS using a plunger (Miltenyi Biotec).

2.3 RNA EXTRACTION AND cDNA SYNTHESIS

RNA was extracted from asynchronous cells (10^7) using Trizol (Invitrogen) or CONCERT cytoplasmic RNA reagent (Invitrogen) according to the manufacturer's protocol. All the reagents used with both of these protocols were prepared with 0.2% diethylpyrocarbonate (DEPC) in purified water (Sigma). All instruments and workspaces were treated with RNase-away prior to performing extractions. In order to reduce genomic contamination, RNA samples were treated with 20 units of RNase-free DNase I (Roche) at room temperature for 30 minutes before heat inactivating the DNase I at 65°C for 10 minutes. DNA was synthesized with the iScript cDNA synthesis kit (Bio-Rad) according to manufactures protocol using a programmable thermal cycler set for 5 minutes at 25°C, then 30 minutes at 42°C, followed by 5 minutes at 85°C. This kit utilizes a random hexamer primer mix for cDNA synthesis. Prior to cDNA synthesis RNA was quantified via spectrophotometry, so that 5 μg of total RNA could be used per 20 μL iScript reaction.

2.4 REVERSE TRANSCRIPTASE REAL-TIME PCR

2.4a Relative Reverse Transcriptase Real-Time PCR

RNA samples were reverse transcribed into cDNA in a separate step prior to performing real-time PCR. Real-time PCR was performed using iQ SYBR Green Supermix (Bio-Rad) on an iCycler (Bio-Rad) and data expressed according to the Michael Pfaffl method, using EF1α as an internal control for

normalization (157). A five-point standard curve was constructed by serial diluting target DNA to evaluate PCR efficiency for every primer pair in every experiment. Only experiments with PCR efficiencies in the range of 90-110% were included in data analysis. All samples, including those used to construct standard curves for PCR efficiency, were loaded in triplicate for all experiments. Real-time PCR products were electrophoresed on 1.5% agarose gels to verify the specificity of each primer pair (See supplementary data, **Figure 3.21**). Melt curves were analyzed for every experiment to ensure that amplification products were primer pair specific.

2.4b Absolute Reverse Transcriptase Real-Time PCR

RNA samples were reverse transcribed into cDNA in a separate step prior to performing real-time PCR. Real-time PCR was performed using iQ SYBR Green Supermix (Bio-Rad) on an iCycler (Bio-Rad). Reference plasmids containing H1 isoform inserts and cDNA samples were quantified using an intercalating agent that specifically binds double-strand DNA quantitatively (Picogreen, Molecular Probes) on a spectrofluorometer. Plasmid and cDNA concentrations were determined by extrapolation from a standard curve constructed from lambda phage DNA of known concentration (See supplementary data, **Figure 3.16A**). Avogadro's number was used to calculate copy number from plasmid size and concentration. Quantified reference plasmids were then serial diluted to yield samples from 500 to 50 million molecules. The serial diluted samples served to evaluate efficiency during real-

time PCR and to construct a standard curve. The C_T for each reference plasmid was plotted against the natural log of the molecule number so that we could extrapolate the number of linker histone molecules (transcripts) per picogram of cDNA analyzed by real-time PCR (See supplementary data, **Figure 3.16B**). H1 transcripts (copy numbers) are then expressed as molecules/pg of cDNA. Melt curves were analyzed for every experiment to ensure that amplification products were primer pair specific. All samples, including those used to construct standard curves, were loaded in triplicate for all experiments. This protocol was adapted from the method described by Michael Whelan, et. al. (158).

2.4c Primer Sequences for Real-Time PCR

The following primer sequences were used for real-time PCR:

H2A Fwd AGCTCAACAAGCTTCTGGGCAA;

H2A Rev TTGTGGTGGCTCTCGGTCTTCTT;

H2B Fwd TGCGCCCAAGAAGGGTTCTAAA;

H2B Rev ACGAAGGAGTTCATGATGCCCA;

H3 Fwd TGCTCATCCGCAAACTGCCATT;

H3 Rev AGTGACACGCTTGGCGTGAATA;

H4 Fwd ACCGTAAAGTACTGCGCGACAA;

H4 Rev TTCTCCAGGAACACCTTCAGCA;

H1S-1 Fwd CCTGTAAAGAAGAAGGCGGCCAAA;

H1S-1 Rev CAGAGAAACTCCGCTACGCTCTTT;

H1S-2 Fwd CCCAGTATCTGAGCTTATCACCAAGG;

H1S-2 Rev TTTCTTAAGCGCGGCCAGAGAAAC;

H1S-3 Fwd CCCGGCTAAGAAGAAGGCAACTAA;

H1S-3 Rev GAAAGGCCATTGCGCTCCTTAGAA;

H1S-4 Fwd CCGGTGTCCGAGCTCATTACTAAA;

H1S-4 Rev GCTTTCTTGAGAGCGGCCAAAGAT;

EF1α Fwd GCCTCTCCAGGATGTCTACAAA;

EF1α Rev GTTTGAGAACACCAGTCTCCACTC;

Tax Fwd TTCTACCCGAAGACTGTTTGCCCA;

Tax Rev TGTCCAAATAAGGCCTGGAGTGGT.

2.5 NORTHERN BLOTS

2.5a Electrophoresis, Transfer, Probe Preparation and Hybridization

RNA extracts were quantified by spectrophotometry so that 10 μg of total RNA could be resolved on 1% agarose / 6.6% formaldehyde gels containing 20 mM MOPS, 2 mM sodium acetate and 1 mM EDTA pH 8.0. All aqueous solutions used in this protocol were prepared with purified water containing 0.2% diethylpyrocarbonate (DEPC) to deactivate potential contaminating RNases. Prior to electrophoresis of the RNA extracts, the gel box and comb were treated with 3% hydrogen peroxide to deactivate potential contaminating RNases. RNA extracts were prepared in a solution containing 5% glycerol, 0.0001% bromophenol blue (BPB), 20 mM MOPS, 2 mM sodium acetate, 1 mM EDTA pH

8.0 and 3.7% formaldehyde by incubating at 70°C for 10 minutes. Immediately after heat denaturation, the prepared samples were incubated on ice for two minutes prior to loading. Samples were electrophoresed at 50V until the βPB dye front had migrated approximately two-thirds the length of the gel.

After electrophoresis, the gel was removed and washed 4 times with 200 mL DEPC-treated water. The fourth wash was allowed to incubate for 20 minutes. The gel was then treated with 200 mL of 50 mM sodium hydroxide for 15 minutes. After the base treatment, the gel was washed quickly with 200 mL DEPC-treated water and incubated in 200 mL of 250 mM sodium phosphate pH 6.5 for 30 minutes. RNA samples were then transferred to a nylon membrane overnight, by using a downward capillary action setup with 25 mM sodium phosphate pH 6.5 as transfer buffer.

To prepare ^{32}P-radiolabeled probes a random hexanucleotide mixture (Roche; Random Primed DNA Labeling Kit) was utilized. DNA templates were denatured by incubating at 100°C for 5 minutes and immediately cooled on ice. Denatured DNA (25 ng) was mixed with 0.025 mM each of dCTP, dGTP and dTTP, 60 μCi [α^{32}P] labeled dATP, 10 units of Klenow fragment DNA polymerase (Fermentas) and a proprietary hexanucleotide mixture in reaction buffer (Roche; Random Primed DNA Labeling Kit). This mixture was incubated at 37°C for 30 minutes after which EDTA pH 8.0 was added to a final concentration of 25 mM to stop the reaction. Unincorporated dNTPs were then separated from the generated probes by centrifugation through a Micro Bio-Spin 6 column (Bio-Rad).

Membranes were probed with histone and EF1α probes simultaneously. Membranes were prepared for hybridization by incubating in a solution of 50% (v/v) stabilized formamide (FORMAzol; Molecular Research Center), 250 mM sodium phosphate pH 7.2, 250 mM sodium chloride, 1 mM EDTA pH 8.0, 100 μg/μL denatured salmon sperm DNA, and 10.5% (w/v) SDS for 120 minutes at 43°C in a rotating hybridization tube. Radiolabeled probes were boiled for 5 minutes and immediately cooled on ice prior to adding to the hybridization solution. Probes were allowed to hybridize overnight (16-24 hours) at 43°C in a rotating hybridization tube. After hybridization, membranes were washed 3 times with 20 mL of 300 mM sodium chloride, 30 mM sodium citrate, and 0.001% SDS (SSC) preheated to 53°C. The membrane was then incubated at 53°C for 20 minutes in 35 mL of SSC in a rotating hybridization tube. The membrane was then washed 2 times with 35 mL of 25 mM sodium phosphate pH 7.2, 1 mM EDTA pH 8.0 and 0.001% SDS by incubating at 53°C for 18 minutes each, in a rotating hybridization tube. Finally, the membrane was washed 2 times with 35 mL of 25 mM sodium phosphate, 1 mM EDTA pH 8.0 and 0.01% SDS by incubating at 53°C for 18 minutes each, in a rotating hybridization tube. The membrane was then allowed to air dry for 3 minutes prior to wrapping in cellophane and exposing to a phosphorimager screen.

Phosphorimager screens were scanned on a STORM (Molecular Probes). Histone signals were quantified with ImageQuant software version 5.1 (Molecular Dynamics) and normalized to EF1α signals.

2.5b Primer Sequences for the Preparation of ^{32}P-Radiolabeled Probes

The DNA templates used for the generation of ^{32}P-radiolabeled probes for histone and EF1α transcripts were prepared by PCR from Jurkat genomic DNA using the following primers:

H1 Fwd AAGGAGCGCAATGGCCTTTCTTTG;

H1 Rev GCCTTCTTGGCCTTTGCAGCTTTA;

H2A Fwd TTCAGTTTCCCGTAGGCCGAGT,

H2A Rev GAAGCTTGTTGAGCTCCTCATCGT;

H2B Fwd AAGAAGGATGGCAAGAAGCGCAAG;

H2B Rev ACTTGGAGCTGGTGTACTTGGTGA;

H3 Fwd ATCGCTATCGGCCTGGTACAGT;

H3 Rev AGCTGGATGTCCTTGGGCATGATA;

H4 Fwd ATGTCAGGACGCGGCAAAGGAGGTAA;

H4 Rev GATCACGTTCTCCAGGAACACCTTCA;

EF1α Fwd TCATTGGACACGTAGATTCGGGCA;

EF1α Rev TTCACACCCAGTGTGTAAGCCAGA;

The DNA template used for the generation of ^{32}P-radiolabeled probes for Tax transcripts was prepared by PCR from pSG-Tax plasmid DNA using the following primers:

Tax Fwd TTCCCAGGGTTTGGACAGAGTCTT;

Tax Rev GCGTGCCATCGGTAAATGTCCAAA.

2.6 PERCHLORIC ACID EXTRACTION OF HISTONE H1

This extraction technique is based upon the fact that histone H1 is soluble in 5% perchloric acid while nearly all other cellular proteins are insoluble, including the core histones. Soluble histone H1 is recovered by precipitation with 30% trichloroacetic acid.

Cultured T-cells (1×10^8 total) were pelleted by centrifugation at 325 x g for 3 minutes. Culture media was decanted and cells were washed with 5 mL phosphate buffered saline (PBS) pH 7.4 by resuspending the cell pellet and centrifuging as above. Wash buffer was decanted and 5% (v/v) perchloric acid (PCA) was added to the cell pellet at a volume of 1 mL per 1.5×10^7 cells. After adding 6.7 mL 5% PCA cells were gently vortexed until suspended and incubated for 60 minutes on ice with periodic swirling at 15 minute intervals. After incubation, the insoluble debris was pelleted by centrifugation at 12000 x g for 10 minutes at 4°C. The volume of the supernatant (acid soluble fraction) was measured as it was transferred to a new tube so that trichloroacetic acid (TCA) could be added to a final concentration of 30% (v/v). After addition of the appropriate volume of 100% TCA, the mixture was gently swirled and incubated on ice for 60 minutes to precipitate histone H1. Histone H1 was pelleted by centrifugation at 17,350 x g for 15 minutes at 4°C. The pellet was washed twice with 15 mL of acetone and centrifuged at 17,350 x g for 5 minutes at 4°C after each wash. After air-drying the pellet for 5-10 minutes it was suspended in 200

μL purified water. Samples were resolved by 15% SDS-PAGE and total protein visualized by coomassie brilliant blue staining.

2.7 WESTERN BLOTS

2.7a Preparation of Whole Cell Extracts

Whole cell extracts (WCEs) were prepared by pelleting 1 x 10^7 cells by centrifugation at 325 x g for 3 minutes. After decanting the culture media, the cell pellet was washed with 5 mL PBS pH 7.4 by resuspending the cell pellet and centrifuging as above. The cell pellet was then resuspended in 200 μL of Laemmli buffer 62.5 mM Tris-HCl pH 6.8, 3% (w/v) SDS, 20% (v/v) glycerol and boiled for 10-20 minutes. Bromophenol blue was excluded from Laemmli buffer and added to whole cell extracts just prior to gel electrophoresis, so that extracts could be quantified first. After boiling, WCEs were centrifuged at 18,000 x g for 10 minutes at 4°C and supernatant was transferred to a microcentrifuge tube for storage at -80°C.

2.7b Quantification of Whole Cell Extracts

Total protein concentration of whole cell extracts was determined by absorption at 280 nm. A standard curve was constructed using purified bovine serum albumin (BSA) of known concentration. Protein concentrations of WCEs were extrapolated from the BSA standard curve. As the Laemmli buffer used to prepare the WCEs contained several components at concentrations known to

interfere with absorption spectra at 280 nm, the WCEs were diluted below the interference limits of these components (159).

WCEs were diluted 1:100 by mixing 5 μL of WCE with 495 μL of purified water (Sigma). Laemmli buffer was also diluted 1:100 with purified water, to use in the preparation of the BSA standards at concentrations of 25, 50, 100, 250, 500 and 1000 ng/μL and to set the background absorption to zero on the spectrophotometer.

2.7c Electrophoresis, Transfer and Antibody Detection

WCEs were resolved by 15% SDS-PAGE and proteins were transferred to a nitrocellulose membrane in a Mini Trans-Blot (Bio-Rad) containing an ice block, at 300 mAmps for 60 minutes. After transfer, the nitrocellulose was blocked with 15 mL 5% (w/v) non-fat dry milk (NFDM) in PBS pH 7.4, containing 0.05% (w/v) sodium azide and 0.002% (v/v) Tween-20. After blocking, the nitrocellulose was incubated with primary antibody overnight at 4°C. Primary antibodies were diluted in 2.5% NFDM in PBS pH 7.4, containing 0.05% sodium azide and 0.002% Tween-20. The concentration of primary antibody was empirically determined for every antibody used. After primary antibody incubation, the nitrocellulose was washed three times with 10 mL 2.5% NFDM in PBS pH 7.4, containing 0.05% sodium azide and 0.002% Tween-20. The membrane was then incubated in 15 mL of secondary antibody for 90 minutes at room temperature. Anti-mouse and anti-rabbit HRP-conjugated secondary antibodies

(Promega) were both diluted 1:10,000 in PBS pH 7.4. After secondary antibody incubation the membrane was washed three times with PBS pH 7.4. Antibody binding was then visualized using the ECL+ detection system (Amersham) and scanning membranes on a STORM (Molecular Probes). One of the western blots presented (H2B, Figure 3.3) was recorded using film, as the STORM was inoperable at the time of this western blot.

2.7d Antibodies

The following antibodies and concentrations were used for western blotting. Mouse monoclonal anti-actin, Clone: C4 (MP Biomedicals) 1:1,000; mouse monoclonal anti-EF1α, Clone CBP-KK1 (Upstate) 1:1250; mouse monoclonal anti-H1, (Biomeda, product number V7013) 1:750, rabbit polyclonal anti-H2A, clone Poly 6194 (Biolegand) 1:450, rabbit polyclonal anti-H2B, ab18977 (Abcam) 1:100, rabbit polyclonal anti-H3, ab1791 (Abcam) 1:35,000, rabbit polyclonal anti-H4 (Biovision, catalog number 3624) 1:200.

2.8 DNA CONTENT/CELL CYCLE ANALYSIS

Cell cultures were diluted to a density of 5 x 10^5 to 1 x 10^6 cells/mL 24 hours prior to fixation to ensure a cell population proliferating in log phase at the time of fixation. Culture media containing 10^6 total asynchronous cells was centrifuged at 325 x g for 3 minutes to pellet the cells. The cell pellet was suspended in 5 mL ice-cold phosphate buffered saline (PBS) pH 7.4 to wash

away residual culture media and cells were once again pelleted as above. The washed cell pellet was suspended in 2 mL ice-cold PBS pH 7.4. 2 mL of ice-cold 100% ethanol was added dropwise to the cell suspension with a Pasteur pipet while vortexing at the lowest setting. The dropwise addition of ethanol was performed by adding 5 drops, waiting 5 seconds, and then repeating this sequence until the entire 2 mL of ethanol was added. An additional 3 mL of ice-cold 100% ethanol was added slightly faster by pipeting continuously while vortexing vigorously. Fixed cells were then incubated at -20°C for approximately 24 hours. After incubating, cells were pelleted again by centrifugation at 325 x g for 3 minutes. Cells were suspended in 1 mL ice-cold PBS pH 7.4 containing 1% BSA to wash away residual ethanol. After centrifuging as before, cells were suspended in 500 μL PBS pH 7.4 containing 1% BSA and then vortexed briefly. In order to extract low molecular weight DNA, cells were incubated in 1 mL of 4 mM sodium citrate and 192 mM dibasic sodium phosphate pH 7.8 for 30 minutes at room temperature. Cells were pelleted as before, buffer was decanted and the cell pellet was suspended in 1 mL of 50 μg/mL propidium iodide containing 730 Kunitz U/mL RNase A and incubated at room temperature for 20 minutes prior to running samples. Data was collected on an EPICS flow cytometer (Beckman Coulter) and cell cycle distributions were calculated using Multicycle (Phoenix Flow Systems).

2.9 HISTONE:DNA RATIOS BY FLOW CYTOMETRY

2.9a Preparation of Cells for Flow Cytometry

Asynchronous cells from log phase (5 x 10^6) were pelleted by centrifugation 325 x g and washed with 5 mL ice-cold PBS. Pellets were resuspended in 500 μL ice-cold PBS and transferred to 4.5 mL ice-cold 1% formaldehyde (methanol-free) in PBS and incubated on ice for 15 minutes to fix cells. After fixation cells were pelleted as above and washed with 4.5 mL ice-cold PBS. Cell pellets were resuspended in 500 μL ice-cold PBS and transferred to 4.5 mL ice-cold 70% ethanol and let stand at -20°C for at least 2 hours to permeablize cells. (A 4 hour incubation, though not absolutely necessary, seemed to yield higher quality DNA histograms) After ethanol permeabilization, cells were centrifuged at 200 x g for 8 minutes at room temperature. Cell pellets were washed 2 times with 2 mL PBS. Cell pellets were then resuspended in 2 mL of 1% BSA-PBS and let stand at room temperature for 5 minutes. After blocking, 100 μL of 1% BSA-PBS containing 5 μg primary antibody (ab1791 rabbit polyclonal to histone H3, Abcam; or V7013 mouse monoclonal antibody to histone H1, Biomeda) was added an incubated overnight at 4°C while rotating. Cells were then washed with 2 mL 1% BSA-PBS and centrifuged at 300 x g for 5 minutes at room temperature. Cell pellets were incubated in 2 mL of 1% BSA-PBS solution containing 5 μg of Alexa Flour 488 goat anti-rabbit secondary antibody (product number A11008, Molecular Probes) for histone H3 analysis or Alexa fluor 488 goat anti-mouse secondary antibody (product number A11029,

Molecular Probes) for histone H1 analysis, for 1 hour at room temperature. Cells were washed with 5 mL 1% BSA-PBS and centrifuged at 300 x g for 5 minutes at room temperature. Cell pellets were incubated in 1 mL PBS containing 25 μg/mL propidium iodide (PI) (Sigma) and 40 Kunitz units/mL RNase A (Sigma, certified DNase-free) for 30 minutes at room temperature. During secondary antibody incubation containers were shielded from light. Unstained cells, as well as cells treated with primary antibody only, secondary antibody only, PI only, and primary and secondary antibody only were included as controls in every experiment to determine background fluorescence and in instrument calibration.

Cells were analyzed on a MoFlo (Dako Cytomation) flow cytometer/cell sorter with laser excitation at 488 nm with 110 mW. Data was interpreted using Summit software, version 4.0 (Dako Cytomation).

2.9b Data Analysis

Mean histone signal intensity was traced from G1 through G2/M by setting a narrow window on the DNA histogram and recording the histone signal associated with the cell population defined by the window. During flow cytometry, a cell is assigned to an appropriate channel based on the DNA content of the cell, thus cell populations are defined by DNA content. By moving from the G1 peak (1X DNA content) to the G2/M peak (~2X DNA content) in defined increments, histone signals were recorded for particular DNA contents. Histone:DNA ratios can be determined directly from this data and expressed as a

whole raw number or relative to Jurkat. In order facilitate the comparison of individual experiments, the G1 histone:DNA ratio of Jurkat was then set equal to 1 and the values of the other T-cell lines examined expressed relative to Jurkat. This was necessary due to individual experimental variations in histone and DNA signals based on instrument calibration and settings. While it is impossible to compare histone and DNA signals directly between individual experiments, histone:DNA ratios calculated are comparable and highly reproducible.

2.10 CO-TRANSFECTION AND MAGNETIC SELECTION OF TRANSFECTANTS

2.10a Electroporation

Jurkat cells were co-transfected with pSG-Tax/pMACS Kk or pUC-19/pMACS K^k at 20 μg total DNA per 1 x 10^7 cells by electroporation in 0.4 cm cuvettes using Genepulse (Bio-Rad). Cells were collected by centrifugation at 325 x g for 3 minutes and washed with non-supplemented Iscove's Modified Dulbecco's Medium (IMDM) (Sigma). Washed cells were resuspended in 500 μL of non-supplemented IMDM containing 20 μg total DNA and incubated for 10 minutes prior to electroporation. The electroporation settings were as follows: voltage; 250V, amperage; 1500 μF and ohms; set to infinity. Both the pSG-Tax and pUC-19 plasmids were used in 3.5 molar excess of the pMACS K^k plasmid, in order to increase the probability that cells expressing the selection marker also contained the experimental plasmid. The 500 μL of transfected cell suspension

was transferred to 25 cm^2 filter-cap T-flasks, carefully avoiding transfer of lysed cells floating on the surface. Transfected cells were then plated at a density of 1 x 10^6 cells/mL in supplemented IMDM and incubated for 24 hours prior to enrichment with the pMACS K^k magnetic selection system (Miltenyi Biotec).

2.10b Magnetic Separation

The pMACS Kk expression plasmid encodes a truncated mouse MHC class I molecule. Cells receiving plasmid by electroporation express a unique surface marker distinguishing transfected cells from untransfected cells. Magnetic beads conjugated to an antibody specific for the mouse MHC class I molecule are then used to retain transfected cells within a column placed in a magnetic field, while untransfected cells are washed away. This procedure results in the enrichment of transfected cells.

Transfected cells were pelleted by centrifugation at 150 x g for 10 minutes. After decanting media, cells were resuspended in 320 μL of PBS pH 7.4 with 5 mM EDTA (PBE) per 10^7 total cells. After resuspending cells, 150 μL of MACSelect K^k microbeads (Miltenyi Biotec) were added to the cell suspension and incubated for 15 minutes, while rotating at 4°C. After incubating, PBE was added to a final volume of 2 mL. A LS magnetic separation column (Miltenyi Biotec) was placed into a magnetic field stand (Miltenyi Biotec) and equilibrated with 3 mL of PBE prior to loading the cell/bead suspension. As dead cells result in clogging of the separation column, pre-separation filters (Miltenyi Biotec) were

used. After loading the cell/bead suspension, the columns were washed 4 times with 3 mL of PBE. The column was then removed from the magnetic field stand and bound cells were flushed out with 4.5 mL of supplemented IMDM using a plunger (Miltenyi Biotech). Enriched cell populations were plated at a density of 1 x 10^6 cells/mL and cultured for an additional 24 hours prior to harvesting cells for RNA extraction and DNA content analysis.

2.11 Preparation of T-Cell Lines for Harvesting of Metaphase Spreads

T-cell lines were incubated in media containing 100 ng/mL colcemid for 3 hours. After colcemid treatment, cells were pelleted by centrifugation at 150 x g for 5 minutes. After decanting media, 5 mL of 75 mM potassium chloride was added dropwise while vortexing gently. Cells were incubated in potassium chloride for 15 minutes at room temperature. After incubating, 1 mL of (3:1) methanol:acetic acid was added dropwise while gently vortexing. Cells were immediately pelleted by centrifugation at 150 x g for 5 minutes. The initial fixative was decanted and 5 mL of (3:1) methanol:acetic acid was added dropwise while gently vortexing. Cells were then allowed to incubate for 10 minutes at room temperature. Cells were then pelleted by centrifugation at 150 x g for 5 minutes and the fixation sequence described above was repeated once. Cells were then stored at -20°C prior to analyzing metaphase spreads.

Cells were centrifuged 150 x g for 5 minutes and the fixative was aspirated off the cell pellet. Fixative, (3:1) methanol:acetic acid, was then added at a volume that just covered the cell pellet. Glass slides were cleaned with ethanol and rinsed with sterile water prior to placing slides on a steaming apparatus. Approximately 3 drops of the cell suspension was dropped onto glass slides with a Pastuer pipet from a distance of about 30 cm. Slides were allowed to steam for 8 seconds. Slides were then placed on a warming tray until dry. Slides were visualized on a Zeiss phase microscope.

2.12 Micrococcal Nuclease Digestion of Nuclei

Nuclei were isolated and micrococcal nuclease (MNase) digestions performed exactly as described in detail by Hager and Fragoso (160).

Chapter 3

Human T Lymphotropic Virus Type 1 Protein Tax Reduces Histone Levels

The findings described and discussed in this chapter have been published in the open-access journal, Retrovirology. However, this chapter includes evidence, in addition to published data, demonstrating that HTLV-1 infection and Tax expression reduce histone levels. The materials and methods used to complete the experiments included in this section have been described in Chapter 2. The citation for the manuscript is as follows:

Bogenberger, JM and Laybourn, PJ Human T Lymphotropic Virus Type 1 Protein Tax reduces histone levels. Retrovirology, 2008 Jan 31; 5(1):9

3.1 ABSTRACT

ATLL cells exhibit many chromosomal abnormalities. The nuclei of ATLL cells are often enlarged, with chromatin appearing more homogenous than that of normal T-cells. HTLV-1 infected and Tax expressing T-cells contain micronuclei, a potential indication of DNA damage. While DNA damage and genomic instability have been observed in many types of transformed cells, defects in chromatin structure/assembly have not been correlated with transformed phenotypes. Defects in chromatin assembly may represent a novel means for the induction of DNA damage and genomic instability. The viral transcription factor Tax is thought to deregulate the expression of hundreds of cellular genes. Mechanisms for the deregulation of many of these genes have been described. Chromatin is an integral component in the regulation of eukaryotic transcription. Thus, it is possible that defects in chromatin structure contribute to the mechanisms of deregulation previously described for Tax deregulated genes. In addition, defects in chromatin structure/assembly may represent a novel means for the deregulation of gene expression.

We were interested in investigating the possibility that the aforementioned attributes of ATLL, HTLV-1 infected and Tax expressing T-cells result, in part, from defects in forming proper chromatin structure. Since histones are critical to the formation of proper chromatin structure, we hypothesized that HTLV-1 infection and Tax perturb histone gene expression. This study demonstrates that histone protein and transcript levels are reduced in HTLV-1 infected T-cell lines as compared to uninfected T-cell lines. Additionally, our findings suggest that

HTLV-1 infection uncouples replication-dependent histone gene expression and DNA replication, allowing the depletion of histone protein with cell division. Furthermore, this study demonstrates that Tax expression in uninfected Jurkat T-cells is sufficient for reduction of replication-dependent histone transcript levels.

3.2 INTRODUCTION

While HTLV-1 infected and Tax-expressing cells exhibit chromosomal abnormalities including deletions, duplications, translocations and aneuploidy, it is not known exactly how these diverse abnormalities arise. There is no evidence linking a specific chromosomal abnormality to the development of ATLL. The chromatin of ATLL cells has been described as being clumped and relatively more homogenous than that of normal T-cells (5). Tax expressing cells exhibit a reduction of heterochromatin at the nuclear periphery (5, 118). Studies have shown that Tax deregulates the mitotic spindle assembly checkpoint (SAC), which can result in aneuploidy in HTLV-1 infected T-cells (82). While Tax effects on the SAC are sufficient to explain aneuploidy in HTLV-1 infected cells, they do not likely explain the observed defects in chromatin appearance. Additionally, Tax has been shown to deregulate checkpoints involved in DNA damage repair, at multiple levels (161). While damage checkpoint deregulation occurring in the presence of Tax promoted cell survival could result in T-cells that are accumulating mutations, it does not likely account for gross chromatin abnormalities.

Histone proteins form the foundation of eukaryotic chromatin. While there are no previous reports of histone level reductions associated with viral infection or transformed phenotypes, reduction of histone levels has been achieved experimentally. The linker histone isoforms have been systematically evaluated by the creation of knockout mice lacking a single H1 isoform or combinations thereof. While ablation of a single H1 isoform did not alter viability, combinatorial knockouts resulting in a reduction of total linker histone to 50% or more, resulted in death during mid-gestation (162). A study evaluating partial depletion of histone H4 in a *Saccharomyces cerevisiae* strain that can be gradually depleted of histone H4 demonstrates that a 29% reduction in H4 protein levels results in only a slight decrease in the rate of cell proliferation. Furthermore, this study demonstrates that a 29% reduction in histone H4 protein levels does not effect global nucleosome repeat length or micrococcal nuclease sensitivity of the resultant chromatin (127).

A group of protists known as the dinoflagellates represent an anomaly amongst eukaryotes in terms of chromosome structure. Dinoflagellates contain haploid genomes ranging in size from 2 to 200 gigabases, yet lack nucleosomes and histone proteins altogether. The chromosomes of the dinoflagellates occur in a liquid crystalline state and are condensed even during interphase. While the dinoflagellates utilize basic proteins to package genomic DNA, the basic protein to DNA ratio in dinoflagellates is an astounding 1:10 (163).

While the histones package genomic DNA within the nuclei of nearly all eukaryotes, they also function in the regulation of all processes involving DNA,

including replication, transcription, repair and recombination. The regulatory functions of histones in DNA-based metabolism are not necessarily distinct from the packaging function, as evidence indicates that the degree of chromatin compaction correlates with varying activities. Chromatin structure is likely integrated into of all aspects of DNA function. Modifications to the histone tails, while capable of altering chromatin structure, may have additional roles with respect to the storage of epigenetic information and interaction with non-architectural chromatin binding proteins. Defects in chromatin assembly will affect all processes involving DNA and will have deleterious consequences for cellular homeostasis. This study provides a previously unidentified mechanism by which Tax may directly induce chromosomal instability and deregulate gene expression through reduced histone levels.

3.3 RESULTS

3.3a Acid Extraction of Histone H1 Indicates a Reduction of Histone H1 Protein in HTLV-1 Infected T-Cell Lines

In order to specifically extract histone H1 protein from T-cell lines, perchloric acid extractions were performed. Perchloric acid extracts from whole cells are a nearly homogenous mixture of histone H1 isoforms without further purification, as judged by gel electrophoresis and visualization with a non-specific protein stain. The H1 isoforms are resolved as two separate bands on 15% polyacrylamide gels. $H1^S$-2, $H1^S$-3 and $H1^S$-4 are indistinguishable in a slower

migrating band, while $H1^S$-1 migrates slightly faster. Perchloric acid was used to extract H1 isoforms from both uninfected and HTLV-1 infected T-cell lines. Electrophoretic resolution of acid extracts indicates a reproducible reduction of all H1 isoforms in the HTLV-1 infected T-cell lines examined (**Figure 3.1A & B**). In order to illustrate the separation of the isoforms, a gel with increased resolution was included (**Figure 3.1B**). Additionally, comparison of these two gels shows that there was not a problem with the loading or extracting of the MT-2 sample in figure 3.1A, as histone H1 levels are actually significantly lower in the MT-2 samples shown (**Figure 3.1B**). Although these results indicate a reproducible reduction of histone H1 protein in the two HTLV-1 infected T-cell lines examined, the results obtained through this methodology are difficult to rigorously quantify. While these extracts were normalized against total cell number, it is often difficult to attain highly accurate cell counts. Tax is cytotoxic in cultured cells and results in an increase in non-viable cells, making counting difficult despite the use of cell viability dyes. Therefore, we sought to measure histone H1 levels by western blotting.

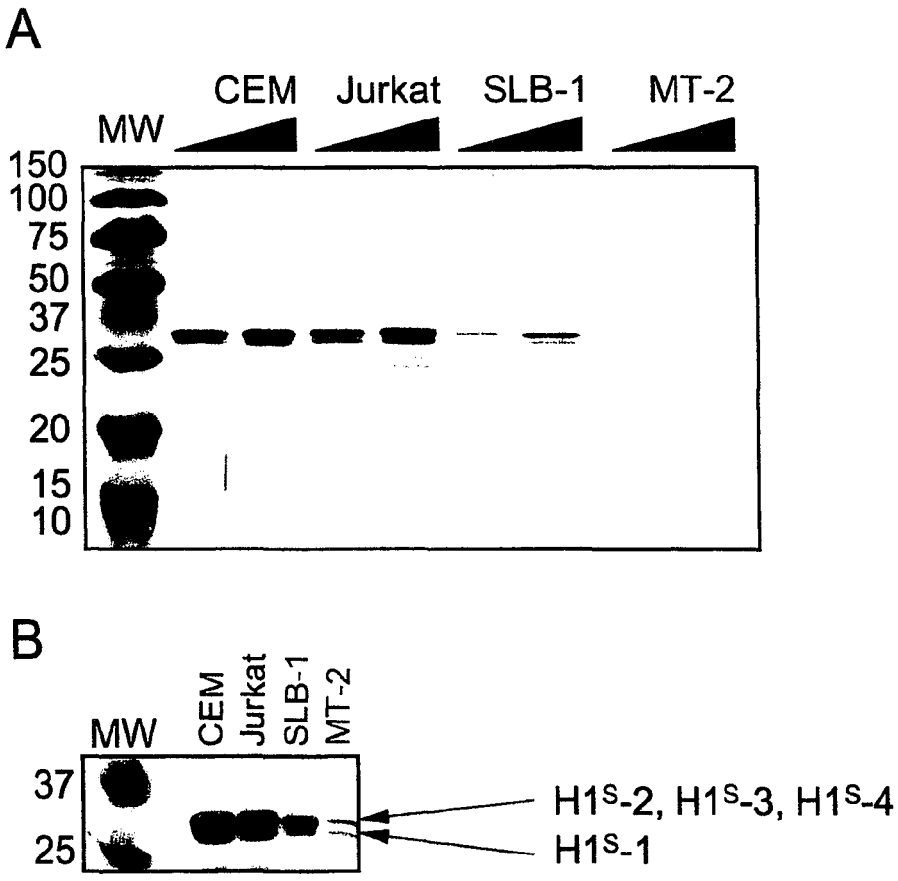

Figure 3.1. Acid extraction indicates a reduction of histone H1 protein in HTLV-1 infected T-cell lines. Histone H1 isoforms were specifically extracted from an equal number of cells with 5% perchloric acid. Extracts were resolved by 15% SDS-PAGE and visualized by coomassie brilliant blue staining. The T-cell lines used for extract preparation are indicated on the top of the gels. Uninfected T-cell lines are labeled in blue, while HTLV-1 infected T-cell lines are labeled in red. The sizes of the molecular weight markers (MW) are indicated in kilodaltons on the left of the gels (**A & B**). The black triangles on the top correspond to different amounts of extract loaded, with the thinner portion representing a 1X volume and the thicker portion representing a 2X volume (**A**). The arrows point to the two migratory species of histone H1, with the slower migrating band composed of $H1^S$-2, $H1^S$-3 and $H1^S$-4 and the faster migrating band composed of only $H1^S$-1 (**B**).

3.3b Western Blots Show a Reduction of Core and Linker Histones in HTLV-1 Infected T-Cell Lines

As the acid extraction method discussed in 3.3a lacks an internal control for normalization we decided to perform western blots to determine histone H1 protein levels in HTLV-1 infected and uninfected T-cell lines. Whole cell extracts were prepared from three uninfected T-cell lines (CEM, Jurkat and Molt-4) and four HTLV-1 infected T-cell lines (SLB-1, MT-2, HuT102 and C81). Extracts were prepared from an equal number of starting cells for each T-cell line examined. In addition, we measured the level of a "housekeeping" gene product concurrently, as an internal control.

To improve the accuracy of cell count determination for extract preparation, a Coulter counter was used. As this instrument utilizes the electrical resistance of the plasma membrane to count cells in a single-cell stream passing though a detector, it is more reliable than a hemacytometer in determining cell density. Initially an antibody directed against actin was used for normalization. A membrane probed with an anti-total H1 antibody revealed a reduction in total H1 protein in HTLV-1 infected T-cells lines (**Figure 3.2A**). The same membrane was stripped and re-probed with an anti-total actin antibody. Surprisingly, the levels of total actin were considerably elevated in the HTLV-1 infected T-cell lines (**Figure 3.2B**). Although the Coulter counter should be more accurate than manual counting, we wanted to verify that this was not an artifact of a miscount, and so we prepared another set of extracts using a hemacytometer.

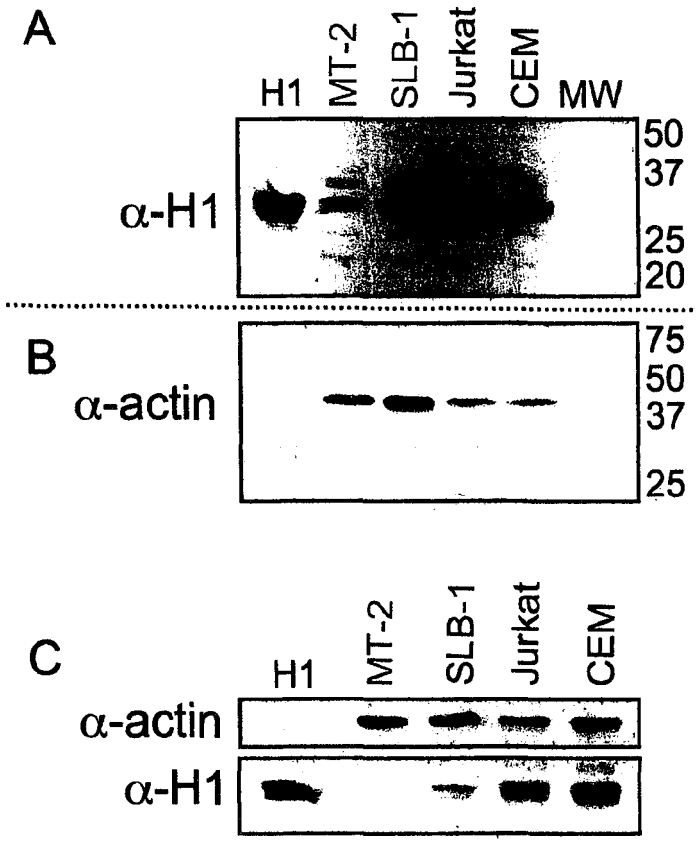

Figure 3.2. Western blots show a reduction of histone H1 protein in HTLV-1 infected T-cell lines. Whole cell extracts were resolved by 15% SDS-PAGE and probed with the antibodies indicated to the left of the membrane scans. The T-cell lines examined are indicated at the top of the membrane scans. HTLV-1 infected T-cell lines are labeled in red, while uninfected T-cell lines are labeled in blue. Acid extracted H1 (200ng) was loaded as a marker (**A, B & C**). The sizes of the molecular weight markers (MW) are indicated in kilodaltons to the right of the upper membrane scan. The extracts were prepared by using an equal number of cells as determined with a Coulter counter (**A & B**). The same membrane probed with α-H1 (**A**) was stripped and re-probed with α-actin (**B**). The extracts were prepared by using an equal number of cells as determined with a hemocytometer (**C**).

The results from a second preparation of extracts were similar, with total H1 being reduced and total actin being elevated in the HTLV-1 infected T-cell lines (**Figure 3.2C**). This finding is rationalized by evidence that HTLV-1 infected cells undergo polarization of the actin cytoskeleton upon cell-to-cell contact in the formation of a virological synapse (30). Additionally, our measurement of an increase in total actin protein levels is substantiated by the finding that at least one actin subunit is up-regulated in fresh ATLL cells and HTLV-1 infected T-cells, as determined by microarray analysis (164, 165). While this was encouraging with respect to our ability to prepare and quantify whole cell extracts, this meant that actin would not be suitable as an internal control.

We decided to employ an antibody for translation elongation factor 1 alpha (EF1α) as a normalization control based on data from the Laybourn lab that suggested EF1α levels were constant between uninfected and HTLV-1 infected T-cell lines. In addition, total protein concentration was determined for each extract, so that total protein resolved by gel electrophoresis would be equal for each sample. As the replication-dependent histones are coordinately regulated, we were interested in analyzing core histone protein levels in our panel of T-cell lines by western blotting. We were surprised to find a reduction of all four core histones in our whole cell extracts, in addition to the previously observed reduction in H1 levels (**Figure 3.3**). Additionally, it appeared as though EF1α levels were similar between infected and uninfected T-cell lines. Many western blots were performed and a reduction of both core and linker histone protein

levels in HTLV-1 infected cells was reproducible. However, several aspects of the western blotting technique made quantification of the actual level of reduction quite difficult. In addition, differences in the amount of DNA in these cell lines could account for changes in histone protein levels, as the amount of histone protein in a cell is proportional to DNA content. Thus, we became interested in employing a technique that would enable us to determine histone and DNA content concurrently.

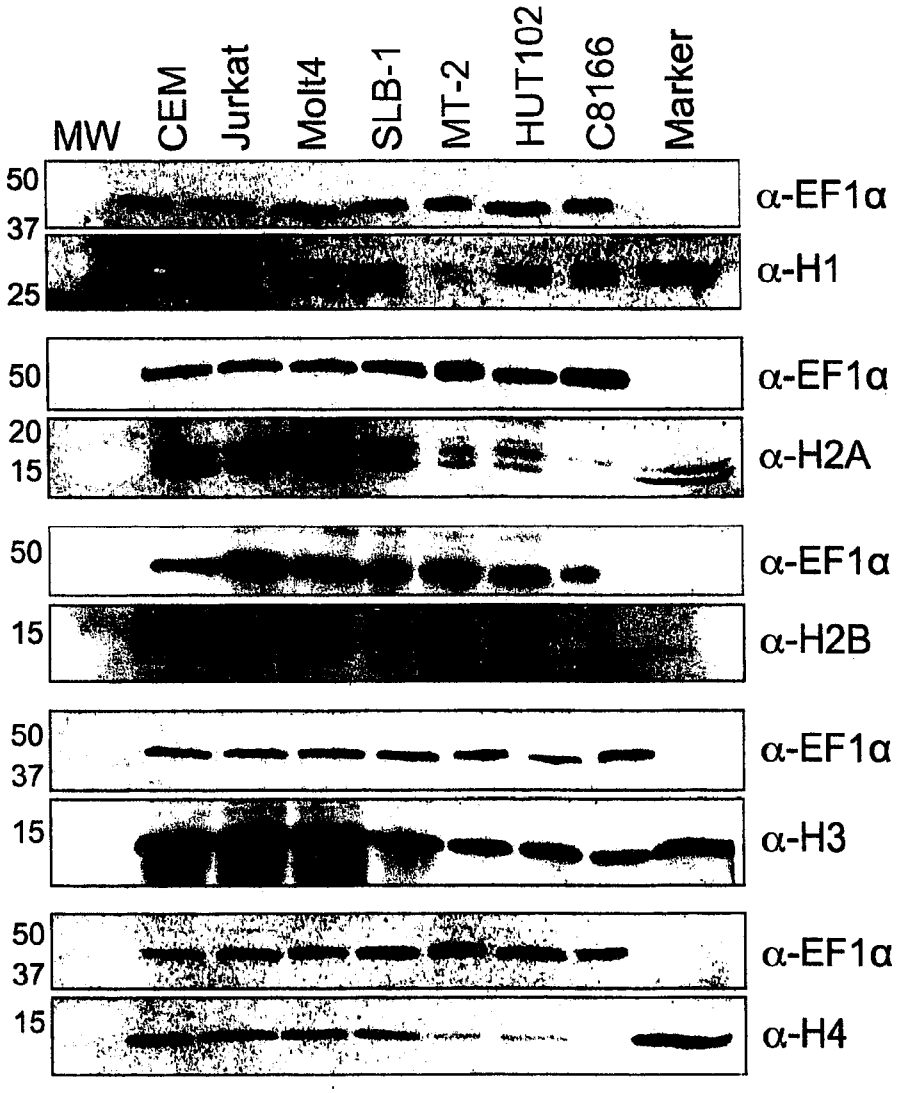

Figure 3.3. Western blots demonstrate a reduction of both core and linker histone protein levels in HTLV-1 infected T-cell lines. Whole cell extracts were quantified by A_{280} so that 60 μg of total protein could be resolved by 15% SDS-PAGE. All gels were loaded identically with the positions of each extract (T-cell line) indicated at the top of the first gel. Uninfected T-cell lines are labeled in blue while HTLV-1 infected T-cell lines are labeled in red. The sizes of the molecular weight markers are indicated in kilodaltons to the left of each membrane scan. The antibodies used to probe the membranes are indicated to the right of each membrane scan. Acid extracted histone H1 (200 ng) was loaded as a marker for the H1 western blot, whereas purified recombinant mouse octamer (800 ng) was loaded for the core histone western blots.

3.3c Flow Cytometry Demonstrates Reduced Histone H3:DNA Ratios in HTLV-1 Infected T-Cell Lines

To quantify histone protein levels more accurately, we measured histone protein and DNA content simultaneously using a flow cytometry-based assay. This assay has several advantages over the previously used methods for measuring cellular histone protein levels. In normal cells, histone protein levels are dependent on cellular DNA content. This fact has several important consequences for the measurement of histone protein levels in different cell lines. Differences in the amount of DNA per haploid complement will result in concomitant differences in histone protein levels during interphase. Additionally, as cells replicate genomic DNA during S-phase, histone protein levels will increase along with the DNA content. Therefore, differences in cell cycle distributions represent another putative source for observed differences in histone protein levels. The simultaneous quantification of histone protein and DNA content allowed us to normalize histone protein levels to DNA content. The ability to detect the slight increases in both histone protein and DNA content as cells progress through S-phase, attests to the quantitative sensitivity of our assay.

Histone H3 and DNA content were measured simultaneously by flow cytometry. The antibody used is directed against the H3 carboxyl-terminus and recognizes modified forms of H3 and H3 variants. In addition, H3 forms the core heterotetramer of nucleosomes, along with histone H4. It is important to note

that somatic cells, regardless of cell cycle phase, contain no significant histone pools and levels of the four core histones and total linker histone are finely balanced. It has been estimated that even during S phase, the soluble histone pool not associated with DNA represents about 0.1% of total histone in human cells (132, 133). Therefore, the levels of H3 measured using this antibody are indicative of the nucleosomal levels on the chromosomes. During flow cytometry, the level of anti-H3 antibody bound per cell was measured using an Alexa 488-conjugated secondary antibody.

Mean histone H3 signal intensity was traced from G1 through G2/M and plotted against mean genomic DNA content. This was accomplished by setting up a series of windows or data filters. The first window (R1) was created on the side light scatter (SCC) versus forward light scatter (FSC) histogram (**Figure 3.4A**). This histogram is generated from the light characteristics of cells as they pass through the flow cell. This window ensures that the cell population we are observing in subsequent analysis is composed of cells with similar light scattering characteristics. In addition, a clump gate was set during the collection of our data to eliminate cells that may pass through the flow cell attached to another cell from our analysis. A narrow DNA content window (R2) was then defined on each DNA histogram, so that the histone H3 levels for the corresponding cell population defined by the window could be determined at that particular DNA content level. An example of this procedure is shown for the determination of histone H3 content during G1 (**Figure 3.4B & C**).

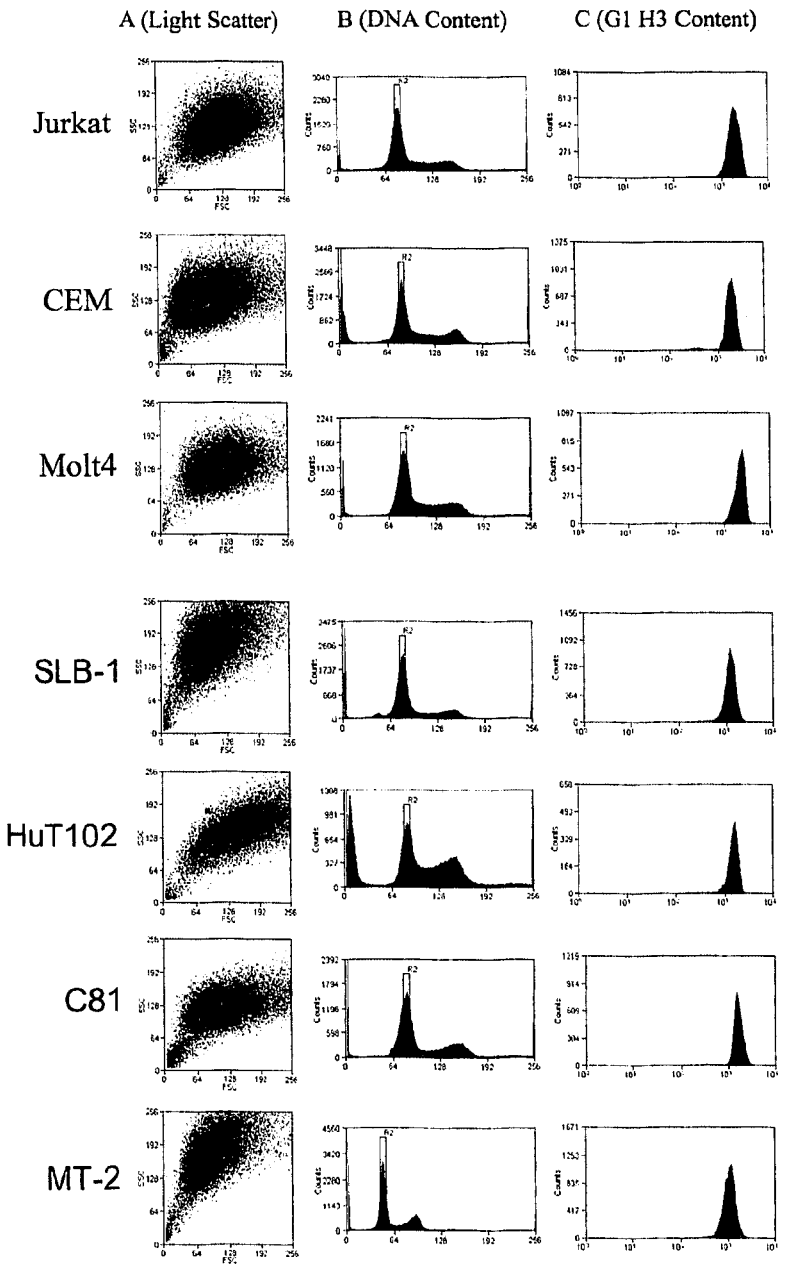

Figure 3.4. Example of the data filtering procedure used in the calculation of G1 histone:DNA ratios. Side scattered light (SSC) is plotted against forward scattered light (FSC). The ellipsoid shape draw on the SSC versus FSC histogram is the first window applied and is labeled R1 (**A**). Cell counts (y-axis) are assigned to channel numbers (x-axis) based on propidium iodide content (DNA content). The bar shaped window (R2) placed over the G1 peak is set to analyze only the cell population within this window (**B**). The corresponding G1 histone H3 content of the population defined by the R2 window is shown (**C**).

The data filtering procedure described in the previous paragraph and shown in figure 3.4 was used to trace histone H3 content from G1 through G2/M. This allowed us to graph histone H3 levels as a function of DNA content levels (**Figure 3.5**). Our results show that upon initiation of DNA replication at the onset of S phase, cells exhibit a near linear increase in both DNA and histone H3 content. As cells approach G2/M histone H3 immunofluoresence was observed to plateau in all T-cell lines examined (both HTLV-1 infected and uninfected), while PI fluorescence (DNA content) continued to increase in a near linear fashion. The plateau in H3 immunofluoresence observed may be explained by a decrease in H3 antibody epitope accessibility during chromosome condensation. Nevertheless, the simultaneous measurement of histone levels and DNA content using flow cytometry is clearly sensitive and quantitative enough to accurately measure the slight increase in both DNA and histone associated with genome replication as cells progress through S phase of the cell cycle. To display the histone H3 levels measured for each of the cell lines examined, the average histone H3:DNA ratios corresponding to G1, Mid-S and G2/M cell populations were calculated for each cell line and expressed relative to Jurkat (**Figure 3.6**).

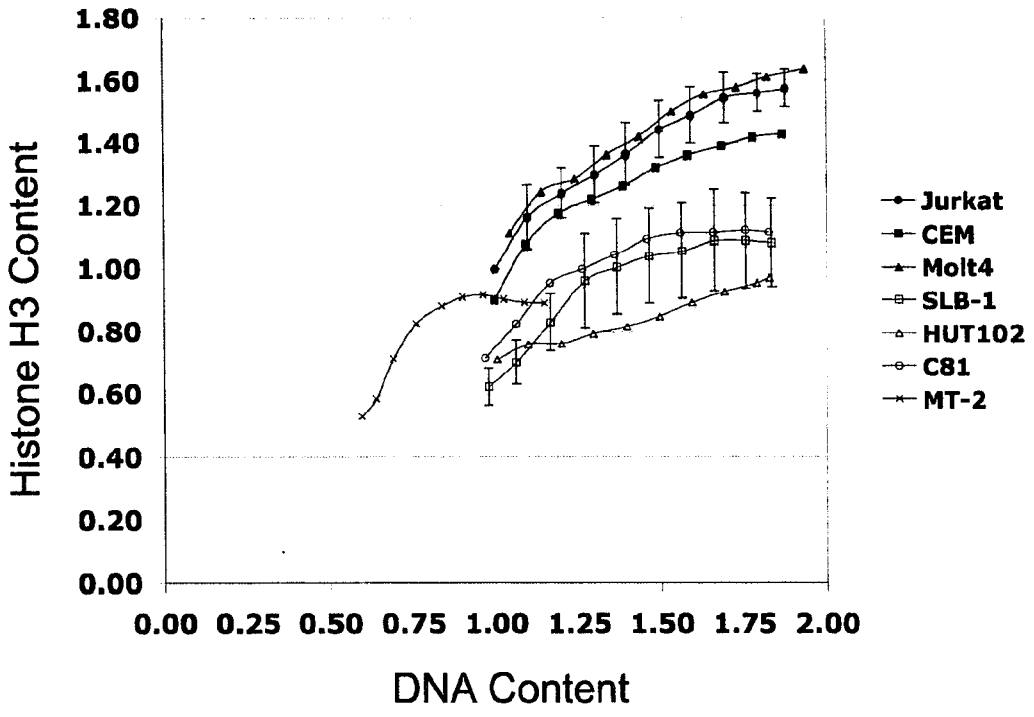

Figure 3.5. A plot of mean histone H3 vs DNA content demonstrates that histone H3 levels are reduced throughout the cell cycle of HTLV-1 infected T-cell lines. Histone H3 and genomic DNA content were measured simultaneously in uninfected T-cell lines (labeled in blue) and HTLV-1 infected T-cells lines (labeled in red) using flow cytometry. H3 levels were measured using a primary antibody against the C-terminal domain and an Alexa-488 conjugated secondary antibody. DNA content was measured using propidium iodide. Mean histone H3 signal intensity was traced from G1 through G2/M by defining a narrow window on the DNA histogram and plotted against the genomic DNA content for the corresponding cell population defined by the window.

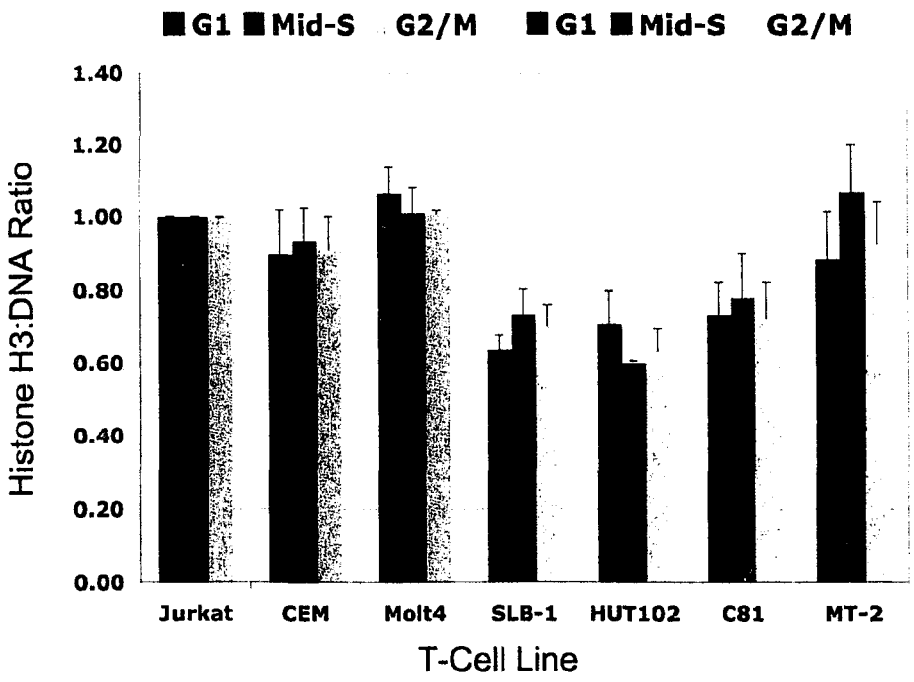

Figure 3.6. Simultaneous measurement of histone H3 and DNA content demonstrates that mean histone H3:DNA ratios are reduced 20-40% in HTLV-1 infected T-cell lines. The average histone H3:DNA ratios during G1, Mid-S and G2/M are shown for uninfected (labeled in shades of blue) and HTLV-1 infected T-cell lines (labeled in shades of red). Ratios were determined as outlined in figure 3.4. P-values associated with these measurements are shown in Table 1.

To summarize our results, mean histone H3:DNA ratios are not significantly different between each of the three uninfected T-cell lines, Jurkat, CEM and Molt4. In clear contrast, mean histone H3:DNA ratios are reduced 20 to 40% in the HTLV-1 infected T-cell lines, SLB-1, HuT102 and C81, relative to Jurkat cells. The reduction of histone H3 observed is consistent throughout the cell cycle. Mean histone H3:DNA ratios were reduced 10% on average in MT-2 cells. While the histone H3 content was much lower in MT-2 cells at all stages of the cell cycle, the DNA content was also much lower. The p-values associated with the measurement of mean histone H3:DNA ratios are shown in **table 1**.

MT-2 cells with an equal DNA content exhibit variation in histone H3 content (**Figure 3.7**). In other words, MT-2 cells in culture are heterogeneous in terms of histone H3 content. Notice that cells with an identical G1 DNA content (x-axis) exhibit histone H3 contents varying 8-fold (spanning the y-axis). Although the mean histone H3:DNA ratio for MT-2 cells was the greatest of all the HTLV-1 infected T-cell lines, a fraction of MT-2 cells exhibited histone H3:DNA ratios much lower than any of the other HTLV-1 infected T-cell lines. This heterogeneity in histone H3 content was not observed with any of the other cell lines examined.

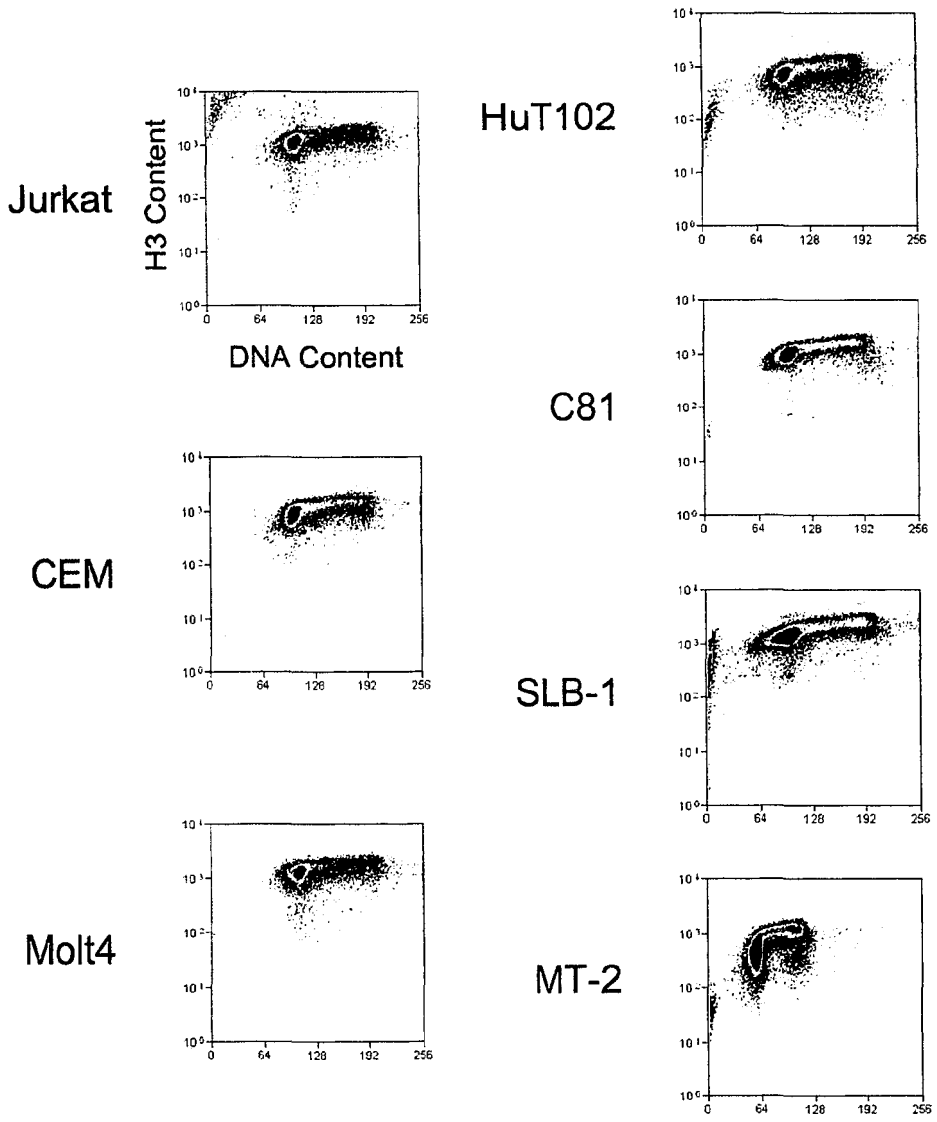

Figure 3.7. Histone H3 vs DNA histograms demonstrate that MT-2 cells are a heterogeneous population with respect to histone H3 content. Histone H3 and DNA content were determined as described in detail in Chapter 2. Histone H3 signal (logarithmic scale) is plotted against DNA content (linear scale). Uninfected T-cell lines are in the left column (labeled in blue) while HTLV-1 infected T-cell lines are in the right column (labeled in red). Notice that MT-2 cells with an identical G1 DNA content (x-axis) exhibit histone H3 contents varying 8-fold (spanning the y-axis).

Table 1

H3:DNA	G1	Mid-S	G2/M
CEM	1.7×10^{-1}	2.2×10^{-1}	1.5×10^{-1}
Molt4	1.6×10^{-1}	4.2×10^{-1}	2.6×10^{-1}
MT-2	1.7×10^{-1}	2.6×10^{-1}	2.2×10^{-1}
SLB-1	3.0×10^{-3}	1.5×10^{-2}	1.1×10^{-2}
HuT102	2.2×10^{-2}	9.4×10^{-5}	6.4×10^{-3}
C81	2.6×10^{-2}	6.0×10^{-2}	3.3×10^{-2}

Table 1. P-values associated with the measurement of histone H3:DNA ratios by flow cytometry. T-tests were performed by Microsoft Excel using the paired two sample for means function. The p-values in this table are comparing the histone H3:DNA ratios of Jurkat (set equal to 1) with the relative histone H3:DNA ratios of the listed T-cell lines. Histone H3:DNA ratios were set equal to 1 and ratios of the other T-cell lines expressed relative to Jurkat, so that ratios between individual experiments could be compared.

3.3d Flow Cytometry Demonstrates Reduced Histone H1:DNA Ratios in HTLV-1 Infected T-Cell Lines

Histone H1 protein levels were determined using the same flow cytometry-based assay as for determining histone H3:DNA ratios. These experiments were performed in order to measure protein levels for a different histone, using a different primary antibody. Mean histone H1 levels are plotted against genomic DNA content (**Figure 3.8**) and mean histone H1:DNA ratios were determined (**Figure 3.9**). Mean histone H1:DNA ratios are not significantly different in the three uninfected T-cell lines examined, Jurkat, CEM and Molt4. Mean histone H1:DNA ratios are reduced by 40% on average in two of the HTLV-1 infected T-cell lines examined, C81 and HuT102 as compared to Jurkat cells. The p-values associated with the measurement of H1:DNA ratios are shown in **table 2**. The reduction of H1 observed in C81 and HuT102 cells is also consistent throughout the cell cycle.

One of the HTLV-1 infected T-cell lines that exhibited a reduction in mean histone H3:DNA ratio by flow cytometry measurements (SLB-1), appeared to have a normal mean histone H1:DNA ratio on average (**Figure 3.8 & 3.9**). However, histograms plotting histone H1 against DNA content show that SLB-1 cell populations do in fact contain cells with reduced histone H1 levels. Furthermore, SLB-1 cells that were observed to have a DNA content equal to that of the uninfected T-cell lines during H3 flow cytometry analysis, now exhibited a lower DNA content, equal to that of MT-2 cells. On average, MT-2

cells also appeared to have a mean histone H1:DNA closer to the uninfected T-cell lines, as observed for that of the H3:DNA ratios determined for this T-cell line. However, histograms plotting histone H1 against DNA content reveal that both SLB-1 and MT-2 are heterogeneous populations with respect to histone H1 content for a specific DNA content (**Figure 3.10**). The mean histone H1:DNA ratios in MT-2 and SLB-1 cells are presented here for consistency. However, the histone H1 levels in MT-2 and SLB-1 cells as compared to uninfected T-cell lines, are not accurately reflected by mean histone H1:DNA ratios, due to the heterogeneity in histone H1 content in these HTLV-1 infected T-cell lines.

When histone H1 content is plotted against DNA content, on a per cell basis rather than a population mean, an interesting and consistent difference is observed between uninfected and HTLV-1 infected T-cell lines (**Figure 3.10**). HTLV-1 infected T-cell lines exhibit a variable amount of histone H1 for a specific DNA content. In other words, HTLV-1 infected T-cell lines consist of a heterogeneous population of cells with varying histone H1 contents for a specific DNA content. This can be seen by observing the cells spanning the y-axis (varying histone H1 content) for a single point on the x-axis (a specific DNA content) (**Figure 3.10**). This heterogeneity in terms of histone H1 content is not observed in the uninfected T-cell lines. The percent contribution of these sub-populations with reduced histone levels to the total cell population was substantial. Data windows were used to determine the percent contribution of the sub-populations to the total cell population. The sub-populations under the G1 peaks of MT-2, SLB-1 and HuT102 represented 20% +/- 6%, 4% +/- 1% and

12% +/- 2% of the total cell population, respectively (**Figure 3.10**). In addition, histone H1 levels vary 20 to 30-fold in MT-2 cells with identical G1 DNA content. The reduction of histone H1 in the sub-population of MT-2 cells is greater than that observed for any of the other HTLV-1 infected T-cell lines. Although the mean histone H1:DNA ratios calculated for MT-2 and SLB-1 cells indicate a ratio closer to that of the uninfected T-cell lines, histograms plotting histone H1 against DNA clearly demonstrate that histone H1 levels are reduced in at least a portion of all HTLV-1 infected T-cell lines.

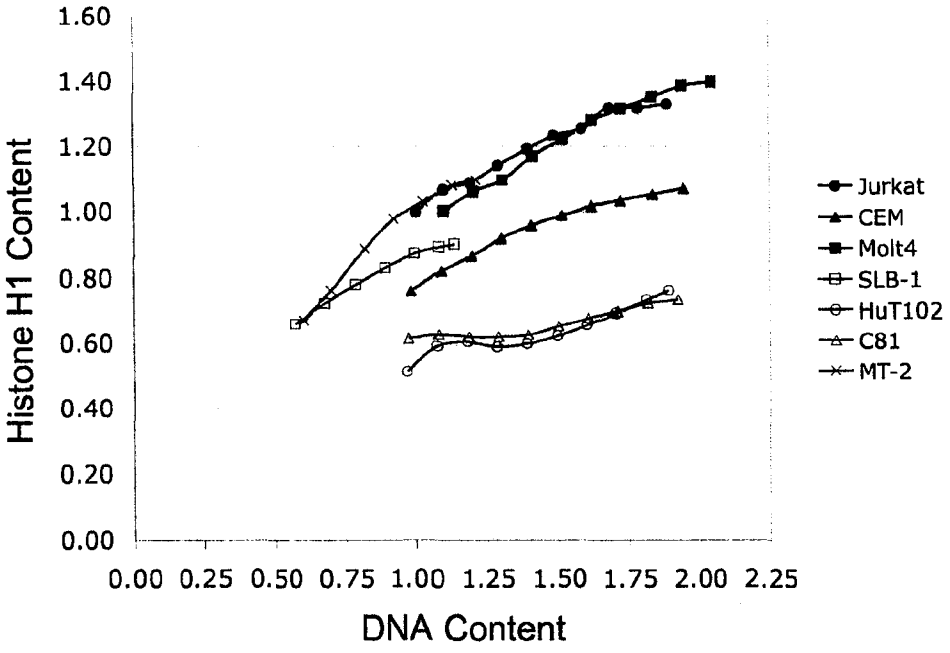

Figure 3.8. A plot of mean histone H1 vs DNA content demonstrates that histone H1 levels are reduced throughout the cell cycle in HTLV-1 infected T-cell lines. Histone H1 and genomic DNA content were measured simultaneously in uninfected (labeled in blue) and HTLV-1 infected T-cell lines (labeled in red) using flow cytometry. H1 levels were measured using a primary antibody directed against the C-terminal domain of histone H1 and an Alexa-488 conjugated secondary antibody. DNA content was measured using propidium iodide. Mean histone H1 signal intensity was traced from G1 through G2/M by defining a narrow window on the DNA histogram and plotted against the genomic DNA content for the corresponding cell population defined by the window.

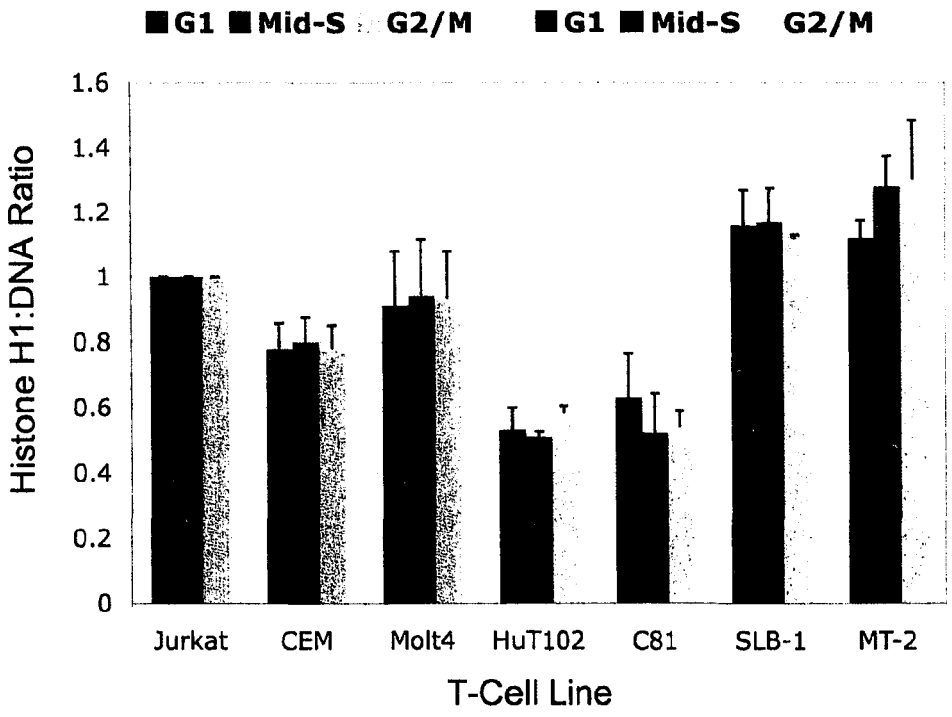

Figure 3.9. Simultaneous determination of histone H1 and DNA content demonstrates that mean histone H1:DNA ratios are reduced in HTLV-1 infected T-cell lines. The average histone H1:DNA ratios during G1, Mid-S and G2/M are shown for uninfected (labeled in shades of blue) and HTLV-1 infected T-cell lines (labeled in shades of red). Ratios were determined by the procedure outlined in figure 3.4. The p-values associated with these measurements are shown in table 2.

Table 2

H1:DNA	G1	Mid-S	G2/M
CEM	1.0×10^{-1}	1.1×10^{-1}	1.0×10^{-1}
Molt4	3.5×10^{-1}	3.9×10^{-1}	2.5×10^{-1}
MT-2	1.4×10^{-1}	1.1×10^{-1}	1.8×10^{-1}
SLB-1	1.9×10^{-1}	1.8×10^{-1}	1.0×10^{-3}
HuT102	5.0×10^{-2}	1.0×10^{-2}	2.0×10^{-2}
C81	1.1×10^{-1}	8.0×10^{-2}	6.0×10^{-2}

Table 2. P-values associated with the measurement of histone H1:DNA ratios by flow cytometry. T-tests were performed by Microsoft Excel using the paired two sample for means function. The p-values in this table are comparing the histone H1:DNA ratios of Jurkat (set equal to 1) with the relative histone H1:DNA ratios of the listed T-cell lines. Histone H1:DNA ratios were set equal to 1 and ratios of the other T-cell lines expressed relative to Jurkat, so that ratios between individual experiments could be compared.

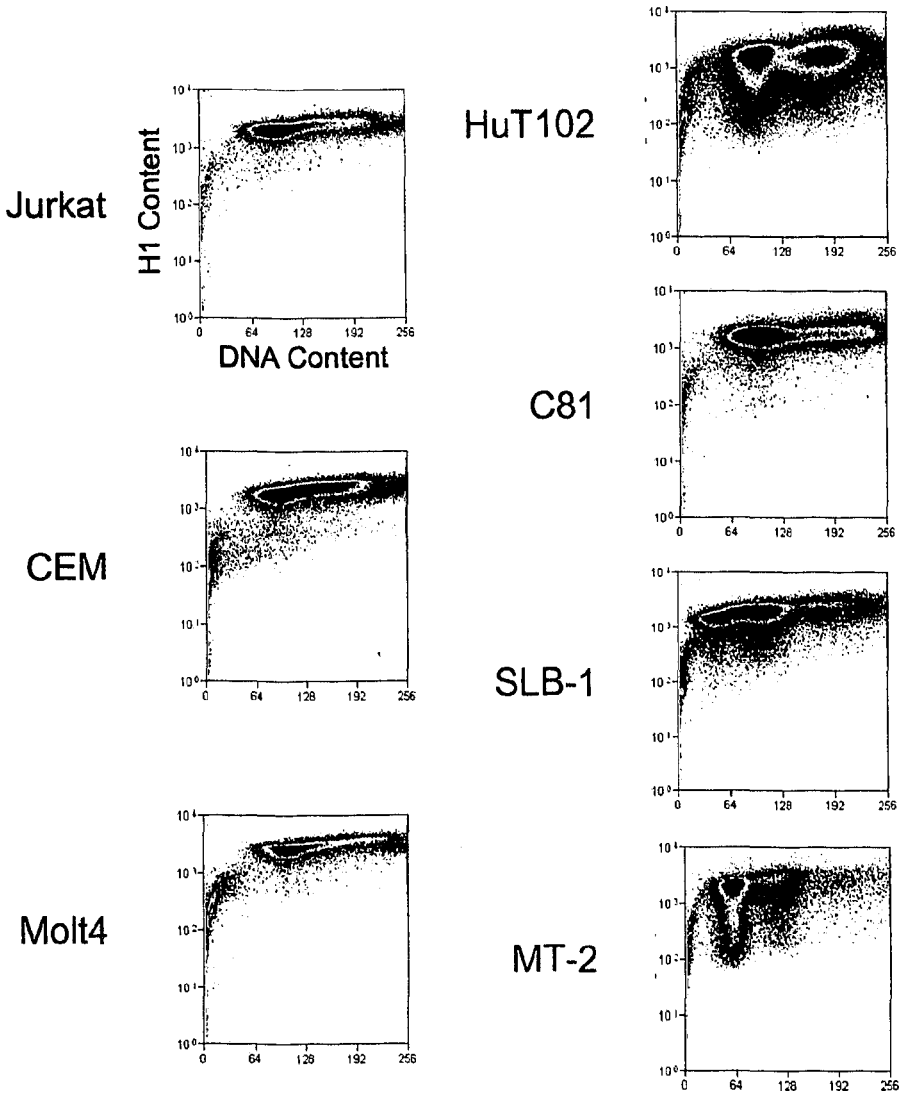

Figure 3.10. Cell populations with identical DNA content but varying histone H1 content are revealed in HTLV-1 infected T-cell lines. Histone H1 and DNA content were determined as described in detail in Chapter 2. Histone H1 signal (logarithmic scale) is plotted against DNA content (linear scale). Uninfected T-cell liness are in the left column (labeled in blue), while HTLV-1 infected T-cell liness are in the right column (labeled in red). Observe the cells spanning the y-axis (varying histone H1 content) for a single point on the x-axis (a specific DNA content).

During the simultaneous measurement of histone H1 and DNA content in SLB-1 cells, a reduction of DNA content was observed as compared to that determined for histone H3:DNA measurements by flow cytometry. Close inspection of the DNA histogram for SLB-1 in **figure 3.4b** reveals the presence of a small sub-G1 DNA content peak. The sub-G1 DNA content peak in the SLB-1 DNA histogram corresponds to the same channel number (DNA content) as the G1 peak of the MT-2 sample in **figure 3.4b**. SLB-1 and MT-2 were observed to have nearly identical G1 DNA contents during H1:DNA measurements. This same phenomenon was observed in DNA content analysis performed with SLB-1 cells prior to the development of our assay for simultaneous measurement of histone and DNA content (**Figure 3.11**). The sub-G1 DNA content peak in the DNA histograms of SLB-1 cells from these previous experiments are more pronounced than that in **figure 3.4b**. This sub-G1 DNA content peak observed represents a cell population with a reduced DNA content. This peak is not from apoptotic cells, as low molecular weight DNA was extracted from fixed cells prior to DNA content analysis (see chapter 2 section 2.8 for details). Analysis of metaphase spreads (discussed in section 3.5b) prepared from both uninfected and HTLV-1 infected T-cell lines indicate that MT-2 cell populations were composed of mostly diploid cells whereas SLB-1 cell populations were composed of both diploid and tetraploid cells (**Figure 3.18**). All of the other T-cell lines for which metaphase spreads were prepared (Jurkat, CEM, Molt4 and C81) were observed to be tetraploid.

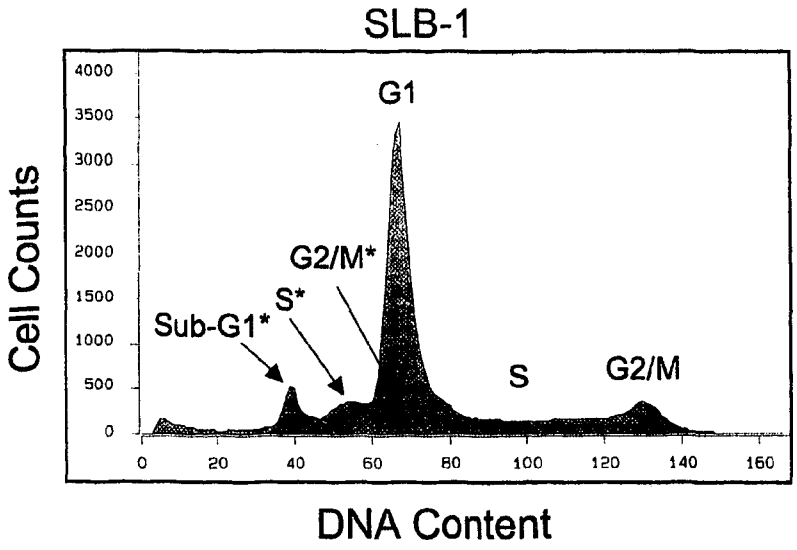

Figure 3.11. A DNA histogram of SLB-1 cells shows two cell populations with distinct DNA contents (ploidy). DNA content was measured as described in detail in section 2.8. Cell cycle phases with asterisks denote the sub-G1 population. These populations are not a result of observing apoptotic cells, as low molecular weight DNA was extracted from these cells prior to DNA content analysis. The abnormal S* peak results from an overlap or stacking of S* cells and cells from the G1 shoulder.

3.3e Replication-Dependent Histone Transcript Levels are Reduced in HTLV-1 Infected T-Cell Lines

After demonstrating a reduction of histone protein levels we wanted to determine if this reduction was occurring through repression of histone gene expression. The replication-dependent histones are expressed from multiple gene copies. While their amino acid sequences are highly conserved, the histones are divergent enough in their DNA sequences as to require a separate primer set for the measurement of transcript from each of the gene copies by real-time PCR. Therefore, northern blot analysis was employed allowing the measurement of total transcript levels for each replication-dependent histone type. Histone transcript levels in each cell line were normalized against EF1α. Northern blot analyses revealed a reduction of histone transcripts from all of the replication-dependent histone genes in HTLV-1 infected T-cell lines (**Figure 3.12A**). Quantification of the Northern blot results revealed a two to five-fold reduction in both core and linker histone transcript levels in HTLV-1 infected T-cell lines (HUT102, SLB-1 and C81) as compared to Jurkat T-cells (**Figure 3.12B**). Total histone transcripts are reduced by 66%, 61% and 50% in SLB-1, HuT102 and C81 cells respectively. Histone transcript levels in the other uninfected T-cell lines examined, Molt4 and CEM, were either not significantly different from or slightly higher than Jurkat. These results demonstrate reduced histone transcript levels in HTLV-1 infected T-cell lines as compared to uninfected T-cell lines.

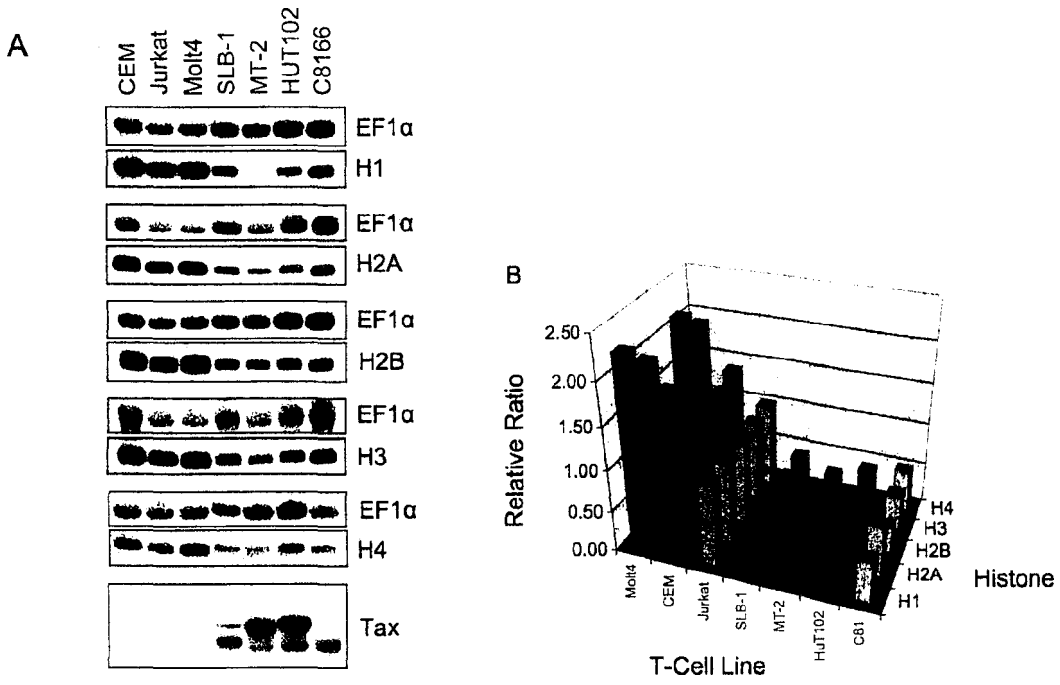

Figure 3.12. Northern blots demonstrate a reduction of replication-dependent core and linker histone transcripts in HTLV-1 infected T-cell lines. Core and linker histones were measured in uninfected T-cell lines labeled in blue (CEM, Jurkat and Molt4), and HTLV-1 infected T-cell lines labeled in red (SLB-1, MT-2, HuT102 and C81) by northern blotting (**A**). Graphical representation of northern blot quantification is shown. Histone transcript signals were normalized to EF1α transcript signals. Values for all T-cell lines are expressed relative to Jurkat. The p-values associated with northern blot measurements of histone transcripts for each cell line were: CEM – 2.3×10^{-3}, Molt4 – 1.1×10^{-4}, SLB-1 – 5.8×10^{-12}, HuT102 – 2.9×10^{-8}, C81 – 2.8×10^{-6} (**B**).

3.3e All Linker Histone Isoform Transcript Levels are Reduced in HTLV-1 Infected T-Cell Lines

As northern blots demonstrated a reduction of histone transcripts, we wanted to verify this result using a complementary approach. We used reverse-transcription and real-time PCR to determine the transcript levels of each of the somatic linker histone isoforms. Real-time PCR quantification of linker histone cDNAs generated from an uninfected T-cell line (Jurkat) and from an HTLV-1 infected T-cell line (SLB-1) reveal a significant reduction of somatic linker histone transcripts in the HTLV-1 infected T-cell line when compared to the uninfected T-cell line. $H1^S$-1, $H1^S$-2, $H1^S$-3, and $H1^S$-4 transcripts are 6, 14, 9 and 4-fold lower in SLB-1 cells, respectively, relative to Jurkat T-cells (**Figure 3.13**).

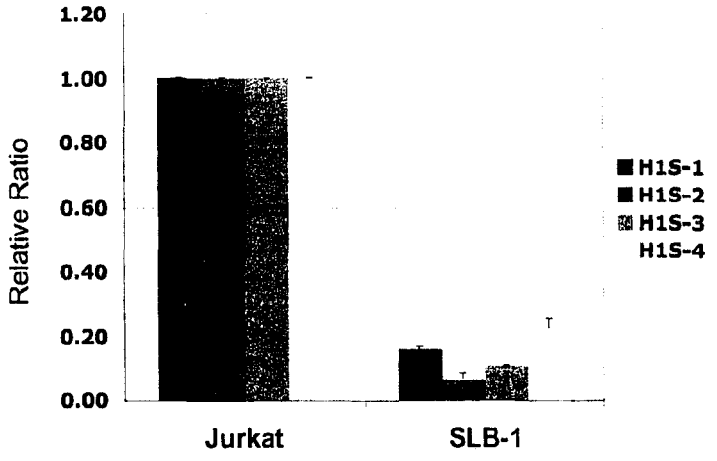

Figure 3.13. Reverse transcription and real-time PCR demonstrate a reduction of all linker histone isoform transcript levels in HTLV-1 infected T-cell lines. Somatic linker histone transcripts were measured in an uninfected T-cell line (Jurkat) and an HTLV-1 infected T-cell (SLB-1), using reverse-transcriptase, real-time PCR. Linker histone transcript levels were normalized to EF1α transcript levels and values were expressed relative to Jurkat.

3.3f Tax Expression Alone Reduces Histone Transcript Levels in an Uninfected T-Cell Line

The HTLV-1 provirus encodes several viral proteins, but only the Tax protein is known to be oncogenic. To determine if Tax alone is sufficient to repress histone gene expression, we transiently transfected an uninfected T-cell line (Jurkat) with a Tax expression vector (pSG-Tax) or empty vector (pUC-19). Both sets of cells were cotransfected with a vector encoding a surface molecule (truncated mouse MHC Class I) to allow selection of transfectants by their retention on magnetic beads conjugated to antibody recognizing this unique surface marker. Reverse-transcription and real-time PCR were used to evaluate all of the somatic linker histone mRNAs and representative family members of the core histone genes in Tax expressing and mock transfected Jurkat cells. Tax expression was verified by both western blot and real-time PCR (See supplementary data, **Figure 3.22** and **Figure 3.23**).

Both core and linker histone mRNAs were reduced in Tax expressing Jurkat cells as compared to pUC-19 transfected Jurkat cells. Core and linker histone mRNA levels are reduced in the range of three- to five-fold, similar to the reduction observed in HTLV-1 infected T-cell lines (**Figure 3.14**).

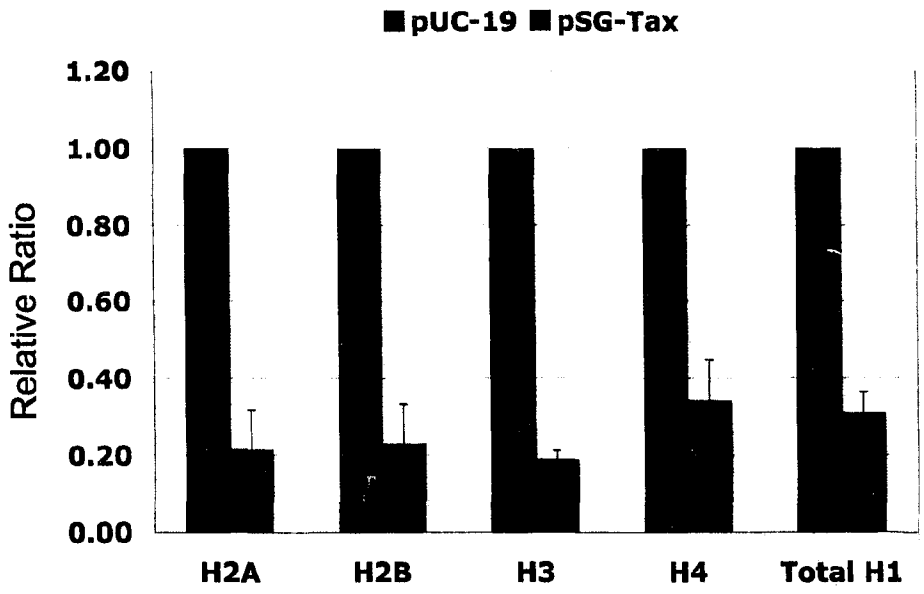

Figure 3.14. Reverse transcription and real-time PCR demonstrate that Tax expression is sufficient for reduction of replication-dependent histone transcript levels. Histone transcript levels were measured in pSG-Tax transfected Jurkat cells and empty vector transfected Jurkat cells using reverse-transcriptase, real-time PCR. P-values associated with the measurement of histone transcripts in pUC-19 versus pSG-Tax transfected Jurkat cells were: H2A – 3.7×10^{-6}, H2B – 3.4×10^{-5}, H3 – 5.6×10^{-3}, H4 - 3.5×10^{-2}, H1 – 1.1×10^{-2}.

3.3g Cell Cycle Analysis of Transfected Cells

Replication-dependent histones are only transcribed in S phase of the cell cycle and histone transcripts are rapidly degraded at the end of S-phase. To eliminate the possibility that Tax expressing cells reduce replication-dependent histone transcript levels by reducing the proportion of cells in S phase, we determined cell cycle distributions of pSG-Tax and pUC-19 transfected Jurkat cells. pSG-Tax and pUC-19 transfected Jurkat cells used for RNA extraction were subjected to cell cycle analysis . The percentage of cells in S phase of Tax expressing Jurkat cells was 31%, while that of pUC-19 transfected Jurkat cells was 36% (**Figure 3.15**). The reduction of histone mRNAs observed in Tax expressing Jurkat cells due to the lower proportion of cells in S phase is no more than 14% (31/36) on average. Therefore, Tax effects on cell cycle distribution do not account for the *remaining* 52 to 76% reduction in histone transcript levels observed in these Tax transfection studies.

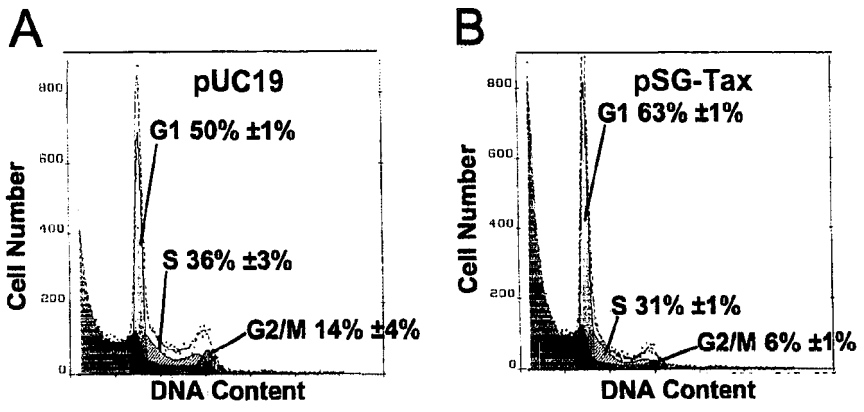

Figure 3.15. DNA content analysis reveals similar cell cycle distributions for pSG-Tax transfected and empty vector transfected Jurkat cells. Cell cycle distributions for empty vector (pUC-19) transfected Jurkat T-cells are shown (A) next to pSG-Tax transfected Jurkat T-cells (B).

3.4 DISCUSSION

3.4a Results

The results in this chapter demonstrate that histone protein levels are reduced 20 to 40% in HTLV-1 infected T-cell lines as compared to uninfected T-cell lines and that this reduction correlates with decreased histone transcript levels. Additionally, we have shown that Tax alone is sufficient to decrease histone transcript levels. Replication-dependent histones are expressed only in S phase, so it was formally possible that the reduction in histone transcript levels observed after Tax expression in an uninfected T-cell line was the result of a significant decrease in the proportion of the cell population in S phase. We have ruled out this possibility by analyzing cell cycle distributions of Tax expressing T-cells as compared to empty vector transfected T-cells. Further, by measuring histone H3 levels and DNA content per cell simultaneously using flow cytometry, we have demonstrated that the reduced histone levels observed in HTLV-1 infected T-cell lines do not occur through a reduction in the amount of genomic DNA in these cells. Rather, our results indicate that Tax directly deregulates histone production and that it occurs, at least in part, through a decrease in histone gene transcripts resulting in reduced histone proteins assembled into nucleosomes on the genomic DNA. Furthermore, our data indicate that HTLV-1 infection can uncouple replication-dependent histone gene expression from DNA synthesis. It is important to point out that we cannot exclude cooperative effects from one or more of the other accessory HTLV-1 proteins in either the reduction

of histone protein levels or the uncoupling of histone expression from DNA replication. However, Tax is sufficient to reduce histone mRNAs.

3.4b Potential Mechanisms of Tax Deregulation of Histone Expression

As the promoters for the replication-dependent histone types have been shown to utilize unique cis-acting elements bound by different sequence-specific trans-acting factors during S-phase induced expression, Tax mediated repression of histone expression is likely to occur through an effect on one or more of the coordinating regulators of histone expression, FLASH, HIRA, NPAT, or SLBP. Alternatively, Tax may reduce histone levels by disrupting the cell cycle signaling regulating histone gene expression. The difference in reduction of histone protein levels (20 to 40%) and histone transcript levels (50 to 80%) suggests some compensation may occur through increased mRNA stability, translation efficiency or protein stability.

3.4c Potential Mechanisms for HTLV-1 Uncoupling of Histone Expression from DNA Synthesis

In properly functioning cells DNA synthesis is inhibited when histones are not immediately deposited at the replication fork. HTLV-1 infected T-cell lines are able to proliferate and synthesis DNA with reduced histone levels. Thus the results from this study suggest that HTLV-1 infection is able to uncouple the

interdependence of histone gene expression and DNA synthesis. There is little known about the mechanism coupling histone synthesis and DNA replication. One candidate for this function is the histone chaperone Asf1 (Asf1a and Asf1b in mammalian cells), which has been shown to regulate histone levels during replicational stress (166). Tax may provide a useful probe to investigate this coupling mechanism, as well as the mechanism of coordinate histone gene regulation in general.

3.4d Effects of Histone Level Reduction

We hypothesize that reduced histone gene expression will have multiple consequences for cellular homeostasis. This hypothesis is based on several observations from several lines of evidence. Chromatin-remodeling, histone replacement, post-translational modifications to the histone tails and DNA methylation are thought to function in the epigenetic control of distinct programs of heritable transcription (121). Aberrations in all of these mechanisms of epigenetic control are known to be associated with neoplastic phenotypes (167-170). We suggest a reduction of histone levels will affect all of the aforementioned epigenetic cancer mechanisms, as these are all nucleosome-based processes. Genomic DNA that has lost histones will necessarily lose the epigenetic information imprinted on the histone tails. We speculate that replacement of replication-dependent histones with histone variants will be hindered with reduced histone levels. Furthermore, reduction of nucleosome assembly has been show to impair double-strand DNA break repair

and directly induce DNA damage (124, 125). We speculate that double-strand DNA breaks occurring in nucleosome-free gaps of the genome will not be repaired as effectively as double-strand DNA breaks occurring in nucleosome-assembled regions of the genome. Defects in double-strand DNA break repair in nucleosome-free gaps may occur through reduced γ-H2A.X signaling and/or defects in nucleosome-based chromatin remodeling activity or recruitment thereof. A partial depletion of histone H4 was achieved experimentally and shown to induce recombination-mediated genetic instability (127). Therefore, we hypothesize that a reduction of histone levels will result in genetic instability contributing to the progression of ATLL. We suggest that genes controlling histone gene expression and genes coupling histone expression to DNA synthesis may be thought of as tumor suppressor genes. We suggest that reduced histone protein levels may be associated with other neoplastic phenotypes.

Many of the effects of Tax are dependent on the continued expression of Tax. While cell proliferation, initiation of pro-survival signals, and deregulation of cell cycle checkpoints could facilitate early steps in transformation; it is likely that genetic lesions accelerate progression of later steps in HTLV-1 T-cell transformation. Epigenetic alterations may also substitute for and/or act in concert with genetic lesions to promote transformation. Epigenteic alterations can result in changes in gene expression of both tumor suppressors and proto-oncogenes. We suggest that reduced histone levels, following transient Tax expression during the cell cycle, provides an unprecedented mechanism by

which the epigenome can be reprogrammed and genetic lesions induced, even after Tax expression is silenced.

3.5 Supplementary Data

3.5a Absolute Real-Time PCR

Data presented in this section provide further evidence of reduced histone transcript levels in HTLV-1 infected T-cell lines. While relative, reverse-transcriptase, real-time PCR (RT^2-PCR) data demonstrating a reduction of linker histone isoform transcripts in HTLV-1 infected T-cell lines has been presented in section 3.3e, the absolute RT^2-PCR data presented here provides additional information and has several advantages. This absolute, RT^2-PCR approach allowed us to determine linker histone isoform composition in uninfected T-cell lines, an HTLV-1 infected T-cell line, and in primary $CD4^+$ lymphocytes. The percent contribution of each isoform towards the total linker histone content cannot be determined with traditional, relative RT^2-PCR. Transcript levels for each isoform are likely to mirror the protein levels for each isoform, given the high conservation of the stem-loop sequence in all the linker histone isoform transcripts.

There are four linker histone isoforms that have been detected in all somatic cells examined to date. These are termed the somatic linker histone isoforms and are known as $H1^S$-1, $H1^S$-2, $H1^S$-3 and $H1^S$-4. Although the functional specialization of the linker histone isoforms remains controversial and

largely uncharacterized, it is hypothesized that specific isoforms are actively depleted from certain regions of chromatin so that distinct properties of isoforms can influence local chromatin structure/function and expression of genes in those regions (171).

The absolute measurement of transcripts with RT^2-PCR yields data that is expressed as molecules (transcripts) per specified quantity of cDNA (molecules/pg cDNA). Data from relative RT^2-PCR can only compare the levels of transcripts that are determined in a single analysis. Absolute RT^2-PCR can be used to compare transcript levels across several individual experiments. Absolute RT^2-PCR represents a powerful method for the standardization of presenting real-time PCR data.

To facilitate the measurement of transcripts with absolute RT^2-PCR, reference plasmids containing histone H1 isoform inserts and cDNA samples were quantified with a double-strand DNA-specific intercalating agent using a spectrofluorometer. Plasmid and cDNA concentrations were determined by extrapolation from a standard curve constructed with lambda phage DNA of known concentration (**Figure 3.16A**). Avogadro's number was used to calculate copy number from the plasmid size and determined concentration. For RT^2-PCR quantification of H1 isoform transcripts in cDNA samples, a five-point standard curve was constructed by serial diluting reference plasmid DNA of known concentration and plotting the cycle threshold (C_T) versus the natural log of the molecule number, for each dilution in a series of 500 to 50 million molecules

(**Figure 3.16B**). This five-point standard curve allowed us to extrapolate absolute values for individual linker histone isoforms in cDNA samples.

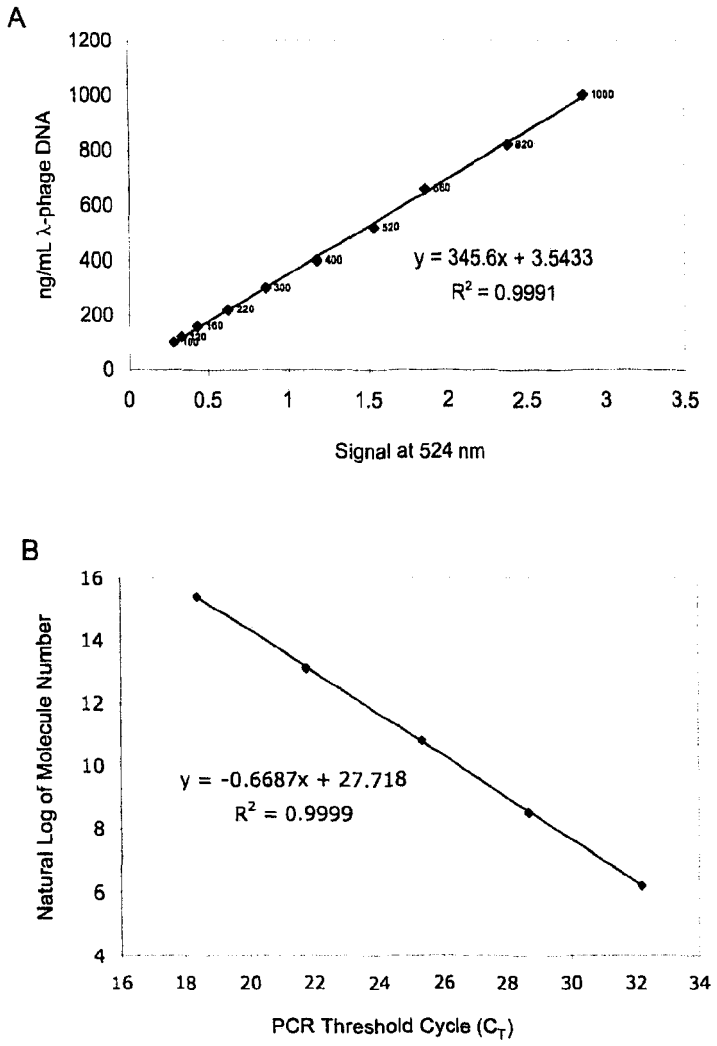

Figure 3.16. Standard curves utilized for the determination of H1 isoform transcript levels by absolute RT^2-PCR. A standard curve was constructed by diluting a known concentration of λ phage DNA and quantifying the dilutions on a spectrofluorometer using a double-strand specific DNA intercalating agent (Picogreen) (**A**). The natural log of the molecule number for each reference plasmid in a serial dilution, ranging from 500 to 50 million copies, was plotted against the threshold cycle (C_T) determined by real-time PCR (**B**).

The uninfected T-cell lines CEM and Jurkat, contained 1770 and 1400 molecules of total linker histone transcripts/pg cDNA, respectively. Total linker histone transcripts in the HTLV-1 infected T-cell line SLB-1, were calculated to be 270 molecules/pg cDNA. This ~five-fold reduction of total linker histone transcripts observed in SLB-1 cells as compared to Jurkat cells (~six-fold as compared to CEM) reinforces data from relative RT^2-PCR. $CD4^+$ lymphocytes isolated from the peripheral blood of two individuals, exhibited 220 and 95 molecules of total linker histone transcripts/pg cDNA. While these levels are much lower than the uninfected T-cell lines examined, the level of total histone H1 transcripts in replicating $CD4^+$ lymphocytes are likely similar to that of uninfected T-cell lines. DNA content analysis was not performed for the $CD4^+$ lymphocytes isolated from these blood samples. Nevertheless, there is ample evidence in the literature suggesting that $CD4^+$ lymphocytes should not be actively dividing. As histone transcripts are only detectable during S phase, reduced histone transcript levels can be reconciled. Furthermore, evidence suggests that quiescent $CD4^+$ lymphocytes are not normally transcribing other mRNAs either. Direct evidence for this is provided by the observed levels of RNA extracted from equivalent numbers of $CD4^+$ T-cells. Total RNA extracted from HTLV-1 infected and uninfected cells is comparable. A typical extraction from a T-cell line yields 12.5 μg total RNA/10^6 cells. For comparison, a typical extraction from $CD4^+$ T-cells yields 0.8 μg total RNA/10^6 cells. The difference in total RNA extracted between T-cell lines and primary $CD4^+$ T-cells is ~16-fold.

Strikingly, absolute RT^2-PCR data indicate a conserved isoform composition amongst all the cells examined (**Figure 3.17**). Interestingly, although the total H1 transcripts were reduced by ~five-fold in SLB-1, the isoform distribution remained very similar. The isoform compositions of the primary $CD4^+$ lymphocytes are nearly identical to that of the transformed T-cell lines with one striking exception. $H1^S$-3 was found to be nearly absent in primary $CD4^+$ lymphocytes. It is hypothesized that local $H1^S$-3 enrichment is associated with actively transcribed regions of chromatin (172, 173). The presence of $H1^S$-3 has been observed to decline during quiescence (174, 175). However, studies in mice suggest that although $H1^S$-3 levels decline in quiescent lymphocytes, $H1^S$-3 levels remain higher than that of other non-dividing cells (176). As $CD4^+$ lymphocyte populations are thought to be circulating in a quiescent state with little cell division or transcription occurring, our observation of $H1^S$-3 levels in primary $CD4^+$ lymphocytes would lend corroborative evidence to the $H1^S$-3 hypothesis mentioned above. It would be interesting to determine if $H1^S$-3 expression levels are increased during T-cell activation. Additionally, it would be interesting to determine if the promoters of genes induced during T-cell activation are locally enriched with the $H1^S$-3 isoform.

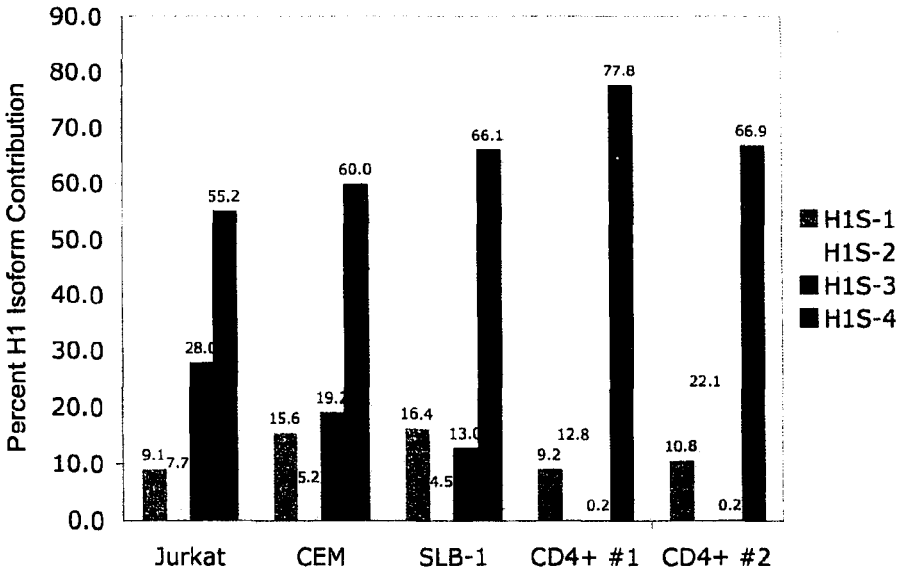

Figure 3.17. Percent H1 isoform content in uninfected T-cell lines, an HTLV-1 infected T-cell line and primary CD4$^+$ lymphocytes isolated from peripheral blood. Jurkat and CEM are uninfected T-cell lines, SLB-1 is an HTLV-1 infected T-cell line and CD4+ #1 and #2 are primary lymphocytes isolated from the peripheral blood of two different individuals. Percent H1 contribution was determined by absolute real-time PCR as described in section 2.3b.

3.5b Metaphase Spreads

Metaphase spreads were prepared from both HTLV-1 infected and uninfected T-cell lines. The metaphase spreads observed indicate that HTLV-1 infected T-cell lines are not defective in forming apparently normal metaphase chromosomes. With the exception of MT-2, all of the uninfected and HTLV-1 infected T-cell line populations examined (Jurkat, CEM, Molt-4, SLB-1 and C81) appeared to be composed of mostly tetraploid cells. While the SLB-1 cells examined appeared to be composed of mostly tetraploid cells, diploid cells were observed. Metaphase spreads are shown for SLB-1 and MT-2 and appear to be diploid (**Figure 3.18**). This procedure was performed as a qualitative check for the formation of metaphase chromosomes, and no quantitative or statistical analysis was performed.

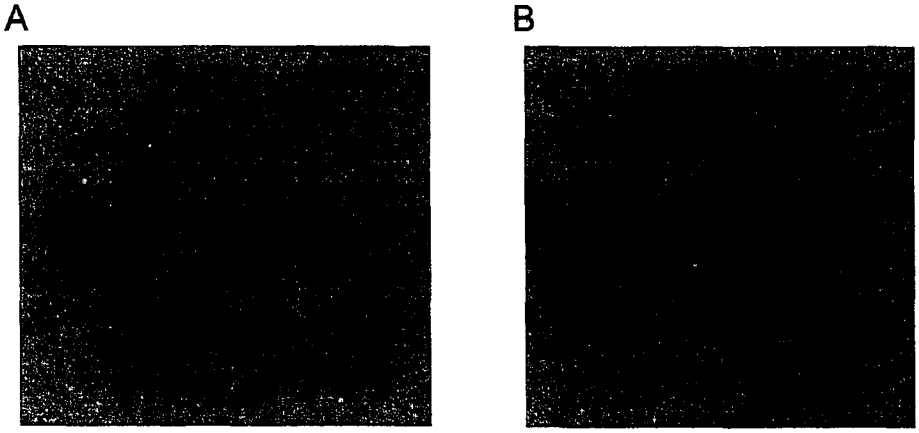

Figure 3.18. Metaphase spreads indicate that HTLV-1 infected T-cell lines are not defective in forming apparently normal metaphase chromosomes. Metaphase spreads were analyzed as described in section 2.13. A metaphase spread for SLB-1 (**A**) and MT-2 (**B**) are shown.

3.5c Micrococcal Nuclease Digestions

To determine the nucleosomal repeat length of genomic DNA that is accessible to micrococcal nuclease digestion, we isolated nuclei from an uninfected and an HTLV-1 infected T-cell line for digestion with this nuclease. Micrococcal nuclease digestions were performed with nuclei prepared from an uninfected (Jurkat) and an HTLV-1 infected T-cell line (HuT102). The digestion indicates that a 20-40% reduction of histone proteins does not result in a noticeable genome-wide increase in nucleosome spacing or nuclease sensitivity (**Figure 3.19**). In support of this data, a study has shown that *Saccharomyces cerevisiae* cells with a 29% reduction of histone H4 do not display a global increase in nucleosomal repeat length nor an increase in micrococcal nuclease sensitivity (127). As there is not a global increase in nucleosome repeat length, this data indicates that there is an increase in the frequency of nucleosome-free regions.

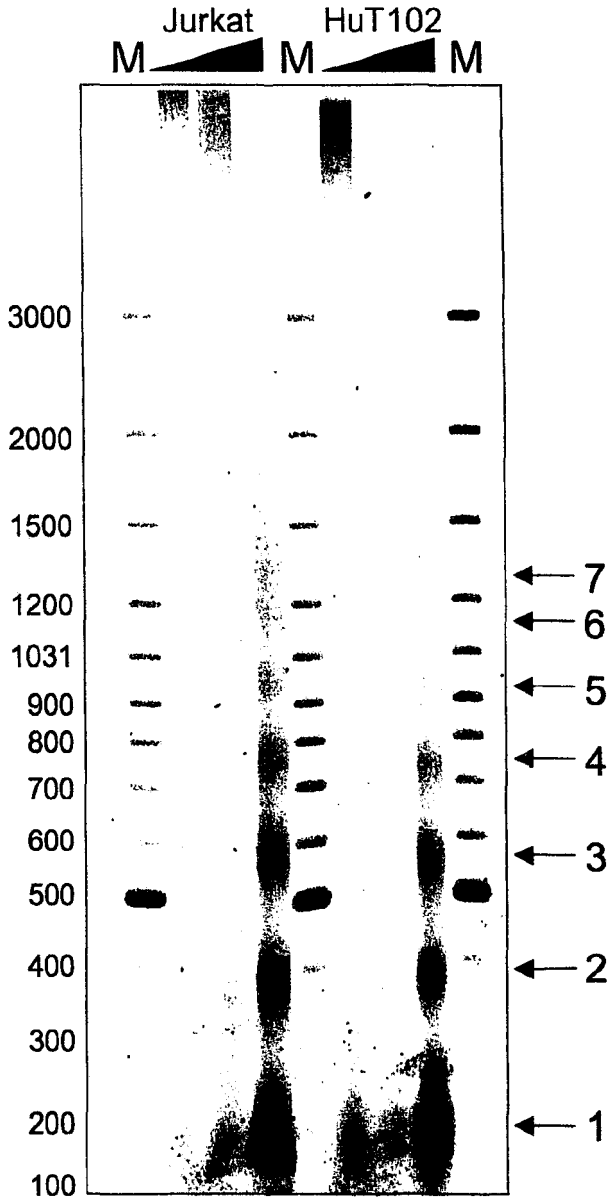

Figure 3.19. Micrococcal nuclease digestions of nuclei from an uninfected and an HTLV-1 infected T-cell line indicate similar nucleosome spacing. Micrococcal nuclease (MNase) digestions were performed as described in section 2.14 and extracted DNA was resolved by 1% agarose gel electrophoresis. The uninfected T-cell line (Jurkat) is on the left while the HTLV-1 infected T-cell line (HuT102) is on the right. The triangles at the top of the gel scan indicate increasing MNase concentrations. The sizes of the marker (M) are indicated to the left of the gel scan in base pairs. The numbers on the right indicate DNA bands corresponding to the number of nucleosomes indicated.

3.5d Western Blots Indicate that Tax Expression May be Sufficient to Reduce Histone Protein Levels

Jurkat cells were cotransfected with pUC-19/pMACS K_k and pSG-Tax/pMACS K_k as described in detail in section 2.10. Transfected cells were plated at a density of 5 x 10^5 cells/mL after magnetic separation of electroporated cells, which was performed 24 hours post-electroporation. Cell densities were monitored periodically and whole cell extracts were prepared once the total cell number of the culture had roughly doubled. A doubling of total cell number, which corresponds roughly to one cell division, occurred 100 hours after electroporation. Cells were harvested at densities of 1.1 x 10^6 and 9.4 x 10^5 cells/mL for pUC-19 and pSG-Tax transfected cells, respectively. Transfected cells were allowed time to double, as a reduction in histone protein levels is only possible as cells are dividing.

Whole cell extracts of pUC-19 and pSG-Tax transfected Jurkat cells were prepared from en equal number of total cells (4.5 x 10^6). Western blots were performed with α-H1, α-H2A and α-actin antibodies. Western blots show a 32% reduction of histone H1 in pSG-Tax transfected Jurkat cells as compared to pUC-19 transfected cells (**Figure 3.20A**), while showing a 34% of histone H2A in pSG-Tax transfected cells as compared to pUC-19 transfected cells (**Figure 3.20B**). Histone H1 and H2A signals were quantified by ImageQuant analysis and normalized to actin signals. While ATLL and HTLV-1 infected T-cells have

been reported to up-regulate β-actin expression (164, 165), a microarray study conducted with a Tax-inducible T-cell line, specifically evaluating cytoskeleton elements, failed to report up-regulated expression of any actin isoform (177). Tax expression was verified in these whole cell extracts, although the level of Tax at 100 hours was lower than that in pSG-Tax transfected cells harvested 48 hours after electroporation. Due to issues with normalization, maintaining Tax expression through cell division and quantitative sensitivity of western blotting, these experiments were not pursued any further and are presented here as preliminary data.

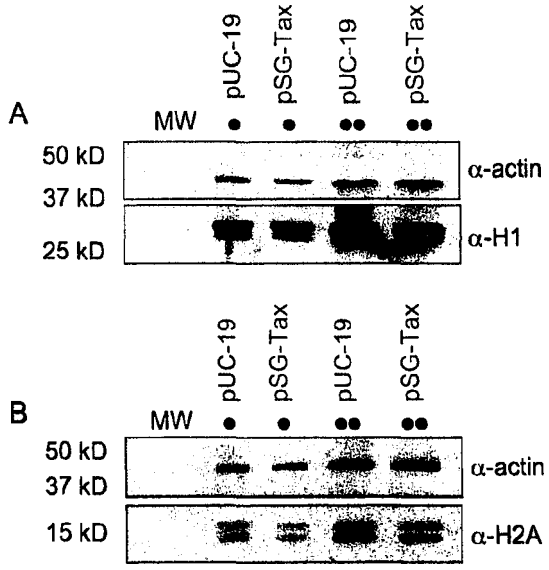

Figure 3.20. Western blots indicate a reduction of histone protein levels in pSG-Tax transfected Jurkat cells after one cell division. Whole cell extracts were resolved by 15% SDS-PAGE and probed with antibodies indicated to the right of the membrane scans. The transfected plasmid is indicated at the top of the membrane scans. The dots correspond to 1X and 2X volumes of whole cell extracts loaded. The sizes of the molecular weight markers (MW) are indicated to the left of the membrane scans. The whole cell extracts were prepared from an equal number of cells, as determined with a hemacytometer (**A & B**)

3.5e Verification of PCR Amplicons

Amplicons from real-time PCR experiments were retrieved from 96-well plates and resolved by gel electrophoresis to ensure these PCR products were primer pair specific (**Figure 3.21**). The expected size of the amplicons in base pairs is as follows: H1a – 158, $H1^0$ – 140, $H1^S$-1 – 105, $H1^S$-2 – 79, $H1^S$-3 – 129, $H1^S$-4 – 105, $H1^S$-4* - 90, H2A – 100, H2B – 174, H3 – 176, H4 -139.

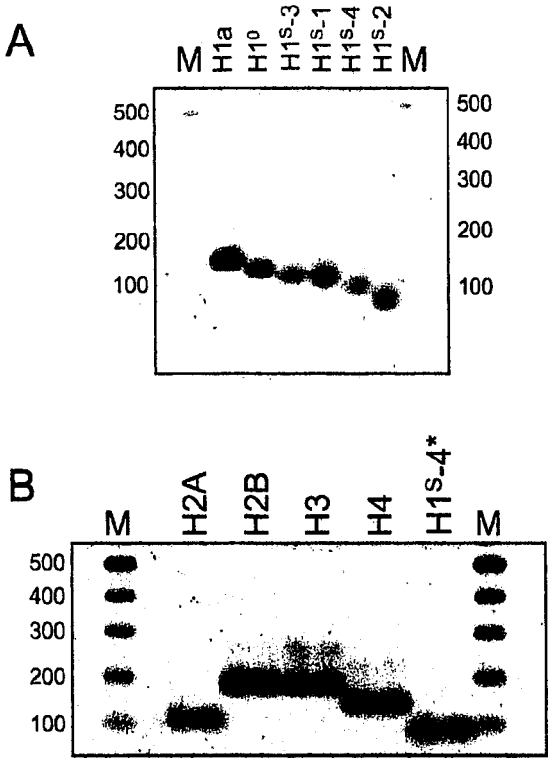

Figure 3.21. Verification of PCR amplicons demonstrates primer pair specific amplification. PCR products were sampled from PCR experiments and resolved by 1.5% agarose gel electrophoresis. Amplicons from primers specific for the H1 isoforms (**A**) and primers for representative family members of the core histones (**B**) are shown. The target genes for the primer pairs used in real-time PCR are shown at the top of the gel scans. The sizes of the marker (M) are indicated in base pairs to the left and right of the gel scan for A and to the left of the gel scan for B.

3.5f Verification of Tax Expression from pSG-Tax Plasmid by Western Blot and RT^2-PCR

Tax expression from the pSG-Tax expression vector used in the transfection experiments described in section 3.3f-g, was verified by both western blotting (**Figure 3.22**) and by reverse transcription and real-time PCR (**Figure 3.23**).

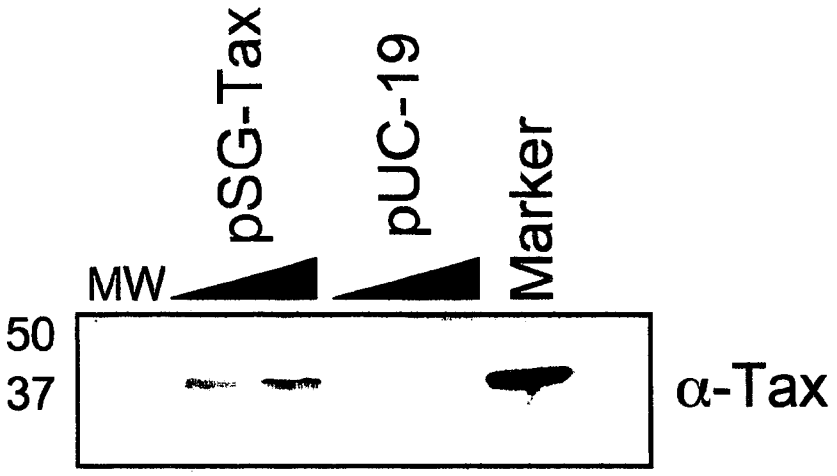

Figure 3.22. Western blots verify Tax protein in pSG-Tax transfected Jurkat cells. The plasmids used for transfection are indicated at the top of the membrane scans. The triangles at the top indicate different amounts of whole cell extracts loaded, with the thinner portion corresponding to a 1X volume and the thicker portion corresponding to a 2X volume. The marker lane was loaded with 300 ng of purified Tax protein. The sizes of the molecular weight markers (MW) are indicated to the left of the membrane scan.

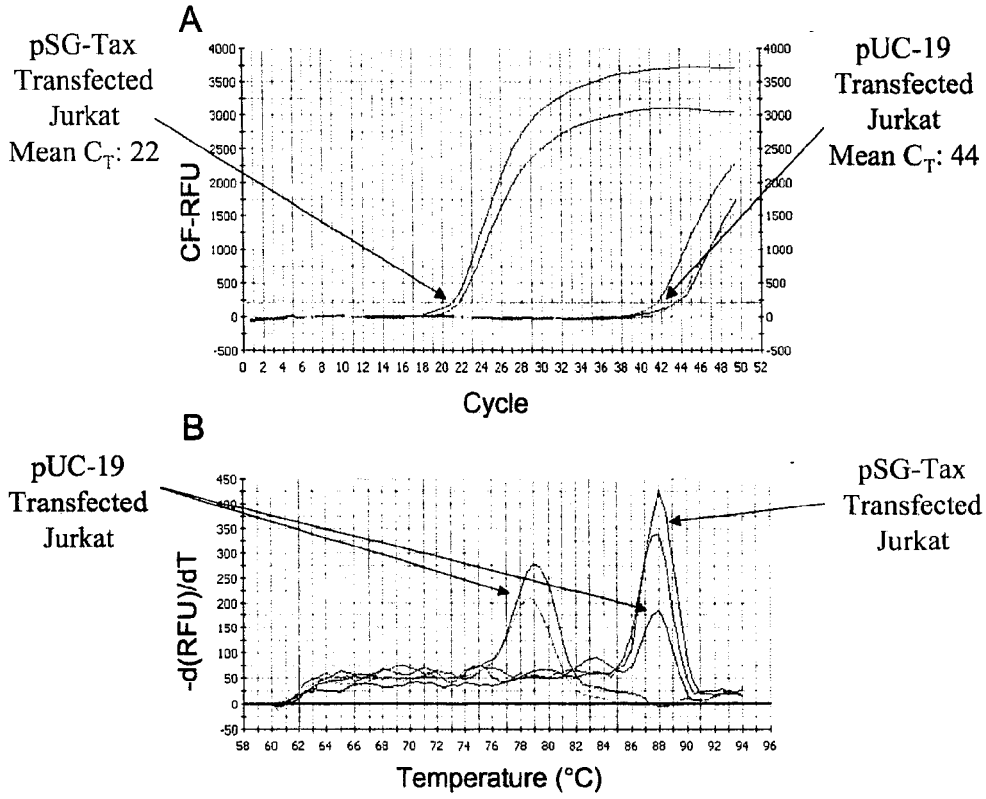

Figure 3.23. Tax transcript levels are detected in pSG-Tax transfected Jurkat cells. A real-time PCR amplification curve using primers specific for Tax transcript is shown for pSG-Tax and pUC-19 transfected Jurkat samples. Curve-fit, relative fluorescent units (CF-RFU) are shown on the y-axis while the threshold cycle (C_T) is shown on the x-axis (**A**). To demonstrate the primer pair specificity of the Tax primers a melt curve is shown. The derivative of the RFU divided by the melting temperature (T_m) is plotted on the y-axis, while T_m is plotted on the x-axis. (**B**) While the amplification curve indicates a product from Tax primers in the pUC-19 transfected Jurkat sample, the melt curve shows that this product is due to non-specific primer dimer amplification.

Chapter 4

Future Directions

4.1 How does HTLV-1 Infection Reduce Histone Levels?

Studies suggest that key regulatory steps in the regulation of histone gene expression are post-transcriptional (153, 154). A reduction in transcription of the histone genes can be compensated for by increased mRNA stability and translation efficiency. Furthermore, the down-regulation of histone gene expression upon completion of the cell cycle or in response to arrest of DNA replication, occurs through decay of histone mRNA (178, 179). There is a considerable body of evidence demonstrating viral protein interaction with host mRNA decay pathways (180). Despite indications that Tax repression of histone gene expression is likely to occur through a post-transcriptional mechanism, it is possible that the observed repression occurs, at least in part, through an effect on transcription. For example, there may be a lower limit for transcription levels at which point, post-transcriptional mechanisms are no longer able to compensate. As transcription of the diverse replication-dependent histone genes are coordinately regulated, Tax may affect the activity of one or more of the regulators responsible for this coordinate expression. This could occur through direct Tax protein interactions with one or more of these regulators, through Tax deregulation of upstream signaling pathways, or through Tax reduction of the expression levels of one or more of these coordinate regulators.

Recently, degradation of histone mRNA transcripts has been found to proceed through the oligouridylation of histone mRNA transcripts. Oligouridylation is a recently discovered mechanism by which a poly-U tail is added to histone mRNA transcripts prior to degradation (181). Tax reduction of histone transcript levels may occur through the induction of transcript degradation. To test this hypothesis, oligouridylated histone transcripts could be quantified in Tax expressing cells using reverse transcription and real-time PCR with an oligo(dA) primer and a histone-specific primer. If Tax induces degradation of histone transcripts, it is likely that an increase in oligouridylated histone transcripts will be observed in Tax expressing cells.

As SLBP regulates the processing, export, stability and translation efficiency of histone transcripts, it represents an attractive target for Tax reduction of histone gene expression. SLBP levels are not regulated transcriptionally during the cell cycle. SLBP stability is regulated through the phosphorylation of threonine 60 and 61. Degradation of SLBP at the end of S phase initiates an abrupt decline in histone mRNAs (178). Therefore, putative Tax deregulation of SLBP function may occur through modification of SLBP phosphorylation state. Phosphorylation-specific SLBP antibodies are currently unavailable. However, mutation of either threonine 60 or 61 to an alanine renders SLBP resist to degradation. Therefore, if Tax reduces histone transcript levels by stimulating SLBP phosphorylation, the ectopic expression of a threonine 60 to alanine mutant would counteract Tax reduction of histone gene expression.

Alternatively, Tax may directly interact with SLBP and interfere with SLBP function in histone mRNA maturation, translation efficiency or stability. Co-immunoprecipitation assays using anti-Tax and anti-SLBP antibodies would indicate whether Tax forms a complex with SLBP or SLBP/histone RNA complexes.

To distinguish between a putative Tax effect on histone transcript maturation versus stability or translation efficiency, an in vitro pre-mRNA processing assay could be used. If Tax interferes with histone mRNA processing, the addition of Tax to an in vitro processing reaction utilizing nuclear extracts, should inhibit the formation of mature histone mRNAs.

Tax may reduce histone transcript levels through an effect on transcription or though a combination of transcriptional and post-transcriptional mechanisms. Tax effects on histone transcription may be facilitated by a decrease in NPAT protein levels. NPAT antibodies are available and protein levels could be determined by western blotting. NPAT protein levels are consistent throughout the cell cycle. NPAT activity is regulated by phosphorylation upon entry into S phase. Phosphorylation of NPAT on tyrosine 1270 and 1350 by cyclin E/Cdk2 regulate NPAT activity and nuclear localization to histone gene loci (141). Phospho-specific antibodies are available and could used in conjunction with flow cytometry, as this would be advantageous for observing phosphorylation levels at specific times during the cell cycle. Flow cytometry measurement of nuclear protein requires a large quantity of antibody that may be difficult to obtain. As an alternative approach, flow cytometry could be used to sort cells based on DNA

content and the sorted populations could be used in the preparation of whole cell extracts for western blotting.

HIRA is the mammalian homolog of the yeast proteins, Hir1p and Hir2p, known to regulate histone gene transcription (182). HIRA is likely to regulate histone transcription in mammals. HIRA is a cell cycle regulator for which protein levels are consistent throughout the cell cycle. Phosphorylation of HIRA on threonine 555 correlates with S phase progression whereas unphosphorylated HIRA induces S phase arrest (140). HIRA protein levels and phosphorylation status could be determined as described for NPAT.

FLASH is another component of the histone gene expression machinery localized to histone gene promoters and represents an additional putative Tax target for reducing histone levels. FLASH-specific antibodies could be used to determine FLASH protein levels in whole cell extracts or in fixed cells using flow cytometry. Additionally, FLASH-specific antibodies could be used to explore the nuclear distribution and thus defects in proper FLASH localization in Tax expressing and HTLV-1 infected cells using fluorescent microscopy.

4.2 What are the Consequences of Reduced Histone Levels?

Several lines of evidence suggest that a reduction of the histone:DNA ratio is likely to promote T-cell transformation. Defects in nucleosome assembly hinder DNA repair and induce double-strand DNA breaks. Thus, we hypothesize

that a reduction of histone proteins will increase the incidence of double-strand DNA breaks, resulting in a mutator phenotype.

Defects in nucleosome assembly during DNA replication may also perturb the passage of epigenetic information from mother to daughter cell. We hypothesize that a reduction of histone protein to levels similar to that observed in HTLV-1 infected T-cell lines will result in the activation and/or repression of cellular proto-oncogenes and tumor suppressors, respectively.

To separate the effects of reduced histone levels from the pleiotropic effects of Tax, an experimental knockdown of histone protein levels can be achieved with SLBP siRNAs. The incidence of double-strand DNA breaks could be measured with a γ-H2A.X-specific antibody using flow cytometry analysis. Additionally, reverse transcription and real-time PCR could be used to measure expression levels of selected cellular transcripts in SLBP knockdowns, although a broader approach such as microarray analysis would be much more suitable. Furthermore, chromatin immunoprecipitation using antibodies against specific modifications to the histone tails could be used in an attempt to correlate epigenetic changes with reductions in expression levels.

Inactivation of viral gene expression through DNA methylation results in retroviral latency, serving as a host cell defense mechanism with implications for retroviral replication cycles. The 5′ LTR of HTLV-1 is hypermethylated in the MT-4 T-cell line and proviral gene expression inactivated. It would be interesting to test if a decreased histone:DNA ratio results in reactivation of proviral gene expression in MT-4 cells.

References

1. Poiesz, B. J., Ruscetti, F. W., Gazdar, A. F., Bunn, P. A., Minna, J. D., and Gallo, R. C. Detection and isolation of type C retrovirus particles from fresh and cultured lymphocytes of a patient with cutaneous T-cell lymphoma. Proc Natl Acad Sci U S A, *77:* 7415-7419, 1980.
2. Grassmann, R., Dengler, C., Muller-Fleckenstein, I., Fleckenstein, B., McGuire, K., Dokhelar, M. C., Sodroski, J. G., and Haseltine, W. A. Transformation to continuous growth of primary human T lymphocytes by human T-cell leukemia virus type I X-region genes transduced by a Herpesvirus saimiri vector. Proc Natl Acad Sci U S A, *86:* 3351-3355, 1989.
3. Hinuma, Y., Nagata, K., Hanaoka, M., Nakai, M., Matsumoto, T., Kinoshita, K. I., Shirakawa, S., and Miyoshi, I. Adult T-cell leukemia: antigen in an ATL cell line and detection of antibodies to the antigen in human sera. Proc Natl Acad Sci U S A, *78:* 6476-6480, 1981.
4. Miyoshi, I., Kubonishi, I., Yoshimoto, S., Akagi, T., Ohtsuki, Y., Shiraishi, Y., Nagata, K., and Hinuma, Y. Type C virus particles in a cord T-cell line derived by co-cultivating normal human cord leukocytes and human leukaemic T cells. Nature, *294:* 770-771, 1981.
5. Uchiyama, T., Yodoi, J., Sagawa, K., Takatsuki, K., and Uchino, H. Adult T-cell leukemia: clinical and hematologic features of 16 cases. Blood, *50:* 481-492, 1977.
6. Yoshida, M., Miyoshi, I., and Hinuma, Y. Isolation and characterization of retrovirus from cell lines of human adult T-cell leukemia and its implication in the disease. Proc Natl Acad Sci U S A, *79:* 2031-2035, 1982.
7. Takatsuki, K. Adult T-cell leukemia. Intern Med, *34:* 947-952, 1995.
8. Silva, M. T., Harab, R. C., Leite, A. C., Schor, D., Araujo, A., and Andrada-Serpa, M. J. Human T lymphotropic virus type 1 (HTLV-1) proviral load in asymptomatic carriers, HTLV-1-associated myelopathy/tropical spastic paraparesis, and other neurological abnormalities associated with HTLV-1 infection. Clin Infect Dis, *44:* 689-692, 2007.
9. Pinheiro, S. R., Martins-Filho, O. A., Ribas, J. G., Catalan-Soares, B. C., Proietti, F. A., Namen-Lopes, S., Brito-Melo, G. E., and Carneiro-Proietti, A. B. Immunologic markers, uveitis, and keratoconjunctivitis sicca associated with human T-cell lymphotropic virus type 1. Am J Ophthalmol, *142:* 811-815, 2006.
10. Osame, M., Nakagawa, M., Umehara, F., Ijichi, S., Moritoyo, T., Higuchi, I., Usuku, K., Arimura, K., and Izumo, S. Recent studies on the epidemiology, clinical features and pathogenic mechanisms of HTLV-I associated myelopathy (HAM/TSP) and other diseases associated to HTLV. J Neurovirol, *3 Suppl 1:* S50-51, 1997.
11. Seiki, M., Hattori, S., Hirayama, Y., and Yoshida, M. Human adult T-cell leukemia virus: complete nucleotide sequence of the provirus genome

integrated in leukemia cell DNA. Proc Natl Acad Sci U S A, *80:* 3618-3622, 1983.

12. Seiki, M., Eddy, R., Shows, T. B., and Yoshida, M. Nonspecific integration of the HTLV provirus genome into adult T-cell leukaemia cells. Nature, *309:* 640-642, 1984.
13. Doi, K., Wu, X., Taniguchi, Y., Yasunaga, J., Satou, Y., Okayama, A., Nosaka, K., and Matsuoka, M. Preferential selection of human T-cell leukemia virus type I provirus integration sites in leukemic versus carrier states. Blood, *106:* 1048-1053, 2005.
14. Wattel, E., Vartanian, J. P., Pannetier, C., and Wain-Hobson, S. Clonal expansion of human T-cell leukemia virus type I-infected cells in asymptomatic and symptomatic carriers without malignancy. J Virol, *69:* 2863-2868, 1995.
15. Yoshida, M., Seiki, M., Yamaguchi, K., and Takatsuki, K. Monoclonal integration of human T-cell leukemia provirus in all primary tumors of adult T-cell leukemia suggests causative role of human T-cell leukemia virus in the disease. Proc Natl Acad Sci U S A, *81:* 2534-2537, 1984.
16. Kiyokawa, T., Seiki, M., Imagawa, K., Shimizu, F., and Yoshida, M. Identification of a protein (p40x) encoded by a unique sequence pX of human T-cell leukemia virus type I. Gann, *75:* 747-751, 1984.
17. Hidaka, M., Inoue, J., Yoshida, M., and Seiki, M. Post-transcriptional regulator (rex) of HTLV-1 initiates expression of viral structural proteins but suppresses expression of regulatory proteins. Embo J, *7:* 519-523, 1988.
18. Hiraragi, H., Kim, S. J., Phipps, A. J., Silic-Benussi, M., Ciminale, V., Ratner, L., Green, P. L., and Lairmore, M. D. Human T-lymphotropic virus type 1 mitochondrion-localizing protein p13(II) is required for viral infectivity in vivo. J Virol, *80:* 3469-3476, 2006.
19. Kiyokawa, T., Seiki, M., Iwashita, S., Imagawa, K., Shimizu, F., and Yoshida, M. p27x-III and p21x-III, proteins encoded by the pX sequence of human T-cell leukemia virus type I. Proc Natl Acad Sci U S A, *82:* 8359-8363, 1985.
20. Seiki, M., Hikikoshi, A., Taniguchi, T., and Yoshida, M. Expression of the pX gene of HTLV-I: general splicing mechanism in the HTLV family. Science, *228:* 1532-1534, 1985.
21. Seiki, M., Inoue, J., Hidaka, M., and Yoshida, M. Two cis-acting elements responsible for posttranscriptional trans-regulation of gene expression of human T-cell leukemia virus type I. Proc Natl Acad Sci U S A, *85:* 7124-7128, 1988.
22. Seiki, M., Inoue, J., Takeda, T., Hikikoshi, A., Sato, M., and Yoshida, M. The p40x of human T-cell leukemia virus type I is a trans-acting activator of viral gene transcription. Jpn J Cancer Res, *76:* 1127-1131, 1985.
23. Grassmann, R., Berchtold, S., Radant, I., Alt, M., Fleckenstein, B., Sodroski, J. G., Haseltine, W. A., and Ramstedt, U. Role of human T-cell

leukemia virus type 1 X region proteins in immortalization of primary human lymphocytes in culture. J Virol, *66:* 4570-4575, 1992.

24. Grossman, W. J., Kimata, J. T., Wong, F. H., Zutter, M., Ley, T. J., and Ratner, L. Development of leukemia in mice transgenic for the tax gene of human T-cell leukemia virus type I. Proc Natl Acad Sci U S A, *92:* 1057-1061, 1995.
25. Pozzatti, R., Vogel, J., and Jay, G. The human T-lymphotropic virus type I tax gene can cooperate with the ras oncogene to induce neoplastic transformation of cells. Mol Cell Biol, *10:* 413-417, 1990.
26. Smith, M. R. and Greene, W. C. Type I human T cell leukemia virus tax protein transforms rat fibroblasts through the cyclic adenosine monophosphate response element binding protein/activating transcription factor pathway. J Clin Invest, *88:* 1038-1042, 1991.
27. Tanaka, A., Takahashi, C., Yamaoka, S., Nosaka, T., Maki, M., and Hatanaka, M. Oncogenic transformation by the tax gene of human T-cell leukemia virus type I in vitro. Proc Natl Acad Sci U S A, *87:* 1071-1075, 1990.
28. Derse, D., Hill, S. A., Lloyd, P. A., Chung, H., and Morse, B. A. Examining human T-lymphotropic virus type 1 infection and replication by cell-free infection with recombinant virus vectors. J Virol, *75:* 8461-8468, 2001.
29. Fan, N., Gavalchin, J., Paul, B., Wells, K. H., Lane, M. J., and Poiesz, B. J. Infection of peripheral blood mononuclear cells and cell lines by cell-free human T-cell lymphoma/leukemia virus type I. J Clin Microbiol, *30:* 905-910, 1992.
30. Igakura, T., Stinchcombe, J. C., Goon, P. K., Taylor, G. P., Weber, J. N., Griffiths, G. M., Tanaka, Y., Osame, M., and Bangham, C. R. Spread of HTLV-I between lymphocytes by virus-induced polarization of the cytoskeleton. Science, *299:* 1713-1716, 2003.
31. Richardson, J. H., Hollsberg, P., Windhagen, A., Child, L. A., Hafler, D. A., and Lever, A. M. Variable immortalizing potential and frequent virus latency in blood-derived T-cell clones infected with human T-cell leukemia virus type I. Blood, *89:* 3303-3314, 1997.
32. Yamano, Y., Nagai, M., Brennan, M., Mora, C. A., Soldan, S. S., Tomaru, U., Takenouchi, N., Izumo, S., Osame, M., and Jacobson, S. Correlation of human T-cell lymphotropic virus type 1 (HTLV-1) mRNA with proviral DNA load, virus-specific CD8(+) T cells, and disease severity in HTLV-1-associated myelopathy (HAM/TSP). Blood, *99:* 88-94, 2002.
33. Okochi, K. and Sato, H. Transmission of ATLV (HTLV-I) through blood transfusion. Princess Takamatsu Symp, *15:* 129-135, 1984.
34. Taylor, G. P., Goon, P., Furukawa, Y., Green, H., Barfield, A., Mosley, A., Nose, H., Babiker, A., Rudge, P., Usuku, K., Osame, M., Bangham, C. R., and Weber, J. N. Zidovudine plus lamivudine in Human T-Lymphotropic Virus type-I-associated myelopathy: a randomised trial. Retrovirology, *3:* 63, 2006.

35. Van Dooren, S., Pybus, O. G., Salemi, M., Liu, H. F., Goubau, P., Remondegui, C., Talarmin, A., Gotuzzo, E., Alcantara, L. C., Galvao-Castro, B., and Vandamme, A. M. The low evolutionary rate of human T-cell lymphotropic virus type-1 confirmed by analysis of vertical transmission chains. Mol Biol Evol, *21:* 603-611, 2004.
36. Lemoine, F. J. and Marriott, S. J. Accelerated G(1) phase progression induced by the human T cell leukemia virus type I (HTLV-I) Tax oncoprotein. J Biol Chem, *276:* 31851-31857, 2001.
37. Arisawa, K., Soda, M., Endo, S., Kurokawa, K., Katamine, S., Shimokawa, I., Koba, T., Takahashi, T., Saito, H., Doi, H., and Shirahama, S. Evaluation of adult T-cell leukemia/lymphoma incidence and its impact on non-Hodgkin lymphoma incidence in southwestern Japan. Int J Cancer, *85:* 319-324, 2000.
38. Tsukasaki, K., Koeffler, P., and Tomonaga, M. Human T-lymphotropic virus type 1 infection. Baillieres Best Pract Res Clin Haematol, *13:* 231-243, 2000.
39. Duensing, S. and Munger, K. Mechanisms of genomic instability in human cancer: insights from studies with human papillomavirus oncoproteins. Int J Cancer, *109:* 157-162, 2004.
40. Furukawa, Y., Kubota, R., Tara, M., Izumo, S., and Osame, M. Existence of escape mutant in HTLV-I tax during the development of adult T-cell leukemia. Blood, *97:* 987-993, 2001.
41. Takeda, S., Maeda, M., Morikawa, S., Taniguchi, Y., Yasunaga, J., Nosaka, K., Tanaka, Y., and Matsuoka, M. Genetic and epigenetic inactivation of tax gene in adult T-cell leukemia cells. Int J Cancer, *109:* 559-567, 2004.
42. Lengauer, C., Kinzler, K. W., and Vogelstein, B. Genetic instabilities in human cancers. Nature, *396:* 643-649, 1998.
43. Jacobson, S. Immunopathogenesis of human T cell lymphotropic virus type I-associated neurologic disease. J Infect Dis, *186 Suppl 2:* S187-192, 2002.
44. Asquith, B., Mosley, A. J., Heaps, A., Tanaka, Y., Taylor, G. P., McLean, A. R., and Bangham, C. R. Quantification of the virus-host interaction in human T lymphotropic virus I infection. Retrovirology, *2:* 75, 2005.
45. Kannagi, M., Sugamura, K., Sato, H., Okochi, K., Uchino, H., and Hinuma, Y. Establishment of human cytotoxic T cell lines specific for human adult T cell leukemia virus-bearing cells. J Immunol, *130:* 2942-2946, 1983.
46. Parker, C. E., Daenke, S., Nightingale, S., and Bangham, C. R. Activated, HTLV-1-specific cytotoxic T-lymphocytes are found in healthy seropositives as well as in patients with tropical spastic paraparesis. Virology, *188:* 628-636, 1992.
47. Goon, P. K., Biancardi, A., Fast, N., Igakura, T., Hanon, E., Mosley, A. J., Asquith, B., Gould, K. G., Marshall, S., Taylor, G. P., and Bangham, C. R. Human T cell lymphotropic virus (HTLV) type-1-specific CD8+ T cells:

frequency and immunodominance hierarchy. J Infect Dis, *189:* 2294-2298, 2004.

48. Jacobson, S., Shida, H., McFarlin, D. E., Fauci, A. S., and Koenig, S. Circulating CD8+ cytotoxic T lymphocytes specific for HTLV-I pX in patients with HTLV-I associated neurological disease. Nature, *348:* 245-248, 1990.
49. Kubota, R., Hanada, K., Furukawa, Y., Arimura, K., Osame, M., Gojobori, T., and Izumo, S. Genetic stability of human T lymphotropic virus type I despite antiviral pressures by CTLs. J Immunol, *178:* 5966-5972, 2007.
50. Cavrois, M., Leclercq, I., Gout, O., Gessain, A., Wain-Hobson, S., and Wattel, E. Persistent oligoclonal expansion of human T-cell leukemia virus type 1-infected circulating cells in patients with Tropical spastic paraparesis/HTLV-1 associated myelopathy. Oncogene, *17:* 77-82, 1998.
51. Etoh, K., Yamaguchi, K., Tokudome, S., Watanabe, T., Okayama, A., Stuver, S., Mueller, N., Takatsuki, K., and Matsuoka, M. Rapid quantification of HTLV-I provirus load: detection of monoclonal proliferation of HTLV-I-infected cells among blood donors. Int J Cancer, *81:* 859-864, 1999.
52. Nagai, M., Usuku, K., Matsumoto, W., Kodama, D., Takenouchi, N., Moritoyo, T., Hashiguchi, S., Ichinose, M., Bangham, C. R., Izumo, S., and Osame, M. Analysis of HTLV-I proviral load in 202 HAM/TSP patients and 243 asymptomatic HTLV-I carriers: high proviral load strongly predisposes to HAM/TSP. J Neurovirol, *4:* 586-593, 1998.
53. Asquith, B., Mosley, A. J., Barfield, A., Marshall, S. E., Heaps, A., Goon, P., Hanon, E., Tanaka, Y., Taylor, G. P., and Bangham, C. R. A functional CD8+ cell assay reveals individual variation in CD8+ cell antiviral efficacy and explains differences in human T-lymphotropic virus type 1 proviral load. J Gen Virol, *86:* 1515-1523, 2005.
54. Fujisawa, J., Seiki, M., Kiyokawa, T., and Yoshida, M. Functional activation of the long terminal repeat of human T-cell leukemia virus type I by a trans-acting factor. Proc Natl Acad Sci U S A, *82:* 2277-2281, 1985.
55. Kimzey, A. L. and Dynan, W. S. Specific regions of contact between human T-cell leukemia virus type I Tax protein and DNA identified by photocross-linking. J Biol Chem, *273:* 13768-13775, 1998.
56. Lenzmeier, B. A., Baird, E. E., Dervan, P. B., and Nyborg, J. K. The tax protein-DNA interaction is essential for HTLV-I transactivation in vitro. J Mol Biol, *291:* 731-744, 1999.
57. Lenzmeier, B. A., Giebler, H. A., and Nyborg, J. K. Human T-cell leukemia virus type 1 Tax requires direct access to DNA for recruitment of CREB binding protein to the viral promoter. Mol Cell Biol, *18:* 721-731, 1998.
58. Lundblad, J. R., Kwok, R. P., Laurance, M. E., Huang, M. S., Richards, J. P., Brennan, R. G., and Goodman, R. H. The human T-cell leukemia virus-1 transcriptional activator Tax enhances cAMP-responsive element-binding protein (CREB) binding activity through interactions with the DNA minor groove. J Biol Chem, *273:* 19251-19259, 1998.

59. Zhang, X., Odom, D. T., Koo, S. H., Conkright, M. D., Canettieri, G., Best, J., Chen, H., Jenner, R., Herbolsheimer, E., Jacobsen, E., Kadam, S., Ecker, J. R., Emerson, B., Hogenesch, J. B., Unterman, T., Young, R. A., and Montminy, M. Genome-wide analysis of cAMP-response element binding protein occupancy, phosphorylation, and target gene activation in human tissues. Proc Natl Acad Sci U S A, *102:* 4459-4464, 2005.
60. Konesky, K. L., Nyborg, J. K., and Laybourn, P. J. Tax abolishes histone H1 repression of p300 acetyltransferase activity at the human T-cell leukemia virus type 1 promoter. J Virol, *80:* 10542-10553, 2006.
61. Kim, Y. M., Ramirez, J. A., Mick, J. E., Giebler, H. A., Yan, J. P., and Nyborg, J. K. Molecular characterization of the Tax-containing HTLV-1 enhancer complex reveals a prominent role for CREB phosphorylation in Tax transactivation. J Biol Chem, *282:* 18750-18757, 2007.
62. Geiger, T. R., Sharma, N., Kim, Y. M., and Nyborg, J. K. The human T-cell leukemia virus type 1 tax protein confers CBP/p300 recruitment and transcriptional activation properties to phosphorylated CREB. Mol Cell Biol, *28:* 1383-1392, 2008.
63. Santiago, F., Clark, E., Chong, S., Molina, C., Mozafari, F., Mahieux, R., Fujii, M., Azimi, N., and Kashanchi, F. Transcriptional up-regulation of the cyclin D2 gene and acquisition of new cyclin-dependent kinase partners in human T-cell leukemia virus type 1-infected cells. J Virol, *73:* 9917-9927, 1999.
64. Robek, M. D. and Ratner, L. Immortalization of CD4(+) and CD8(+) T lymphocytes by human T-cell leukemia virus type 1 Tax mutants expressed in a functional molecular clone. J Virol, *73:* 4856-4865, 1999.
65. Sherr, C. J. The Pezcoller lecture: cancer cell cycles revisited. Cancer Res, *60:* 3689-3695, 2000.
66. Cross, S. L., Feinberg, M. B., Wolf, J. B., Holbrook, N. J., Wong-Staal, F., and Leonard, W. J. Regulation of the human interleukin-2 receptor alpha chain promoter: activation of a nonfunctional promoter by the transactivator gene of HTLV-I. Cell, *49:* 47-56, 1987.
67. Inoue, J., Seiki, M., Taniguchi, T., Tsuru, S., and Yoshida, M. Induction of interleukin 2 receptor gene expression by p40x encoded by human T-cell leukemia virus type 1. Embo J, *5:* 2883-2888, 1986.
68. Leung, K. and Nabel, G. J. HTLV-1 transactivator induces interleukin-2 receptor expression through an NF-kappa B-like factor. Nature, *333:* 776-778, 1988.
69. Fraedrich, K., Muller, B., and Grassmann, R. The HTLV-1 Tax protein binding domain of cyclin-dependent kinase 4 (CDK4) includes the regulatory PSTAIRE helix. Retrovirology, *2:* 54, 2005.
70. Haller, K., Wu, Y., Derow, E., Schmitt, I., Jeang, K. T., and Grassmann, R. Physical interaction of human T-cell leukemia virus type 1 Tax with cyclin-dependent kinase 4 stimulates the phosphorylation of retinoblastoma protein. Mol Cell Biol, *22:* 3327-3338, 2002.

71. Kehn, K., Fuente Cde, L., Strouss, K., Berro, R., Jiang, H., Brady, J., Mahieux, R., Pumfery, A., Bottazzi, M. E., and Kashanchi, F. The HTLV-I Tax oncoprotein targets the retinoblastoma protein for proteasomal degradation. Oncogene, *24:* 525-540, 2005.
72. Low, K. G., Dorner, L. F., Fernando, D. B., Grossman, J., Jeang, K. T., and Comb, M. J. Human T-cell leukemia virus type 1 Tax releases cell cycle arrest induced by p16INK4a. J Virol, *71:* 1956-1962, 1997.
73. Suzuki, T., Kitao, S., Matsushime, H., and Yoshida, M. HTLV-1 Tax protein interacts with cyclin-dependent kinase inhibitor p16INK4A and counteracts its inhibitory activity towards CDK4. Embo J, *15:* 1607-1614, 1996.
74. Riou, P., Bex, F., and Gazzolo, L. The human T cell leukemia/lymphotropic virus type 1 Tax protein represses MyoD-dependent transcription by inhibiting MyoD-binding to the KIX domain of p300. A potential mechanism for Tax-mediated repression of the transcriptional activity of basic helix-loop-helix factors. J Biol Chem, *275:* 10551-10560, 2000.
75. Suzuki, T., Narita, T., Uchida-Toita, M., and Yoshida, M. Down-regulation of the INK4 family of cyclin-dependent kinase inhibitors by tax protein of HTLV-1 through two distinct mechanisms. Virology, *259:* 384-391, 1999.
76. Jeang, K. T., Widen, S. G., Semmes, O. J. t., and Wilson, S. H. HTLV-I trans-activator protein, tax, is a trans-repressor of the human beta-polymerase gene. Science, *247:* 1082-1084, 1990.
77. Park, H. U., Jeong, J. H., Chung, J. H., and Brady, J. N. Human T-cell leukemia virus type 1 Tax interacts with Chk1 and attenuates DNA-damage induced G2 arrest mediated by Chk1. Oncogene, *23:* 4966-4974, 2004.
78. Ariumi, Y., Kaida, A., Lin, J. Y., Hirota, M., Masui, O., Yamaoka, S., Taya, Y., and Shimotohno, K. HTLV-1 tax oncoprotein represses the p53-mediated trans-activation function through coactivator CBP sequestration. Oncogene, *19:* 1491-1499, 2000.
79. Miyazato, A., Sheleg, S., Iha, H., Li, Y., and Jeang, K. T. Evidence for NF-kappaB- and CBP-independent repression of p53's transcriptional activity by human T-cell leukemia virus type 1 Tax in mouse embryo and primary human fibroblasts. J Virol, *79:* 9346-9350, 2005.
80. Pise-Masison, C. A., Mahieux, R., Jiang, H., Ashcroft, M., Radonovich, M., Duvall, J., Guillerm, C., and Brady, J. N. Inactivation of p53 by human T-cell lymphotropic virus type 1 Tax requires activation of the NF-kappaB pathway and is dependent on p53 phosphorylation. Mol Cell Biol, *20:* 3377-3386, 2000.
81. Tabakin-Fix, Y., Azran, I., Schavinky-Khrapunsky, Y., Levy, O., and Aboud, M. Functional inactivation of p53 by human T-cell leukemia virus type 1 Tax protein: mechanisms and clinical implications. Carcinogenesis, *27:* 673-681, 2006.

82. Jin, D. Y., Spencer, F., and Jeang, K. T. Human T cell leukemia virus type 1 oncoprotein Tax targets the human mitotic checkpoint protein MAD1. Cell, *93:* 81-91, 1998.
83. Peloponese, J. M., Jr. and Jeang, K. T. Role for Akt/protein kinase B and activator protein-1 in cellular proliferation induced by the human T-cell leukemia virus type 1 tax oncoprotein. J Biol Chem, *281:* 8927-8938, 2006.
84. Iha, H., Kibler, K. V., Yedavalli, V. R., Peloponese, J. M., Haller, K., Miyazato, A., Kasai, T., and Jeang, K. T. Segregation of NF-kappaB activation through NEMO/IKKgamma by Tax and TNFalpha: implications for stimulus-specific interruption of oncogenic signaling. Oncogene, *22:* 8912-8923, 2003.
85. Xiao, G., Cvijic, M. E., Fong, A., Harhaj, E. W., Uhlik, M. T., Waterfield, M., and Sun, S. C. Retroviral oncoprotein Tax induces processing of NF-kappaB2/p100 in T cells: evidence for the involvement of IKKalpha. Embo J, *20:* 6805-6815, 2001.
86. Koiwa, T., Hamano-Usami, A., Ishida, T., Okayama, A., Yamaguchi, K., Kamihira, S., and Watanabe, T. 5'-long terminal repeat-selective CpG methylation of latent human T-cell leukemia virus type 1 provirus in vitro and in vivo. J Virol, *76:* 9389-9397, 2002.
87. Tamiya, S., Matsuoka, M., Etoh, K., Watanabe, T., Kamihira, S., Yamaguchi, K., and Takatsuki, K. Two types of defective human T-lymphotropic virus type I provirus in adult T-cell leukemia. Blood, *88:* 3065-3073, 1996.
88. Matsuoka, M. and Jeang, K. T. Human T-cell leukaemia virus type 1 (HTLV-1) infectivity and cellular transformation. Nat Rev Cancer, *7:* 270-280, 2007.
89. Nicot, C., Harrod, R. L., Ciminale, V., and Franchini, G. Human T-cell leukemia/lymphoma virus type 1 nonstructural genes and their functions. Oncogene, *24:* 6026-6034, 2005.
90. Collins, N. D., Newbound, G. C., Albrecht, B., Beard, J. L., Ratner, L., and Lairmore, M. D. Selective ablation of human T-cell lymphotropic virus type 1 p12I reduces viral infectivity in vivo. Blood, *91:* 4701-4707, 1998.
91. Silverman, L. R., Phipps, A. J., Montgomery, A., Ratner, L., and Lairmore, M. D. Human T-cell lymphotropic virus type 1 open reading frame II-encoded p30II is required for in vivo replication: evidence of in vivo reversion. J Virol, *78:* 3837-3845, 2004.
92. Younis, I., Yamamoto, B., Phipps, A., and Green, P. L. Human T-cell leukemia virus type 1 expressing nonoverlapping tax and rex genes replicates and immortalizes primary human T lymphocytes but fails to replicate and persist in vivo. J Virol, *79:* 14473-14481, 2005.
93. Ye, J., Silverman, L., Lairmore, M. D., and Green, P. L. HTLV-1 Rex is required for viral spread and persistence in vivo but is dispensable for cellular immortalization in vitro. Blood, *102:* 3963-3969, 2003.

94. Ding, W., Albrecht, B., Luo, R., Zhang, W., Stanley, J. R., Newbound, G. C., and Lairmore, M. D. Endoplasmic reticulum and cis-Golgi localization of human T-lymphotropic virus type 1 p12(I): association with calreticulin and calnexin. J Virol, *75:* 7672-7682, 2001.
95. Johnson, J. M., Nicot, C., Fullen, J., Ciminale, V., Casareto, L., Mulloy, J. C., Jacobson, S., and Franchini, G. Free major histocompatibility complex class I heavy chain is preferentially targeted for degradation by human T-cell leukemia/lymphotropic virus type 1 p12(I) protein. J Virol, *75:* 6086-6094, 2001.
96. Awasthi, S., Sharma, A., Wong, K., Zhang, J., Matlock, E. F., Rogers, L., Motloch, P., Takemoto, S., Taguchi, H., Cole, M. D., Luscher, B., Dittrich, O., Tagami, H., Nakatani, Y., McGee, M., Girard, A. M., Gaughan, L., Robson, C. N., Monnat, R. J., Jr., and Harrod, R. A human T-cell lymphotropic virus type 1 enhancer of Myc transforming potential stabilizes Myc-TIP60 transcriptional interactions. Mol Cell Biol, *25:* 6178-6198, 2005.
97. Zhang, W., Nisbet, J. W., Albrecht, B., Ding, W., Kashanchi, F., Bartoe, J. T., and Lairmore, M. D. Human T-lymphotropic virus type 1 p30(II) regulates gene transcription by binding CREB binding protein/p300. J Virol, *75:* 9885-9895, 2001.
98. Zhang, W., Nisbet, J. W., Bartoe, J. T., Ding, W., and Lairmore, M. D. Human T-lymphotropic virus type 1 p30(II) functions as a transcription factor and differentially modulates CREB-responsive promoters. J Virol, *74:* 11270-11277, 2000.
99. Nicot, C., Dundr, M., Johnson, J. M., Fullen, J. R., Alonzo, N., Fukumoto, R., Princler, G. L., Derse, D., Misteli, T., and Franchini, G. HTLV-1-encoded p30II is a post-transcriptional negative regulator of viral replication. Nat Med, *10:* 197-201, 2004.
100. D'Agostino, D. M., Ranzato, L., Arrigoni, G., Cavallari, I., Belleudi, F., Torrisi, M. R., Silic-Benussi, M., Ferro, T., Petronilli, V., Marin, O., Chieco-Bianchi, L., Bernardi, P., and Ciminale, V. Mitochondrial alterations induced by the p13II protein of human T-cell leukemia virus type 1. Critical role of arginine residues. J Biol Chem, *277:* 34424-34433, 2002.
101. Inoue, J., Seiki, M., and Yoshida, M. The second pX product p27 chi-III of HTLV-1 is required for gag gene expression. FEBS Lett, *209:* 187-190, 1986.
102. Inoue, J., Yoshida, M., and Seiki, M. Transcriptional (p40x) and post-transcriptional (p27x-III) regulators are required for the expression and replication of human T-cell leukemia virus type I genes. Proc Natl Acad Sci U S A, *84:* 3653-3657, 1987.
103. Black, A. C., Chen, I. S., Arrigo, S., Ruland, C. T., Allogiamento, T., Chin, E., and Rosenblatt, J. D. Regulation of HTLV-II gene expression by Rex involves positive and negative cis-acting elements in the 5'long terminal repeat. Virology, *181:* 433-444, 1991.

104. Gaudray, G., Gachon, F., Basbous, J., Biard-Piechaczyk, M., Devaux, C., and Mesnard, J. M. The complementary strand of the human T-cell leukemia virus type 1 RNA genome encodes a bZIP transcription factor that down-regulates viral transcription. J Virol, *76:* 12813-12822, 2002.
105. Larocca, D., Chao, L. A., Seto, M. H., and Brunck, T. K. Human T-cell leukemia virus minus strand transcription in infected T-cells. Biochem Biophys Res Commun, *163:* 1006-1013, 1989.
106. Basbous, J., Arpin, C., Gaudray, G., Piechaczyk, M., Devaux, C., and Mesnard, J. M. The HBZ factor of human T-cell leukemia virus type I dimerizes with transcription factors JunB and c-Jun and modulates their transcriptional activity. J Biol Chem, *278:* 43620-43627, 2003.
107. Lemasson, I., Lewis, M. R., Polakowski, N., Hivin, P., Cavanagh, M. H., Thebault, S., Barbeau, B., Nyborg, J. K., and Mesnard, J. M. Human T-cell leukemia virus type 1 (HTLV-1) bZIP protein interacts with the cellular transcription factor CREB to inhibit HTLV-1 transcription. J Virol, *81:* 1543-1553, 2007.
108. Satou, Y., Yasunaga, J., Yoshida, M., and Matsuoka, M. HTLV-I basic leucine zipper factor gene mRNA supports proliferation of adult T cell leukemia cells. Proc Natl Acad Sci U S A, *103:* 720-725, 2006.
109. Fujimoto, T., Hata, T., Itoyama, T., Nakamura, H., Tsukasaki, K., Yamada, Y., Ikeda, S., Sadamori, N., and Tomonaga, M. High rate of chromosomal abnormalities in HTLV-I-infected T-cell colonies derived from prodromal phase of adult T-cell leukemia: a study of IL-2-stimulated colony formation in methylcellulose. Cancer Genet Cytogenet, *109:* 1-13, 1999.
110. Kamada, N., Sakurai, M., Miyamoto, K., Sanada, I., Sadamori, N., Fukuhara, S., Abe, S., Shiraishi, Y., Abe, T., Kaneko, Y., and et al. Chromosome abnormalities in adult T-cell leukemia/lymphoma: a karyotype review committee report. Cancer Res, *52:* 1481-1493, 1992.
111. Majone, F., Semmes, O. J., and Jeang, K. T. Induction of micronuclei by HTLV-I Tax: a cellular assay for function. Virology, *193:* 456-459, 1993.
112. Semmes, O. J., Majone, F., Cantemir, C., Turchetto, L., Hjelle, B., and Jeang, K. T. HTLV-I and HTLV-II Tax: differences in induction of micronuclei in cells and transcriptional activation of viral LTRs. Virology, *217:* 373-379, 1996.
113. Lynch, A. M. and Parry, J. M. The cytochalasin-B micronucleus/kinetochore assay in vitro: studies with 10 suspected aneugens. Mutat Res, *287:* 71-86, 1993.
114. Yager, J. W., Eastmond, D. A., Robertson, M. L., Paradisin, W. M., and Smith, M. T. Characterization of micronuclei induced in human lymphocytes by benzene metabolites. Cancer Res, *50:* 393-399, 1990.
115. Majone, F. and Jeang, K. T. Clastogenic effect of the human T-cell leukemia virus type I Tax oncoprotein correlates with unstabilized DNA breaks. J Biol Chem, *275:* 32906-32910, 2000.

116. Lemoine, F. J. and Marriott, S. J. Genomic instability driven by the human T-cell leukemia virus type I (HTLV-I) oncoprotein, Tax. Oncogene, *21:* 7230-7234, 2002.
117. Liang, M. H., Geisbert, T., Yao, Y., Hinrichs, S. H., and Giam, C. Z. Human T-lymphotropic virus type 1 oncoprotein tax promotes S-phase entry but blocks mitosis. J Virol, *76:* 4022-4033, 2002.
118. Bennett, J. M., Catovsky, D., Daniel, M. T., Flandrin, G., Galton, D. A., Gralnick, H. R., and Sultan, C. Proposals for the classification of chronic (mature) B and T lymphoid leukaemias. French-American-British (FAB) Cooperative Group. J Clin Pathol, *42:* 567-584, 1989.
119. Kornberg, R. D. and Thomas, J. O. Chromatin structure; oligomers of the histones. Science, *184:* 865-868, 1974.
120. Luger, K., Mader, A. W., Richmond, R. K., Sargent, D. F., and Richmond, T. J. Crystal structure of the nucleosome core particle at 2.8 A resolution. Nature, *389:* 251-260, 1997.
121. Cavalli, G. Chromatin and epigenetics in development: blending cellular memory with cell fate plasticity. Development, *133:* 2089-2094, 2006.
122. Karagiannis, T. C. and El-Osta, A. Epigenetic changes activate widespread signals in response to double-strand breaks. Cancer Biol Ther, *3:* 617-623, 2004.
123. Osley, M. A., Tsukuda, T., and Nickoloff, J. A. ATP-dependent chromatin remodeling factors and DNA damage repair. Mutat Res, *618:* 65-80, 2007.
124. Lewis, L. K., Karthikeyan, G., Cassiano, J., and Resnick, M. A. Reduction of nucleosome assembly during new DNA synthesis impairs both major pathways of double-strand break repair. Nucleic Acids Res, *33:* 4928-4939, 2005.
125. Ye, X., Franco, A. A., Santos, H., Nelson, D. M., Kaufman, P. D., and Adams, P. D. Defective S phase chromatin assembly causes DNA damage, activation of the S phase checkpoint, and S phase arrest. Mol Cell, *11:* 341-351, 2003.
126. Karagiannis, T. C. and El-Osta, A. Double-strand breaks: signaling pathways and repair mechanisms. Cell Mol Life Sci, *61:* 2137-2147, 2004.
127. Prado, F. and Aguilera, A. Partial depletion of histone H4 increases homologous recombination-mediated genetic instability. Mol Cell Biol, *25:* 1526-1536, 2005.
128. Zhao, J. Coordination of DNA synthesis and histone gene expression during normal cell cycle progression and after DNA damage. Cell Cycle, *3:* 695-697, 2004.
129. Gunjan, A., Paik, J., and Verreault, A. Regulation of histone synthesis and nucleosome assembly. Biochimie, *87:* 625-635, 2005.
130. Sogo, J. M., Stahl, H., Koller, T., and Knippers, R. Structure of replicating simian virus 40 minichromosomes. The replication fork, core histone segregation and terminal structures. J Mol Biol, *189:* 189-204, 1986.

131. Tyler, J. K., Adams, C. R., Chen, S. R., Kobayashi, R., Kamakaka, R. T., and Kadonaga, J. T. The RCAF complex mediates chromatin assembly during DNA replication and repair. Nature, *402:* 555-560, 1999.
132. Bonner, W. M., Wu, R. S., Panusz, H. T., and Muneses, C. Kinetics of accumulation and depletion of soluble newly synthesized histone in the reciprocal regulation of histone and DNA synthesis. Biochemistry, *27:* 6542-6550, 1988.
133. Oliver, D., Granner, D., and Chalkley, R. Identification of a distinction between cytoplasmic histone synthesis and subsequent histone deposition within the nucleus. Biochemistry, *13:* 746-749, 1974.
134. Marzluff, W. F., Gongidi, P., Woods, K. R., Jin, J., and Maltais, L. J. The human and mouse replication-dependent histone genes. Genomics, *80:* 487-498, 2002.
135. Heintz, N., Sive, H. L., and Roeder, R. G. Regulation of human histone gene expression: kinetics of accumulation and changes in the rate of synthesis and in the half-lives of individual histone mRNAs during the HeLa cell cycle. Mol Cell Biol, *3:* 539-550, 1983.
136. Marzluff, W. F. and Duronio, R. J. Histone mRNA expression: multiple levels of cell cycle regulation and important developmental consequences. Curr Opin Cell Biol, *14:* 692-699, 2002.
137. Osley, M. A. The regulation of histone synthesis in the cell cycle. Annu Rev Biochem, *60:* 827-861, 1991.
138. Spector, M. S., Raff, A., DeSilva, H., Lee, K., and Osley, M. A. Hir1p and Hir2p function as transcriptional corepressors to regulate histone gene transcription in the Saccharomyces cerevisiae cell cycle. Mol Cell Biol, *17:* 545-552, 1997.
139. Ray-Gallet, D., Quivy, J. P., Scamps, C., Martini, E. M., Lipinski, M., and Almouzni, G. HIRA is critical for a nucleosome assembly pathway independent of DNA synthesis. Mol Cell, *9:* 1091-1100, 2002.
140. Hall, C., Nelson, D. M., Ye, X., Baker, K., DeCaprio, J. A., Seeholzer, S., Lipinski, M., and Adams, P. D. HIRA, the human homologue of yeast Hir1p and Hir2p, is a novel cyclin-cdk2 substrate whose expression blocks S-phase progression. Mol Cell Biol, *21:* 1854-1865, 2001.
141. Ma, T., Van Tine, B. A., Wei, Y., Garrett, M. D., Nelson, D., Adams, P. D., Wang, J., Qin, J., Chow, L. T., and Harper, J. W. Cell cycle-regulated phosphorylation of p220(NPAT) by cyclin E/Cdk2 in Cajal bodies promotes histone gene transcription. Genes Dev, *14:* 2298-2313, 2000.
142. Zhao, J., Kennedy, B. K., Lawrence, B. D., Barbie, D. A., Matera, A. G., Fletcher, J. A., and Harlow, E. NPAT links cyclin E-Cdk2 to the regulation of replication-dependent histone gene transcription. Genes Dev, *14:* 2283-2297, 2000.
143. Gao, G., Bracken, A. P., Burkard, K., Pasini, D., Classon, M., Attwooll, C., Sagara, M., Imai, T., Helin, K., and Zhao, J. NPAT expression is regulated by E2F and is essential for cell cycle progression. Mol Cell Biol, *23:* 2821-2833, 2003.

144. Gall, J. G. The centennial of the Cajal body. Nat Rev Mol Cell Biol, *4:* 975-980, 2003.
145. Kolev, N. G. and Steitz, J. A. Symplekin and multiple other polyadenylation factors participate in 3'-end maturation of histone mRNAs. Genes Dev, *19:* 2583-2592, 2005.
146. Abbott, J., Marzluff, W. F., and Gall, J. G. The stem-loop binding protein (SLBP1) is present in coiled bodies of the Xenopus germinal vesicle. Mol Biol Cell, *10:* 487-499, 1999.
147. Frey, M. R. and Matera, A. G. Coiled bodies contain U7 small nuclear RNA and associate with specific DNA sequences in interphase human cells. Proc Natl Acad Sci U S A, *92:* 5915-5919, 1995.
148. Liu, J. L., Murphy, C., Buszczak, M., Clatterbuck, S., Goodman, R., and Gall, J. G. The Drosophila melanogaster Cajal body. J Cell Biol, *172:* 875-884, 2006.
149. Barcaroli, D., Bongiorno-Borbone, L., Terrinoni, A., Hofmann, T. G., Rossi, M., Knight, R. A., Matera, A. G., Melino, G., and De Laurenzi, V. FLASH is required for histone transcription and S-phase progression. Proc Natl Acad Sci U S A, *103:* 14808-14812, 2006.
150. DeLisle, A. J., Graves, R. A., Marzluff, W. F., and Johnson, L. F. Regulation of histone mRNA production and stability in serum-stimulated mouse 3T6 fibroblasts. Mol Cell Biol, *3:* 1920-1929, 1983.
151. Birchmeier, C., Folk, W., and Birnstiel, M. L. The terminal RNA stem-loop structure and 80 bp of spacer DNA are required for the formation of 3' termini of sea urchin H2A mRNA. Cell, *35:* 433-440, 1983.
152. Dominski, Z., Zheng, L. X., Sanchez, R., and Marzluff, W. F. Stem-loop binding protein facilitates 3'-end formation by stabilizing U7 snRNP binding to histone pre-mRNA. Mol Cell Biol, *19:* 3561-3570, 1999.
153. Wang, Z. F., Whitfield, M. L., Ingledue, T. C., 3rd, Dominski, Z., and Marzluff, W. F. The protein that binds the 3' end of histone mRNA: a novel RNA-binding protein required for histone pre-mRNA processing. Genes Dev, *10:* 3028-3040, 1996.
154. Ling, J., Morley, S. J., Pain, V. M., Marzluff, W. F., and Gallie, D. R. The histone 3'-terminal stem-loop-binding protein enhances translation through a functional and physical interaction with eukaryotic initiation factor 4G (eIF4G) and eIF3. Mol Cell Biol, *22:* 7853-7867, 2002.
155. Sanchez, R. and Marzluff, W. F. The stem-loop binding protein is required for efficient translation of histone mRNA in vivo and in vitro. Mol Cell Biol, *22:* 7093-7104, 2002.
156. Whitfield, M. L., Zheng, L. X., Baldwin, A., Ohta, T., Hurt, M. M., and Marzluff, W. F. Stem-loop binding protein, the protein that binds the 3' end of histone mRNA, is cell cycle regulated by both translational and posttranslational mechanisms. Mol Cell Biol, *20:* 4188-4198, 2000.
157. Pfaffl, M. W. A new mathematical model for relative quantification in real-time RT-PCR. Nucleic Acids Res, *29:* e45, 2001.

158. Whelan, J. A., Russell, N. B., and Whelan, M. A. A method for the absolute quantification of cDNA using real-time PCR. J Immunol Methods, *278:* 261-269, 2003.
159. Simonian, M. H. Current Protocols in Molecular Biology. *2:* 10.11.11-10.11.10, 1996.
160. Fragoso, G. L. H. a. G. Analysis of Nucleosome Positioning in Mammalian Cells. Methods in Enzymology, *304:* 632-634, 1999.
161. Gatza, M. L., Watt, J. C., and Marriott, S. J. Cellular transformation by the HTLV-I Tax protein, a jack-of-all-trades. Oncogene, *22:* 5141-5149, 2003.
162. Fan, Y., Nikitina, T., Morin-Kensicki, E. M., Zhao, J., Magnuson, T. R., Woodcock, C. L., and Skoultchi, A. I. H1 linker histones are essential for mouse development and affect nucleosome spacing in vivo. Mol Cell Biol, *23:* 4559-4572, 2003.
163. Chan, Y. H. and Wong, J. T. Concentration-dependent organization of DNA by the dinoflagellate histone-like protein HCc3. Nucleic Acids Res, *35:* 2573-2583, 2007.
164. Tsukasaki, K., Tanosaki, S., DeVos, S., Hofmann, W. K., Wachsman, W., Gombart, A. F., Krebs, J., Jauch, A., Bartram, C. R., Nagai, K., Tomonaga, M., Said, J. W., and Koeffler, H. P. Identifying progression-associated genes in adult T-cell leukemia/lymphoma by using oligonucleotide microarrays. Int J Cancer, *109:* 875-881, 2004.
165. Pise-Masison, C. A., Radonovich, M., Mahieux, R., Chatterjee, P., Whiteford, C., Duvall, J., Guillerm, C., Gessain, A., and Brady, J. N. Transcription profile of cells infected with human T-cell leukemia virus type I compared with activated lymphocytes. Cancer Res, *62:* 3562-3571, 2002.
166. Groth, A., Ray-Gallet, D., Quivy, J. P., Lukas, J., Bartek, J., and Almouzni, G. Human Asf1 regulates the flow of S phase histones during replicational stress. Mol Cell, *17:* 301-311, 2005.
167. Ducasse, M. and Brown, M. A. Epigenetic aberrations and cancer. Mol Cancer, *5:* 60, 2006.
168. Feinberg, A. P., Ohlsson, R., and Henikoff, S. The epigenetic progenitor origin of human cancer. Nat Rev Genet, *7:* 21-33, 2006.
169. Feinberg, A. P. and Tycko, B. The history of cancer epigenetics. Nat Rev Cancer, *4:* 143-153, 2004.
170. Ting, A. H., McGarvey, K. M., and Baylin, S. B. The cancer epigenome--components and functional correlates. Genes Dev, *20:* 3215-3231, 2006.
171. Parseghian, M. H. and Hamkalo, B. A. A compendium of the histone H1 family of somatic subtypes: an elusive cast of characters and their characteristics. Biochem Cell Biol, *79:* 289-304., 2001.
172. Parseghian, M. H., Newcomb, R. L., and Hamkalo, B. A. Distribution of somatic H1 subtypes is non-random on active vs. inactive chromatin II: distribution in human adult fibroblasts. J Cell Biochem, *83:* 643-659, 2001.
173. Parseghian, M. H., Newcomb, R. L., Winokur, S. T., and Hamkalo, B. A. The distribution of somatic H1 subtypes is non-random on active vs.

inactive chromatin: distribution in human fetal fibroblasts. Chromosome Res, *8:* 405-424, 2000.

174. Franke, K., Drabent, B., and Doenecke, D. Expression of murine H1 histone genes during postnatal development. Biochim Biophys Acta, *1398:* 232-242, 1998.
175. Wang, Z. F., Sirotkin, A. M., Buchold, G. M., Skoultchi, A. I., and Marzluff, W. F. The mouse histone H1 genes: gene organization and differential regulation. J Mol Biol, *271:* 124-138, 1997.
176. Lennox, R. W. and Cohen, L. H. The histone H1 complements of dividing and nondividing cells of the mouse. J Biol Chem, *258:* 262-268, 1983.
177. Ng, P. W., Iha, H., Iwanaga, Y., Bittner, M., Chen, Y., Jiang, Y., Gooden, G., Trent, J. M., Meltzer, P., Jeang, K. T., and Zeichner, S. L. Genome-wide expression changes induced by HTLV-1 Tax: evidence for MLK-3 mixed lineage kinase involvement in Tax-mediated NF-kappaB activation. Oncogene, *20:* 4484-4496, 2001.
178. Zheng, L., Dominski, Z., Yang, X. C., Elms, P., Raska, C. S., Borchers, C. H., and Marzluff, W. F. Phosphorylation of stem-loop binding protein (SLBP) on two threonines triggers degradation of SLBP, the sole cell cycle-regulated factor required for regulation of histone mRNA processing, at the end of S phase. Mol Cell Biol, *23:* 1590-1601, 2003.
179. Kaygun, H. and Marzluff, W. F. Translation termination is involved in histone mRNA degradation when DNA replication is inhibited. Mol Cell Biol, *25:* 6879-6888, 2005.
180. Sokoloski, K. J., Wilusz, C. J., and Wilusz, J. Viruses: overturning RNA turnover. RNA Biol, *3:* 140-144, 2006.
181. Mullen, T. E. and Marzluff, W. F. Degradation of histone mRNA requires oligouridylation followed by decapping and simultaneous degradation of the mRNA both 5' to 3' and 3' to 5'. Genes Dev, *22:* 50-65, 2008.
182. De Lucia, F., Lorain, S., Scamps, C., Galisson, F., MacHold, J., and Lipinski, M. Subnuclear localization and mitotic phosphorylation of HIRA, the human homologue of Saccharomyces cerevisiae transcriptional regulators Hir1p/Hir2p. Biochem J, *358:* 447-455, 2001.